

©2022

Elizabeth Kelley Wright-Fairbanks

ALL RIGHTS RESERVED

**OBSERVING SEASONAL CYCLES, DRIVERS, AND POTENTIAL
BIOLOGICAL IMPACTS OF OCEAN ACIDIFICATION IN THE MID-
ATLANTIC BIGHT**

By

ELIZABETH KELLEY WRIGHT-FAIRBANKS

A dissertation submitted to the

School of Graduate Studies

Rutgers, The State University of New Jersey

In partial fulfillment of the requirements

For the degree of

Doctor of Philosophy

Graduate Program in Oceanography

Written under the direction of

Grace K. Saba

And approved by

New Brunswick, New Jersey

January 2022

ABSTRACT OF THE DISSERTATION

Observing seasonal cycles, drivers, and potential biological impacts of ocean acidification in the Mid-Atlantic Bight

By ELIZABETH KELLEY WRIGHT-FAIRBANKS

Dissertation Director:

Grace K. Saba

Ocean acidification due to oceanic uptake of atmospheric carbon dioxide is occurring at unprecedented rates globally. Acidification can be further exacerbated or mitigated due to highly variable physical, biological, and chemical processes in economically important coastal zones like the Mid-Atlantic Bight (MAB). In the MAB, the extent of acidification is altered by freshwater input, biological productivity and respiration, periodic upwelling, seasonal changes in temperature and water column structure, and interactions between coastal water masses. The various drivers of acidification change and interact on time scales from minutes to years, and those interactions have historically been missed due to low spatial or temporal resolution monitoring efforts. Organisms living in the coastal shelf zone that utilize carbonate structures, including economically vital shellfish, are especially susceptible to acidification. Therefore, it is necessary to understand how the carbonate system is changing at a scale that could affect biological processes.

This dissertation is composed of three projects that depict cycles, drivers, and impacts of seasonal changes in the MAB carbonate system. Chapter 2 describes the first ever seasonal deployments of a deep-ISFET based pH sensor integrated into a Slocum glider autonomous observing platform. These deployments took place over the course of 2 years in the MAB, and illustrate the seasonal development and degradation of periods of acidification along the coastal shelf. Additionally, quality assurance, quality control, and data analysis techniques distinctive to this sensor are described for the first time.

Chapter 3 further decomposes the seasonal pH glider deployments, employing a first-order Taylor Series Decomposition analysis of the seasonal data to quantify the drivers of carbonate chemistry in the MAB. Water mass mixing and biogeochemical activity are identified as the main drivers of the MAB carbonate system, with freshwater inputs, shelf-break current interactions, photosynthesis, and respiration interacting to exacerbate or mitigate acidification in the coastal zone.

Chapter 4 addresses the biological implications of seasonal carbonate chemistry dynamics in the MAB. A literature review is conducted to develop a general relationship between larval bivalve growth and acidification. This relationship is then applied to a coupled Regional Ocean Modeling System – Individual Based Model using the ROMSPATH program to simulate the impacts of seasonal hydrodynamic conditions on sea scallop larval dispersal in the MAB. Sea scallops that are sensitive to acidification see lower success rates and population connectivity than those that are not sensitive. However, sensitivity to acidification can make up for loss due to high temperatures in high-carbonate saturation state conditions.

This dissertation exemplifies ways in which observing systems, modeling techniques, and laboratory research can be used together to understand the ecological impacts of climate change. The continued development of ocean acidification monitoring platforms, modeling, laboratory studies, and field research is paramount to predicting and preparing for the physical, societal, and economic effects of future change.

ACKNOWLEDGEMENTS

First, I would like to thank my advisor, Grace Saba, for her unwavering support over the past five years. Grace, you are an inspirational mentor through your skills as a research scientist, commitment to student success, and dedication to fostering a respectful workplace. I would not be the scientist I am today without your guidance.

Thank you to my committee members: Travis Miles, Daphne Munroe, and Joe Salisbury. Travis, thank you for spending countless hours going through MATLAB code with me to figure out how to work with pH glider data. Daphne, thank you for providing guidance on conducting shellfish research and for sharing your knowledge of sea scallop larval modeling. Joe, I value the time we spent at sea together during the ECOA-2 cruise, and all the helpful advice you have provided since.

I have been lucky to work with and learn from many researchers in the Department of Marine and Coastal Sciences at Rutgers. The COOL group faculty, Scott Glenn, Oscar Schofield, Josh Kohut, Travis Miles, and Grace Saba, have provided encouragement and assistance through weekly OIB meetings and facility support. Thank you to my professors Bob Chant, Jim Miller, Rob Sherrell, Yair Rosenthal, John Wilkin, Silke Severmann, Carrie Ferraro, Nick Beard, Debashish Bhattacharya, Paul Falkowski, Gary Taghon, and Bob Kopp for teaching me how to be a well-rounded oceanographer.

The work presented here would not have been possible without support from the incredible research and support staff at DMCS. Thank you especially to glider technicians Dave Aragon and Nicole Waite, and ship captain Chip Haldeman, who keep our fleet moving. Thank you to Eli Hunter, Lori Garzio, Laura Nazzaro, and John Kerfoot

for data processing advice. Thank you Patty Gillen and Donna Napoli for handling every equipment order, TABER, and paperwork question I could come up with.

I am grateful to have made many incredible friendships at Rutgers. Schuyler and Emily, thank you for being lovely roommates and friends. To my extended cohort: Jonathan, Vince, Hailey, Chris, Stan, Cliff, and Austin – thank you for all of the memories and for being there through the ups and downs of graduate school.

I would not have made it through a Ph.D. without my support system. Mom and Dad, your generosity, kindness, love, and support of my goals got me here. Dad, thank you for encouraging me to attend the Island School way back when; it made all the difference. Mom, thank you for keeping me organized and for supporting my trips to sea despite the toll they took on your blood pressure. Sam, you are an inspiration to me. To my life-long friends near and far, I hold every message of support, facetime, and visit close to my heart.

Finally, I would like to thank my partner and best friend, Jason, who has been there through it all. I can't wait for what comes next!

TABLE OF CONTENTS

Abstract	ii
Acknowledgements	v
Table of Contents	vii
List of Tables	x
List of Figures	xii
Chapter 1: Introduction	1
1.1 Ocean and Coastal Acidification.....	2
1.2 Acidification in the Mid-Atlantic Bight.....	4
1.3 Biological Implications of Ocean Acidification.....	5
1.4 Monitoring Coastal Carbonate Chemistry.....	6
1.5 Dissertation Questions	8
1.6 References.....	9
Chapter 2: Autonomous Observation of Seasonal Carbonate Chemistry Dynamics in the Mid-Atlantic Bight	14
2.1 Abstract.....	15
2.2 Introduction.....	15
2.3 Materials and Methods.....	19
2.4 Results.....	27
2.5 Discussion.....	34
2.6 Significance.....	41
2.7 Acknowledgements.....	42
2.8 References.....	43

2.9 Figures.....	52
2.10 Supplemental Text.....	61
2.11 Supplemental Figures.....	62
2.12 Supplemental Tables.....	63
 Chapter 3: Quantification of the Dominant Drivers of Acidification in the Coastal	
Mid-Atlantic Bight.....	75
3.1 Abstract.....	76
3.2 Introduction.....	77
3.3 Materials and Methods.....	80
3.4 Results.....	88
3.5 Discussion.....	92
3.6 Conclusions.....	102
3.7 Acknowledgements.....	103
3.8 References.....	104
3.9 Figures.....	110
3.10 Tables.....	122
3.11 Supplemental Figures.....	123
3.12 Supplemental Tables.....	128
 Chapter 4: Meta-Analysis of Larval Bivalve Growth in Response to Ocean	
Acidification and its Application to Sea Scallop Larval Dispersal in the	
Mid-Atlantic Bight.....	137
4.1 Abstract.....	138
4.2 Introduction.....	138

4.3 Methods.....	141
4.4 Results.....	150
4.5 Discussion.....	154
4.6 Conclusions.....	163
4.7 References.....	164
4.8 Figures.....	172
4.9 Tables.....	176
Chapter 5: Conclusions.....	182

LIST OF TABLES

Chapter 2

Supplemental Table S2.1: Average values of glider-measured and -derived variables, split up by deployment region and depth, from four seasonal missions.....	63
Supplemental Table S2.2: Glider pH sensor agreement and field uncertainty (within-mixed-layer variability) during four seasonal deployments.....	66
Supplemental Table S2.3: pH glider offsets at deployment and recovery during four seasonal deployments.....	67
Supplemental Table S2.4: Uncertainty in Ω_{arag} and TA:DIC measurements due to salinity-derived TA offsets.....	70
Supplemental Table S2.5: A comparison of discrete sample TA and TA derived from a seasonal regression analysis of TA-salinity relationships.....	71
Supplemental Table S2.6: Full water column glider-measured and -derived carbonate system parameters from four seasonal missions.....	74

Chapter 3

Table 3.1: Region and depth definitions used in the analysis.....	122
Supplemental Table S3.1: Sensitivities of H^+ and Ω_{arag} to changes in temperature, salinity, TA, DIC, and salinity-normalized DIC.....	128
Supplemental Table S3.2: Anomalies of H^+ and Ω_{arag} as calculated in Analysis 1.....	131
Supplemental Table S3.3: Anomalies of H^+ and Ω_{arag} as calculated in Analysis 2.....	134

Chapter 4

Table 4.1: Scallop larval dispersal model bounds and particle release amounts.....	176
Table 4.2: Habitat preferences for five bivalve species.....	177

Table 4.3: Modeled larval scallop settlement success.....	178
Table 4.4: Non-OA sensitive scallop population connectivity.....	179
Table 4.5: OA sensitive scallop population connectivity.....	180
Table 4.6: Modeled environmental conditions.....	181

LIST OF FIGURES

Chapter 2

Figure 2.1: Seasonal glider deployments completed between May 2018 and November 2019.....	52
Figure 2.2: Comparisons of mixed layer depth (MLD) and maximum buoyancy frequency ($\max(N^2)$) during seasonal glider deployments.....	53
Figure 2.3: Contour plots of temperature, salinity, and density from four seasonal glider deployments in the MAB.....	54
Figure 2.4: Comparisons of physical, biological, and chemical ocean properties during seasonal glider deployments.....	55
Figure 2.5: Contour plots of depth-averaged chlorophyll and oxygen from four seasonal glider deployments in the MAB.....	56
Figure 2.6: Contour plots of <i>in situ</i> pH, Ω_{arag} , and TA:DIC from four seasonal glider deployments in the MAB.....	57
Figure 2.7: Comparisons of carbonate system parameters measured during and derived from seasonal glider deployments.....	58
Figure 2.8: Seasonal differences in surface water pH, Ω_{arag} , and TA:DIC expressed as a function of distance from shore.....	59
Figure 2.9: Seasonal differences in bottom water pH, Ω_{arag} , and TA:DIC expressed as a function of distance from shore.....	60
Supplemental Figure S2.1: Discrete sample salinity vs. total alkalinity from the 2015 ECOA cruise and four seasonal glider deployments.....	62

Chapter 3

Figure 3.1: Map of pH glider deployment tracks, 2018-2019.....	110
--	-----

Figure 3.2: Change in salinity-normalized DIC vs. changes in aragonite saturation state due to biogeochemical activity in four seasons.....	111
Figure 3.3: Influence of water mass mixing on Ω_{arag} and pH in the nearshore.....	112
Figure 3.4: Patterns of Ω_{arag} and pH in Cold Pool-area water.....	113
Figure 3.5: Drivers of Ω_{arag} and pH in summer 2019 Cold Pool water.....	114
Figure 3.6: Drivers of Ω_{arag} and pH in spring 2018 Cold Pool water.....	115
Figure 3.7: Differences in surface water Ω_{arag} and pH anomalies between winter and summer 2019.....	116
Figure 3.8: Drivers of surface shelf water Ω_{arag} and pH in winter and summer 2019.....	117
Figure 3.9: Schematic depiction of the major drivers of Ω_{arag} and pH in each season.....	118
Figure 3.10: Drivers of Ω_{arag} and pH at the shelf break.....	119
Figure 3.11: Relative change in Ω_{arag} at the shelf break in each season.....	120
Figure 3.12: Mid-Atlantic sea surface temperature on October 24, 2019.....	121
Supplemental Figure S3.1: Ω_{arag} sensitivity to changes in temperature, summer 2019...	123
Supplemental Figure S3.2: Drivers of in Ω_{arag} and pH, winter 2019.....	124
Supplemental Figure S3.3: Drivers of in Ω_{arag} and pH, spring 2019.....	125
Supplemental Figure S3.4: Drivers of in Ω_{arag} and pH, summer 2019.....	126
Supplemental Figure S3.5: Drivers of in Ω_{arag} and pH, fall 2019.....	127

Chapter 4

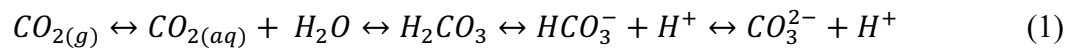
Figure 4.1: Larval sea scallop model release regional bounds.....	172
Figure 4.2: Species-specific larval bivalve growth vs. aragonite saturation state.....	173
Figure 4.3: General larval bivalve growth vs. aragonite saturation state based on sensitivity to ocean acidification.....	174
Figure 4.4: Larval sea scallop seasonal settlement success plotted against temperature and aragonite saturation state.....	175

CHAPTER 1: Introduction

1.1 Ocean and Coastal Acidification

Ocean acidification (OA) results from the ocean's uptake of atmospheric carbon dioxide (CO_2) that creates changes in ocean carbonate chemistry (Gledhill et al., 2015). The ocean has absorbed approximately one-third of the CO_2 emitted by anthropogenic activity since the Industrial Revolution (IPCC, 2021). During this time, atmospheric CO_2 has risen from approximately 280 parts per million (ppm) to 415 ppm (Tans & Keeling, 2021) due to increased rates of emission.

When CO_2 is absorbed by the ocean, it reacts with seawater to form carbonic acid. Carbonic acid quickly dissociates into bicarbonate (HCO_3^-) and carbonate (CO_3^{2-}) ions, releasing two hydrogen ions (H^+ ; Equation 1).



The formation of excess H^+ decreases ocean pH, thereby increasing its acidity. Some excess H^+ is buffered by carbonate ions in a reaction that forms bicarbonate. Therefore, a decrease in pH corresponds to a shifting equilibrium between marine carbonate species, seen as an increase in bicarbonate ions and a decrease in carbonate ions (Stumm & Morgan, 1996). Decreased carbonate ion concentration leads to a lower carbonate saturation state (Ω), reducing stability of two calcium carbonate minerals, calcite and aragonite. Ω governs the formation and dissolution of calcium carbonate, with calcite governed by Ω_{cal} and aragonite governed by Ω_{arag} (Equation 2). A saturation state above 1 indicates that the water is supersaturated with respect to carbonate, meaning precipitation of the mineral is thermodynamically favorable. A saturation state below 1 indicates undersaturated water, meaning dissolution is thermodynamically favorable.

$$\Omega = \frac{[\text{Ca}^{2+}][\text{CO}_3^{2-}]}{K_{sp}^*} \quad (2)$$

The global ocean is acidifying at unprecedented rates, with open ocean surface water pH decreasing by 0.017-0.027 pH units per decade since the late 1980s (Gledhill et al., 2015; IPCC, 2019; Sutton et al., 2016; Zeebe, 2012). Maximum rates of acidification have been detected in high latitude surface waters and upwelling regions (Bopp et al., 2013; IPCC, 2021). Global surface ocean pH is predicted to decline by up to 0.44 pH units by 2099 compared to the preindustrial period under Shared Socioeconomic Pathway (SSP) 5-8.5, and a pH reduction of 0.1 is expected at 1 km depth under SSP3-7.0 (IPCC, 2021). Likewise, the rate of change in Ω_{arag} since the Industrial Revolution has been five times greater than natural variability over the last millennium (Friedrich et al., 2012; Gattuso et al., 2015). Under Representative Concentration Pathway (RCP) 8.5, which is analogous to SSP5-8.5, the total volume of water with Ω_{arag} less than 1.0 will increase from 76% to 91% by the year 2100 (Gattuso et al., 2015). The first large-scale decreases in Ω_{arag} are predicted in high latitude regions (Gattuso et al., 2015; IPCC, 2021), and there is evidence that this process is occurring there at a rate faster than previously projected (Negrete-García et al., 2019).

In socio-economically important coastal oceans, acidification is compounded or mitigated by physical, chemical, and biological processes (Cai et al., 2020; Gledhill et al., 2015; Wootton et al., 2008). These processes can cause highly variable and episodic pockets of acidification that have more immediate impacts on carbonate-dependent organisms than long-term acidification caused by increasing atmospheric CO₂. This is commonly referred to as coastal acidification. Freshwater riverine input and storm water runoff introduce low-alkalinity water into the coastal system, decreasing buffering capacity for CO₂ and increasing acidification (Cai et al., 2020; Kwiatkowski & Orr,

2018). Nutrient runoff can cause eutrophication, increasing photosynthesis, oxygen, and pH in surface water. However, when biological matter sinks, it is respired in subsurface and bottom waters, increasing CO₂ and decreasing oxygen, pH, and Ω_{arag} (Cai et al., 2011). Additionally, coastal current interactions and water column dynamics such as stratification and mixing influence the carbonate system on daily, seasonal, and interannual time scales (Salisbury & Jonsson, 2018; Wanninkhof et al., 2015).

1.2 Acidification in the Mid-Atlantic Bight

The Mid-Atlantic Bight (MAB) encompasses the U.S. east coast continental shelf region bounded by Cape Cod and the Nantucket Shoals to the northeast and Cape Hatteras to the south. This region is highly productive, with seasonal phytoplankton blooms sustaining numerous active fin and shellfisheries in the region. The MAB is adjacent to multiple large city centers, including New York, Philadelphia, Baltimore, and Washington, D.C., as well as significant bays and estuaries including Delaware and Chesapeake Bays. As such, it is subject to anthropogenic inputs year-round. Additionally, the MAB contains multiple offshore wind lease areas, and will be an important site of wind power development in the coming years.

The MAB is prone to acidification due to ongoing CO₂ absorption, seasonal changes in the water column, cycles of biological growth and decay, interactions between coastal currents, several freshwater sources, and episodic upwelling. Seasonal phytoplankton blooms and temperature and salinity cycles in the MAB can alter regional pH and Ω_{arag} (Cai et al., 2011; Cai et al., 2020). Seasonal stratification in the MAB is significant and traps a subsurface water mass (the Cold Pool) on the shelf in the spring

and summer (Houghton et al., 1982; Saba et al., 2019b; Wright-Fairbanks et al., 2020). The Cold Pool exhibits little ventilation to the atmosphere during seasonal stratification, thereby trapping respired CO₂ in the subsurface water mass, and contributing to a decline in pH and Ω_{arag} from spring through summer. The northward-flowing, high- Ω_{arag} Gulf Stream and southward-flowing, low- Ω_{arag} Labrador Current interact offshore of the MAB, influencing shelf water properties including carbonate chemistry (Grotsky et al., 2017; Saba et al., 2016; Salisbury & Jonsson, 2018; Wanninkhof et al., 2015). Nearshore, the Connecticut, Hudson, and Delaware Rivers deliver low-buffering capacity fresh water to the coastal zone, increasing acidification there. Sustained south-southwest winds in the summer can cause upwelling of cold, low- Ω_{arag} bottom waters along the MAB coast, with potential implications for carbonate-bearing organisms (Poach et al., 2019).

1.3 Biological Implications of Ocean Acidification

Ocean acidification has been shown have neutral to negative effects on metabolic processes, growth, development, energy allocation, and acid-base equilibrium in marine life of many kinds, including both calcifying and non-calcifying organisms (Reviewed in: Doney et al., 2009; Fabry et al., 2008; Kroeker et al., 2013; Saba et al., 2019a).

Organisms that build structures with calcium carbonate are especially susceptible to ocean acidification due to decreased Ω_{arag} resulting in reduced calcification rates or depression of metabolic processes. Ecosystem services such as water quality maintenance, shoreline protection, and economic stability depend on these species, which are considered the most vulnerable to acidification (Fay et al., 2017). In laboratory studies, larval and adult bivalves exposed to acidified waters exhibit decreased survival,

growth, shell thickness and integrity, lipid accumulation, calcification, feeding initiation, settlement success, and hinge development (Gazeau et al., 2013; Kroeker et al., 2013; Parker et al., 2013; Ries et al., 2009; Saba et al., 2019a). Many of these species may already live close to their pH or Ω_{arag} tolerance threshold, and will suffer the consequences of additional acidification due to atmospheric or coastal inputs (Baumann et al., 2014).

The Atlantic sea scallop (*Placopecten magellanicus*) is one of the most economically important shellfish in the United States, with a fishery valued at \$486 million in 2016 (NMFS, 2017). The MAB serves as the primary harvest area for sea scallops in the U.S. During development, larval scallops can be transported hundreds of kilometers alongshore (Munroe et al., 2018), encountering variable environmental conditions depending on release date and location. Bivalve larvae are sensitive to their changing environment, as they go through many transitional periods including the first deposition of calcium carbonate which lacks crystalline structure and therefore is particularly susceptible to dissolution (Fabry et al., 2008; Parker et al., 2013). Though OA has been shown to have detrimental effects on larval bivalve success, there have been no published laboratory studies investigating the specific impacts of OA on *P. magellanicus* larvae.

1.4 Monitoring Coastal Carbonate Chemistry

Because coastal carbonate chemistry varies on time scales from minutes to seasons to years, changing at rates that could affect biological processes, it is necessary to monitor changes in the system in high resolution (Gledhill et al., 2015; Huret et al., 2018;

Waldbusser & Salisbury, 2014). Additionally, monitoring the system now provides a baseline that can be used to identify long-term changes in carbonate chemistry as global climate change persists (Gledhill et al., 2015; Goldsmith et al., 2019; Xu et al., 2020). Past acidification monitoring efforts have been limited in temporal and spatial resolution and are scarce in economically important coastal regions like the MAB (Goldsmith et al., 2019). Large shipboard field campaigns across the MAB occur every four to six years during the summer season, covering a large spatial extent but lacking temporal resolution (Cai et al., 2020; Wang et al., 2013; Wanninkhof et al., 2015). More recent shipboard sampling, through the incorporation of carbonate system monitoring during NOAA EcoMon cruises, has provided finer seasonal resolution of carbonate chemistry metrics across the U.S. Northeast Shelf. There are few fixed stations in the MAB, which provide high temporal resolution measurements but lack spatial resolution in terms of location and depth. Satellite imaging can be used to quantify metrics such as biological productivity, $p\text{CO}_2$, and salinity-derived carbonate parameters, but lack depth resolution (Salisbury et al., 2015; Wang et al., 2017). Additionally, many existing MAB monitoring platforms only measure one of the four carbonate system parameters (pH, DIC, TA, and $p\text{CO}_2$), two of which are necessary to fully characterize the carbonate system (Pimenta & Grear, 2018).

In order to fill the gaps left by traditional carbonate system monitoring in the MAB, the work in this dissertation utilizes a newly developed autonomous glider-based ocean pH observing platform. Capable of completing 30-45 day, 600-900 km missions in highly variable currents from surface to 1000 m depth, autonomous underwater gliders are a robust technology that collect spatially and temporally high resolution data

(Rudnick, 2016; Schofield et al., 2007). A deep ion sensitive field-effect transistor (ISFET) pH sensor was recently integrated into a Teledyne-Webb Slocum G2 glider (Saba et al., 2019b). This glider is equipped to measure pH, conductivity (salinity), temperature, dissolved oxygen, chlorophyll fluorescence, and spectral backscatter continuously over the course of deployment. Concurrent measurements from all sensors provide enough information to fully derive the carbonate system and monitor physical, chemical, and biological drivers of change in the system.

1.5 Dissertation Questions

The overall goal of this dissertation is to depict seasonal cycles of MAB carbonate chemistry in high resolution, quantify the drivers of the coastal carbonate system on a seasonal time scale, and provide perspective on how seasonal carbonate chemistry changes may interact with species life histories in the region.

In Chapter 2, the first seasonal deployments of the pH glider are described. For the first time, QA/QC protocols and data analysis techniques for this new sensor are explained in detail, and are then applied to illustrate changes in carbonate chemistry throughout the water column and across the MAB shelf over four seasonal deployments. In Chapter 3, the drivers of the MAB carbonate system are quantified using a first-order Taylor Series decomposition of seasonal glider deployment data. This analysis illustrates the importance of water mass mixing and biogeochemical activity in driving and mitigating acidification in the MAB. Chapter 4 investigates links between carbonate system seasonality and Atlantic sea scallop larval dispersal and success in the MAB. A literature review is conducted to develop a general larval bivalve growth-OA relationship.

That relationship is then integrated into a particle dispersal model along with seasonal carbonate system metrics to simulate the impact of changing Ω_{arag} on growth, dispersal, success, and population connectivity of an under-studied, highly valuable species.

1.6 References

- Baumann, H., Wallace, R. B., Tagliaferri, T., & Gobler, C. J. (2014). Large Natural pH, CO₂ and O₂ Fluctuations in a Temperate Tidal Salt Marsh on Diel, Seasonal, and Interannual Time Scales. *Estuaries and Coasts*, 38(1), 220-231. doi:10.1007/s12237-014-9800-y
- Bopp, L., Resplandy, L., Orr, J. C., Doney, S. C., Dunne, J. P., Gehlen, M., Halloran, P., Heinze, C., Ilyina, T., Séférian, R., Tjiputra, J., & Vichi, M. (2013). Multiple stressors of ocean ecosystems in the 21st century: projections with CMIP5 models. *Biogeosciences*, 10(10), 6225-6245. doi:10.5194/bg-10-6225-2013
- Cai, W.-J., Hu, X., Huang, W.-J., Murrell, M. C., Lehrter, J. C., Lohrenz, S. E., Chou, W.-C., Zhai, W., Hollibaugh, J. T., Wang, Y., Zhao, P., Guo, X., Gundersen, K., Dai, M., & Gong, G.-C. (2011). Acidification of subsurface coastal waters enhanced by eutrophication. *Nature Geoscience*, 4(11), 766-770. doi:10.1038/ngeo1297
- Cai, W.-J., Xu, Y. Y., Feely, R. A., Wanninkhof, R., Jonsson, B., Alin, S. R., Barbero, L., Cross, J. N., Azetsu-Scott, K., Fassbender, A. J., Carter, B. R., Jiang, L. Q., Pepin, P., Chen, B., Hussain, N., Reimer, J. J., Xue, L., Salisbury, J. E., Hernandez-Ayon, J. M., Langdon, C., Li, Q., Sutton, A. J., Chen, C. A., & Gledhill, D. K. (2020). Controls on surface water carbonate chemistry along North American ocean margins. *Nat Commun*, 11(1), 2691. doi:10.1038/s41467-020-16530-z
- Doney, S. C., Fabry, V. J., Feely, R. A., & Kleypas, J. A. (2009). Ocean acidification: the other CO₂ problem. *Ann Rev Mar Sci*, 1, 169-192. doi:10.1146/annurev.marine.010908.163834
- Fabry, V. J., Seibel, B. A., Feely, R. A., & Orr, J. C. (2008). Impacts of ocean acidification on marine fauna and ecosystem processes. *ICES Journal of Marine Science*, 65, 414-432.
- Fay, G., Link, J. S., & Hare, J. A. (2017). Assessing the effects of ocean acidification in the Northeast US using an end-to-end marine ecosystem model. *Ecological Modelling*, 347, 1-10. doi:10.1016/j.ecolmodel.2016.12.016
- Friedrich, T., Timmermann, A., Abe-Ouchi, A., Bates, N. R., Chikamoto, M. O., Church, M. J., Dore, J. E., Gledhill, D. K., González-Dávila, M., Heinemann, M., Ilyina, T., Jungclaus, J. H., McLeod, E., Mouchet, A., & Santana-Casiano, J. M. (2012). Detecting regional anthropogenic trends in ocean acidification against natural variability. *Nature Climate Change*, 2(3), 167-171. doi:10.1038/nclimate1372

- Gattuso, J., -P., Magnan, A., Bille, R., Cheung, W. W. L., Howes, E. L., Joos, F., AlLemand, D., Bopp, L., Cooley, S. R., Eakin, C. M., Hoegh-Guldberg, O., Kelly, R. P., Portner, H. O., Rogers, A. D., Baxter, J. M., Laffoley, D., Osborn, D., Rankovic, A., Rochette, J., Summaila, U. R., Treyer, S., & Turley, C. (2015). Contrasting futures for ocean and society from different anthropogenic CO₂ emissions scenarios. *Science Magazine*, 349(6243). doi:10.1126/10.1126/science.aac4722
- Gazeau, F., Parker, L. M., Comeau, S., Gattuso, J.-P., O'Connor, W. A., Martin, S., Pörtner, H.-O., & Ross, P. M. (2013). Impacts of ocean acidification on marine shelled molluscs. *Marine Biology*, 160(8), 2207-2245. doi:10.1007/s00227-013-2219-3
- Gledhill, D., White, M., Salisbury, J., Thomas, H., Misna, I., Liebman, M., Mook, B., Grear, J., Candelmo, A., Chambers, R. C., Gobler, C., Hunt, C., King, A., Price, N., Signorini, S., Stancioff, E., Stymiest, C., Wahle, R., Waller, J., Rebuck, N., Wang, Z., Capson, T., Morrison, J. R., Cooley, S., & Doney, S. (2015). Ocean and Coastal Acidification off New England and Nova Scotia. *Oceanography*, 25(2), 182-197. doi:10.5670/oceanog.2015.41
- Goldsmith, K. A., Lau, S., Poach, M. E., Sakowicz, G. P., Trice, T. M., Ono, C. R., Nye, J., Shadwick, E. H., StLaurent, K. A., & Saba, G. K. (2019). Scientific considerations for acidification monitoring in the U.S. Mid-Atlantic Region. *Estuarine, Coastal and Shelf Science*, 225. doi:10.1016/j.ecss.2019.04.023
- Grodsky, S. A., Reul, N., Chapron, B., Carton, J. A., & Bryan, F. O. (2017). Interannual surface salinity on Northwest Atlantic shelf. *Journal of Geophysical Research: Oceans*, 122(5), 3638-3659. doi:10.1002/2016jc012580
- Houghton, R. W., Shlitz, R., Beardsley, R. C., Butman, B., & Chamberlin, J. L. (1982). The Middle Atlantic Bight Cold Pool: Evolution of the Temperature Structure During Summer 1979. *American Meteorological Society*, 12, 1019-1029.
- Huret, M., Bourriau, P., Doray, M., Gohin, F., & Petitgas, P. (2018). Survey timing vs. ecosystem scheduling: Degree-days to underpin observed interannual variability in marine ecosystems. *Progress in Oceanography*, 166, 30-40. doi:10.1016/j.pocean.2017.07.007
- IPCC. (2019). Summary for Policymakers. *IPCC Special Report on the Ocean and Cryosphere in a Changing Climate*.
- IPCC. (2021). Climate Change 2021: The Physical Science Basis - Summary for Policymakers. *Sixth Assessment Report of the Intergovernmental Panel on Climate Change*.
- Kroeker, K. J., Kordas, R. L., Crim, R., Hendriks, I. E., Ramajo, L., Singh, G. S., Duarte, C. M., & Gattuso, J. P. (2013). Impacts of ocean acidification on marine organisms: quantifying sensitivities and interaction with warming. *Glob Chang Biol*, 19(6), 1884-1896. doi:10.1111/gcb.12179

- Kwiatkowski, L., & Orr, J. C. (2018). Diverging seasonal extremes for ocean acidification during the twenty-first century. *Nature Climate Change*, 8(2), 141-145. doi:10.1038/s41558-017-0054-0
- Munroe, D. M. H., D., Caracappa, J. C., Klinck, J. M., Powell, E. N., Hofmann, E. E., Shank, B. V., & Hart, D. R. (2018). Modeling larval dispersal and connectivity for Atlantic sea scallop (*Placopecten magellanicus*) in the Middle Atlantic Bight. *Fisheries Research*, 208, 7-15. doi:10.1016/j.fishres.2018.06.020
- Negrete-García, G., Lovenduski, N. S., Hauri, C., Krumhardt, K. M., & Lauvset, S. K. (2019). Sudden emergence of a shallow aragonite saturation horizon in the Southern Ocean. *Nature Climate Change*, 9(4), 313-317. doi:10.1038/s41558-019-0418-8
- NMFS. (2017). Fisheries of the United States, 2016. *U.S. Department of Commerce NOAA Current Fishery Statistics No. 2016*. Retrieved from <https://www.st.nmfs.noaa.gov/commercial-fisheries/fus/fus16/index>
- Parker, L. M., Ross, P. M., O'Connor, W. A., Portner, H. O., Scanes, E., & Wright, J. M. (2013). Predicting the response of molluscs to the impact of ocean acidification. *Biology (Basel)*, 2(2), 651-692. doi:10.3390/biology2020651
- Pimenta, A. R., & Grear, J. S. (2018). Guidelines for Measuring Changes in Seawater pH and Associated Carbonate Chemistry in Coastal Environments of the Eastern United States. *United States Environmental Protection Agency*.
- Poach, M., Munroe, D., Vasslides, J., Abrahamsen, I., & Coffey, N. (2019). Monitoring coastal acidification along the U.S. East coast: concerns for shellfish production. *Bulletin of Japan Fisheries Research and Education Agency*(49), 53-64.
- Ries, J. B., Cohen, A. L., & McCorkle, D. C. (2009). Marine calcifiers exhibit mixed responses to CO₂-induced ocean acidification. *Geology*, 37(12), 1131-1134. doi:10.1130/G30210A.1;1figure;1table;DataRepositoryitem2009279
- Rudnick, D. L. (2016). Ocean Research Enabled by Underwater Gliders. *Ann Rev Mar Sci*, 8, 519-541. doi:10.1146/annurev-marine-122414-033913
- Saba, G. K., Goldsmith, K. A., Cooley, S. R., Grosse, D., Meseck, S. L., Miller, A. W., Phelan, B., Poach, M., Rheault, R., St.Laurent, K., Testa, J. M., Weis, J. S., & Zimmerman, R. (2019a). Recommended priorities for research on ecological impacts of ocean and coastal acidification in the U.S. Mid-Atlantic. *Estuarine, Coastal and Shelf Science*, 225. doi:10.1016/j.ecss.2019.04.022
- Saba, G. K., Wright-Fairbanks, E., Chen, B., Cai, W.-J., Barnard, A. H., Jones, C. P., Branham, C. W., Wang, K., & Miles, T. (2019b). The Development and Validation of a Profiling Glider Deep ISFET-Based pH Sensor for High Resolution Observations of Coastal and Ocean Acidification. *Frontiers in Marine Science*, 6. doi:10.3389/fmars.2019.00664
- Saba, V. S., Griffies, S. M., Anderson, W. G., Winton, M., Alexander, M. A., Delworth, T. L., Hare, J. A., Harrison, M. J., Rosati, A., Vecchi, G. A., & Zhang, R. (2016). Enhanced warming of the Northwest Atlantic Ocean under climate change.

Journal of Geophysical Research: Oceans, 121(1), 118-132.
doi:10.1002/2015jc011346

- Salisbury, J., & Jonsson, B. F. (2018). Rapid warming and salinity changes in the Gulf of Maine alter surface ocean carbonate parameters and hide ocean acidification. *Biogeochemistry*, 141(3), 401-418. doi:10.1007/s10533-018-0505-3
- Salisbury, J., Vandemark, D., Jönsson, B., Balch, W., Chakraborty, S., Lohrenz, S., Chapron, B., Hales, B., Mannino, A., Mathis, J., Reul, N., Signorini, S., Wanninkhof, R., & Yates, K. (2015). How Can Present and Future Satellite Missions Support Scientific Studies that Address Ocean Acidification? *Oceanography*, 25(2), 108-121. doi:10.5670/oceanog.2015.35
- Schofield, O., Kohut, J., Aragon, D., Creed, L., Graver, J., Haldeman, C., Kerfoot, J., Roarty, H., Jones, C., Webb, D., & Glenn, S. (2007). Slocum Gliders: Robust and ready. *Journal of Field Robotics*, 24(6), 473-485. doi:10.1002/rob.20200
- Stumm, W., & Morgan, J. J. (1996). *Aquatic Chemistry: Chemical Equilibria and Rates in Natural Waters*.
- Sutton, A. J., Sabine, C. L., Feely, R. A., Cai, W.-J., Cronin, M. F., McPhaden, M. J., Morell, J. M., Newton, J. A., Noh, J.-H., Ólafsdóttir, S. R., Salisbury, J. E., Send, U., Vandemark, D. C., & Weller, R. A. (2016). Using present-day observations to detect when anthropogenic change forces surface ocean carbonate chemistry outside preindustrial bounds. *Biogeosciences*, 13(17), 5065-5083. doi:10.5194/bg-13-5065-2016
- Tans, P., & Keeling, R. (2021). Trends in Atmospheric Carbon Dioxide. Retrieved from <https://gml.noaa.gov/ccgg/trends/data.html>
- Waldbusser, G. G., & Salisbury, J. E. (2014). Ocean acidification in the coastal zone from an organism's perspective: multiple system parameters, frequency domains, and habitats. *Ann Rev Mar Sci*, 6, 221-247. doi:10.1146/annurev-marine-121211-172238
- Wang, H., Hu, X., Cai, W.-J., & Sterba-Boatwright, B. (2017). Decadal fCO₂ trends in global ocean margins and adjacent boundary current-influenced areas. *Geophysical Research Letters*, 44(17), 8962-8970. doi:10.1002/2017gl074724
- Wang, Z., Wanninkhof, R., Cai, W.-J., Byrne, R. H., Hu, X., Peng, T.-H., & Huang, W.-J. (2013). The marine inorganic carbon system along the Gulf of Mexico and Atlantic coasts of the United States: Insights from a transregional coastal carbon study. *Limnology and Oceanography*, 58(1), 325-342. doi:10.4319/lo.2013.58.1.0325
- Wanninkhof, R., Barbero, L., Byrne, R., Cai, W.-J., Huang, W.-J., Zhang, J.-Z., Baringer, M., & Langdon, C. (2015). Ocean acidification along the Gulf Coast and East Coast of the USA. *Continental Shelf Research*, 98, 54-71. doi:10.1016/j.csr.2015.02.008
- Wootton, J. T., Pfister, C. A., & Forester, J. D. (2008). Dynamic patterns and ecological impacts of declining ocean pH in a high-resolution multi-year dataset. *Proc Natl Acad Sci U S A*, 105(48), 18848-18853. doi:10.1073/pnas.0810079105

- Wright-Fairbanks, E. K., Miles, T. N., Cai, W. J., Chen, B., & Saba, G. K. (2020). Autonomous Observation of Seasonal Carbonate Chemistry Dynamics in the Mid-Atlantic Bight. *Journal of Geophysical Research: Oceans*. doi:10.1029/2020jc016505
- Xu, Y. Y., Cai, W.-J., Wanninkhof, R., Salisbury, J., Reimer, J., & Chen, B. (2020). Long-Term Changes of Carbonate Chemistry Variables Along the North American East Coast. *Journal of Geophysical Research: Oceans*, 125(7). doi:10.1029/2019jc015982
- Zeebe, R. E. (2012). History of Seawater Carbonate Chemistry, Atmospheric CO₂, and Ocean Acidification. *Annual Review of Earth and Planetary Sciences*, 40(1), 141-165. doi:10.1146/annurev-earth-042711-105521

CHAPTER 2: Autonomous Observation of Seasonal Carbonate Chemistry Dynamics in
the Mid-Atlantic Bight*

* This chapter has been published as: **Wright-Fairbanks, E.K.**, Miles, T.N., Cai, W.-J., Chen, B., and Saba, G.K. 2020. Autonomous observation of seasonal carbonate chemistry dynamics in the Mid-Atlantic Bight. *Journal of Geophysical Research: Oceans*, 125, e2020JC016505.

2.1 Abstract

Ocean acidification alters the oceanic carbonate system, increasing potential for ecological, economic, and cultural losses. Historically, productive coastal oceans lack vertically-resolved high-resolution carbonate system measurements on timescales relevant to organism ecology and life history. The recent development of a deep ISFET-based pH sensor system integrated into a Slocum glider has provided a platform for achieving high-resolution carbonate system profiles. From May 2018 to November 2019, seasonal deployments of the pH glider were conducted in the central Mid-Atlantic Bight. Simultaneous measurements from the glider's pH and salinity sensors enabled the derivation of total alkalinity and calculation of other carbonate system parameters including aragonite saturation state. Carbonate system parameters were then mapped against other variables, such as temperature, dissolved oxygen, and chlorophyll, over space and time. The seasonal dynamics of carbonate chemistry presented here provide a baseline to begin identifying drivers of acidification in this vital economic zone.

2.2 Introduction

Ocean acidification (OA) results from the uptake of atmospheric carbon dioxide (CO_2), which alters oceanic carbonate chemistry (Doney et al., 2009; Gledhill et al., 2015; Orr et al., 2005). The ocean has absorbed approximately one-third of the CO_2 emitted by human activities since the Industrial Revolution (Gruber et al., 2019). During this time, atmospheric CO_2 has risen from approximately 280 parts per million (ppm) to 410 ppm (Dlugokencky & Tans, 2020). When CO_2 is absorbed by the ocean, it reacts with seawater and results in complex chemical reactions that reduce seawater pH and

calcium carbonate saturation state, Ω . Saturation states governing the formation and dissolution of the two mineral forms of calcium carbonate, calcite and aragonite, are expressed as Ω_{cal} and Ω_{arag} respectively. A saturation state above 1 indicates carbonate supersaturation and thermodynamic favorability of carbonate calcification, while a saturation state below 1 indicates carbonate undersaturation and thermodynamic favorability of carbonate dissolution. However, carbonate saturation states approaching 1, and as high as 1.92, have been shown to cause negative impacts on calcifying organisms, despite carbonate supersaturation (Gazeau et al., 2007; Gledhill et al., 2015; Gobler & Talmage, 2013, 2014; Hettinger et al., 2012; Talmage & Gobler, 2009, 2010; Waldbusser et al., 2014), likely due to impacts on metabolism and increases in the energetic cost of mitigating stress (Melzner et al., 2019; Miller et al., 2009; Pan et al., 2015).

The rate of oceanic uptake of atmospheric CO_2 has increased in the last two decades due to increasing levels of atmospheric CO_2 (IPCC, 2019). The global ocean is acidifying at unprecedented rates, with open ocean surface water pH decreasing by 0.017-0.027 pH units per decade since the late 1980s (Gledhill et al., 2015; IPCC, 2019; Sutton et al., 2016; Zeebe, 2012). Global surface ocean pH is predicted to decline by up to 0.29 pH units by 2081-2100 relative to 2006-2015 under RCP8.5 (IPCC, 2019). In addition to global changes in pH, the rate of change in global Ω_{arag} since the Industrial Revolution has been 5 times greater than natural variability over the last millennium (Friedrich et al., 2012; Gattuso et al., 2015). Under RCP8.5, there will be no ocean water with Ω_{arag} greater than 3.0, and the total volume of water with Ω_{arag} less than 1.0 will increase from 76% (1990 value) to 91%, by 2100 (Gattuso et al., 2015).

In coastal oceans, carbonate chemistry is influenced by a range of drivers including productivity-respiration cycles, nutrient loading, freshwater inputs, and other coastal processes (Gledhill et al., 2015; Saba et al., 2019a). Because of its multiple contributors, acidification in coastal zones can be highly variable and episodic both spatially and temporally (Baumann & Smith, 2017). The hydrodynamic and biological processes influencing coastal environments can vary on the order of minutes to days (Runcie et al., 2018; Y.-Y. Xu et al., 2017). These extreme short-term events likely have a more immediate impact on carbonate-dependent organisms compared to gradual change due to increases in atmospheric CO₂ (Baumann & Smith, 2017; Cai et al., 2011; Waldbusser & Salisbury, 2014). However, a global increase in atmospheric CO₂ will increase the frequency of extreme acidification events, pushing organisms past critical survival thresholds more regularly (Gledhill et al., 2015). Furthermore, acidification can co-occur with other metabolic stressors, including low dissolved oxygen and warm temperatures (Cai et al., 2011; Cai et al., 2017; Saba et al., 2019a).

The Mid-Atlantic Bight (MAB), located within the U.S. Northeast Shelf (NES), is an ecologically and economically vital coastal zone. This region is home to some of the most profitable commercial and recreational fisheries in the United States (Colvocoresses & Musick, 1984; Hare et al., 2016; NEFSC, 2020), ecosystems that protect coastal communities from inundation, storms, and erosion (NRC, 2010), and offshore wind energy development sites (Musial et al., 2013; NEFSC, 2020). The MAB is prone to acidification due to freshwater sources (primarily riverine), eutrophication and photosynthesis-respiration cycles, coastal upwelling, and other influences. Coastal inputs and biological activity alter carbonate chemistry more quickly than gas equilibrium, and

therefore play a major role in determining the carbonate system, specifically the partial pressure of CO₂ ($p\text{CO}_2$) and pH (Cai et al., 2020). Mid-Atlantic coastal waters are acutely affected by seasonal changes in temperature and inputs from shore. Because MAB oceanography is highly variable between seasons, it is necessary to monitor changes in the carbonate system seasonally (Huret et al., 2018). While there may be no net change in pH or Ω_{arag} over a full annual cycle, seasonal changes operate under a time scale that could affect biological processes in the nearshore (Gledhill et al., 2015; Waldbusser & Salisbury, 2014). Monitoring seasonal changes also provides a basis for identifying long-term changes in carbonate chemistry due to shifts in salinity, temperature, atmospheric CO₂, and coastal inputs (Gledhill et al., 2015; Goldsmith et al., 2019; Y. Y. Xu et al., 2020).

Acidification monitoring efforts to date are limited in temporal and spatial resolution, and lacking in economically important coastal regions including the MAB (Goldsmith et al., 2019). Traditionally, monitoring in the MAB has been conducted through large field campaigns every few years. These ship-based surveys depict large spatial variability and decadal changes of surface water carbonate chemistry in the U.S. NES but lack seasonal resolution across the system (Cai et al., 2020; Z. A. Wang et al., 2013; Wanninkhof et al., 2015). In addition to cruise campaigns, there are few fixed (moored) stations monitoring carbonate system parameters on the MAB shelf. These fixed stations are capable of characterizing temporal changes in carbonate chemistry, but lack spatial resolution in terms of location and depth. Additionally, many existing MAB monitoring stations measure only one of the four carbonate system parameters (pH, dissolved inorganic carbon (DIC), total alkalinity (TA), and $p\text{CO}_2$), two of which are

necessary to fully characterize the carbonate system (Pimenta & Grear, 2018). Along with cruise campaigns and surface-fixed stations, satellite imagery can be used to estimate a suite of surface water carbon system factors, including biological productivity, $p\text{CO}_2$, salinity-derived carbonate parameters, and large-scale coastal inputs (Salisbury et al., 2015; H. Wang et al., 2017).

The ability to monitor carbonate chemistry in high resolution throughout the water column is critical in order to detect low pH in water masses and to derive relationships between physical, biological, and carbonate system variability. Autonomous underwater gliders, capable of collecting data in highly variable currents in water depths up to 1000 m, are a reliable platform that fulfil this role (Rudnick, 2016; Schofield et al., 2007). A deep-ISFET pH sensor was recently developed and integrated into a Teledyne-Webb Slocum G2 glider (Saba et al., 2019b). In addition to measuring pH, this glider has a suite of sensors that provide profiles of conductivity, temperature, dissolved oxygen, chlorophyll fluorescence, and spectral backscatter. This allows users to compare seawater pH to other ocean properties and conduct salinity-based estimates of TA in order to constrain the carbonate system. Here, we present data from four seasonal deployments of the pH glider in the central MAB, which have produced the first spatially and temporally high-resolution characterization of seasonal carbonate system dynamics in this region.

2.3 Materials and methods

2.3.1 Seasonal Deployments

The pH glider was deployed on four seasonal missions in the MAB (May 2-22, 2018 [spring], February 1-19, 2019 [winter], July 17-August 12, 2019 [summer], and

October 15-November 6, 2019 [fall]; Figure 2.1). Before deployment, the glider pH sensor was fully conditioned following the guidelines described in Saba et al. (2019b). After deployment from the small vessel R/V Rutgers, the glider was sent on a shallow mission during discrete water sample collection (see below). Once discrete sampling was completed, the glider was sent to its first offshore waypoint. The winter, summer and fall missions followed a cross-shelf transect starting ~15 km off Sandy Hook, New Jersey, traveling 200 km eastward to the shelf break. The glider then completed various transects and triangles back to shore, covering a total of 469.6 km in winter, 503.5 km in summer, and 471.4 km in fall. The spring mission followed an established glider observation line from Atlantic City, New Jersey, 140 km eastward to the shelf break and back, for a total of 317.0 km.

Timing for sensor repairs and re-calibrations prevented four sequential seasonal deployments on the Sandy Hook transect line. A mission planned for spring of 2019 on the Sandy Hook line was postponed due to technological difficulties and rough seas, and the postponed mission was terminated within hours of deployment due to a glider pump failure. The spring deployment was rescheduled for April 2020, but was canceled due to research restrictions during the COVID-19 pandemic.

Upon each deployment and recovery of the pH glider, discrete water samples were collected following best practice guidelines for autonomous pH measurements with DuraFET sensors (Bresnahan et al., 2014; Johnson et al., 2016; Martz et al., 2015; Saba et al., 2019b). Discrete samples were collected near the glider at various depths either by a hand-lowered 5 L Niskin (spring, winter; within 5 m of glider), or using an SBE55 6-bottle rosette with an SBE19 CTD attached (summer, fall; within 100 m of glider).

Samples were collected into 250 mL borosilicate glass bottles and preserved with 50 μ L of saturated mercuric chloride, then transported to the Cai laboratory (University of Delaware) for analysis.

2.3.2 *Sensor QA/QC*

2.3.2.1 *Glider CTD, oxygen, and chlorophyll sensors*

The glider was equipped with a pumped CTD modified for integration with an ISFET pH sensor, an Aanderaa oxygen optode, and a Sea-Bird Scientific BB2FL ECO puck to measure chlorophyll fluorescence, CDOM, and optical backscatter. The CTD and dissolved oxygen (DO) data were run through QA/QC guidelines outlined in an EPA Quality Assurance Project Plan for glider deployments along the coast of New Jersey (Kohut et al., 2014). Both sensors are factory calibrated annually, and data were verified pre- and post-deployment (Saba et al., 2019b). The BB2FL ECO puck is factory calibrated by WET labs every 1-2 years. Between each seasonal deployment, the integrated CTD/pH sensor was cleaned and re-calibrated by the manufacturer (Sea-Bird Scientific).

2.3.2.2 *Glider pH sensor*

Each time the glider surfaced throughout a mission, a subset of collected data was sent to shore via an Iridium satellite phone located in the tail of the glider. This allowed for preliminary inspection of all science data and software metrics to assess glider functionality. Full data sets were collected post-recovery from memory cards stored in the glider. Data was processed using Slocum Power Tools (<https://github.com/kerfoot/spt/>) and analyzed using MATLAB data analysis software (version R2019a).

pH data was initially inspected for sensor time lags, which were identified as skewed upcast and downcast profiles in pH reference voltage data, and were often associated with areas of steep gradients in salinity or temperature. To correct for sensor lag, upcast and downcast pairs were run through potential time shifts from 0 seconds to 60 seconds at 1 second intervals. The optimal time shift minimized the difference between reference voltage at a certain depth in an upcast/downcast pair (Saba et al., 2019b).

After time shifts were applied, pH data were run through QA/QC measures based on the Integrated Ocean Observing System (IOOS) Manual for Real-Time Quality Control of pH Data Observations (IOOS, 2019). pH reference voltage data was flagged and removed in instances where more than 1 hour has passed between observations (<< 1% of observations), or in instances without a valid time stamp (~20% of observations). Next, observations of other scientific variables without both a corresponding pH reference voltage and pressure value were removed (~40% of observations). Observations outside of the latitude and longitude bounds of the MAB were flagged and removed (<< 1% of observations). pH values were validated in a gross range test, flagging and removing values outside the calibration bounds of the glider pH sensor ($\text{pH} < 6.5$ and $\text{pH} > 9$; << 1% of observations). As more deployments of the pH glider provide a mean climatology for the MAB, the gross range test can be restricted to a user-specified local or seasonal pH range. Next, a spike test identified and removed single value spikes in pH reference voltage observations (<< 1% of observations). Lastly, data were inspected visually for unrealistic rates of change, flat-lining, and attenuated signals, which would indicate sensor failure. Tests for multi-variate failure and comparisons to nearby pH

sensors were not applicable to these deployments, but should be considered in future pH glider deployments.

2.3.2.3 Discrete samples

Discrete sample pH was measured spectrophotometrically at 25 °C using purified *meta*-Cresol Purple dye (Clayton & Byrne, 1993; Liu et al., 2011). pH accuracy was determined against Tris buffers (DelValls & Dickson, 1998; Millero, 1986). Additionally, discrete TA and DIC measurements were used to calculate pH and check the internal accuracy of spectrophotometric measurements. TA titrations were run via open cell Gran titration on an Apollo Scitech TA titrator AS_ALK2 (Cai et al., 2010; B. Chen et al., 2015; Huang et al., 2012). DIC was quantified using a non-dispersive infrared method on an Apollo Scitech DIC Analyzer AS-C3 (B. Chen et al., 2015; Huang et al., 2012). TA and DIC accuracies were determined using Certified Reference Materials (CRMs) from Andrew Dickson's group at the Scripps Institution of Oceanography.

Discrete pH measurements were converted to *in situ* pH values using *in situ*, depth-specific temperature and salinity measured by SBE19 CTD. Discrete pH was then compared to glider ISFET measurements at the same, or closest, depth from the glider's first profile at deployment and its last profile before recovery. Groundtruthing offsets were determined as glider pH – discrete pH at each depth. Glider agreement was calculated as the average absolute offset between all depths at deployment or recovery. Uncertainty in glider agreement was calculated as one standard deviation between glider pH measurements in the surface layer during the discrete sampling period. Because there was little variation in temperature and salinity in the surface layer over a short period of time, variation in glider pH introduced by the environment was small. Glider pH science

bays were sent to SeaBird Scientific for post-deployment analysis, cleaning, and recalibration between deployments.

2.3.3 Data analysis

Salinity was calculated based on glider-measured conductivity, temperature, and pressure. TA and salinity exhibit a conservative relationship in U.S. east coast waters (Cai et al., 2010; Z. A. Wang et al., 2013), thus TA is estimated using glider-derived salinity (Saba et al., 2019b). In each season, a linear regression to estimate TA from salinity was derived from a combination of discrete samples taken at glider deployment/recovery, and discrete samples from transects across the U.S. NES during the East Coast Ocean Acidification (ECO-A)-1 cruise in summer 2015 (supplementary text S1). Discrete samples from glider deployments and the ECO-A-1 cruise were both analyzed by the Cai group using the same method. Sampling during glider deployments and recoveries took place only in relatively low salinity nearshore waters (Figure S2.1). Conversely, the ECO-A-1 cruise sampled across the entire shelf to the shelf break, but missed lower salinity areas. Using both seasonal discrete samples and shelf-wide ECO-A samples ensured that seasonal TA-salinity regressions accounted for the entire scope of salinities the glider encountered in the MAB, while minimizing uncertainty due to seasonal differences in TA-salinity relationships. Full-deployment salinity-estimated TA was also compared to TA derived using the CANYON-B algorithm, which is trained on GLODAPv2 and GO-SHIP bottle samples, and calculates carbonate system parameters using measured latitude, longitude, time, depth, temperature, salinity, and oxygen (Bittig et al., 2018).

Glider pH was calculated on the total hydrogen concentration scale using glider-measured reference voltage, salinity, pressure, temperature, and sensor-specific calibration coefficients (Johnson et al., 2017; Saba et al., 2019b). The remaining carbonate system parameters were calculated using CO2SYS for MATLAB (v3.0) with glider temperature, salinity, pressure, pH, and salinity-derived TA as inputs (Lewis & Wallace, 1998; Sharp et al., 2020; van Heuven et al., 2011). Other CO2SYS inputs included total pH scale ($\text{mol kg}^{-1}\text{-SW}$), K_1 and K_2 constants of Mehrbach et al. (1973) with refits by Dickson and Millero (1987), KSO_4 dissociation constant of Dickson (1990), KHF dissociation constant of Uppstrom (1974), and borate-to-salinity ratio of Perez and Fraga (1987). Carbonate system parameters reported here are pH, Ω_{arag} , and ratio of TA to DIC (TA:DIC). TA:DIC provides context for the CO_2 buffering capacity of seawater. Oceanic buffering capacity for CO_2 reaches a minimum at TA:DIC = 1, meaning water with TA:DIC closest to 1 is most susceptible to acidification (Cai et al., 2020; Egleston et al., 2010; Z. A. Wang et al., 2013).

Slocum gliders are propelled by purposeful changes in buoyancy, allowing the glider to dive and climb in a sawtooth pattern from surface to bottom waters. The pH glider system used here was equipped with a 200-m pump, allowing it to operate in depths as shallow as 4 m and as deep as 200 m. Coastal gliders travel approximately 20 km day^{-1} horizontally, while profiling vertically at 10-15 cm s^{-1} . Sensors sample at 0.5 Hz, providing observations at 20-30 cm intervals vertically. All measured and derived variables were bin-averaged into 1 m depth by 1 km distance bins. At a sampling rate of 0.5 Hz and vertical profiling velocity of 10-15 cm s^{-1} , a 1 m depth average incorporated 3–5 measurements, minimizing the effect of small-scale physical and biological water

column dynamics. At a horizontal speed of 20 km day^{-1} , a 1-km distance bin averaged 1.2 hours of data, which could include between 3 and 30 individual profiles depending on water column depth.

Brunt-Vaisala Frequency squared (N^2) was calculated between adjacent 1 m layers in each depth- and distance-binned profile. The mixed-layer depth (MLD) for each binned profile was determined as the depth of maximum N^2 ($\max(N^2)$) (Carvalho et al., 2017). Each profile's mixed-layer was assigned a quality index (QI), which indicates the significance of the stratification index based on relative homogeneity in and below the mixed-layer (Carvalho et al., 2017; Lorbacher et al., 2006). Profiles with $QI < 0.5$ were considered well-mixed, and removed from MLD analysis.

For analysis, deployment data were split into spatial and depth-defined regions. Distinctions between surface and bottom waters were made using the mean MLD in each season, with surface waters defined as surface to MLD, and bottom waters from MLD to the bottom. During winter, there was no significant MLD ($QI < 0.5$). Therefore, winter surface and bottom parameters were represented by an average of the top 5 m and bottom 5 m of the water column, respectively. The nearshore region was defined as extending from shore to the 35 m isobath, where sea slope begins to increase in the central MAB, or 1–40 km offshore (Levin et al., 2018). Midshelf was defined from the 35–100 m isobaths, or 40–160 km offshore (40–120 km offshore in the spring). The shelf break was defined as beyond the continental shelf ($>160 \text{ km}$ offshore, or $>120 \text{ km}$ offshore in spring), where depth increases to $> 100 \text{ m}$.

Significances of regional and seasonal comparisons of measured and derived variables were calculated using a Kruskal-Wallis analysis with Dunn post-hoc, unless

otherwise noted. Significance is reported as a p-value, with $p < 0.05$ demonstrating a significant difference between the values being compared. All averages are presented as mean \pm 1 standard deviation, and a table of averages is included in the supplemental material (Table S2.1). Along with being depth-averaged into 1 meter bins, chlorophyll and oxygen concentrations were integrated to 35 meters depth to analyze mixed layer productivity. Integration to 35 m, as opposed to full-water column integration, ensured that the majority of mixed layer productivity in each season was captured, while minimizing skewed integrations that could arise due to seasonal differences in profile depths. 35 m-integrated chlorophyll and oxygen are presented along with 1-m depth-averaged chlorophyll and oxygen.

To visualize the spread of data in each season, box-and-whisker plots displaying medians, 25th and 75th percentiles, minimums, and maximums were created for glider-measured and derived variables. To summarize carbonate system interactions with the development and degradation of seasonal stratification and chlorophyll maxima, physical, biological, and carbonate system properties from the first cross-shelf transect of each deployment were plotted on common color axes. Finally, full-deployment carbonate parameters were plotted as a function of distance from shore and season in order to visualize spatial differences in carbonate system seasonality.

2.4 Results

2.4.1 Sensor Performance

A full record of groundtruthing offsets is available in Tables S2.2 and S2.3. Seasonal mean glider agreement ranged from 0.005 to 0.042 pH units and within-mixed-

layer variability ranged from 0.001 to 0.027 pH units. Given these observations, we believe glider pH measurements are accurate to better than 0.05 pH units, which agrees with the manufacturer accuracy specification for this sensor (± 0.05 pH units) and is slightly higher than other studies of autonomous pH sensor deployments (Takeshita et al., 2021; accuracy of 0.01). Short-term reproducibility is likely significantly better than 0.03 because the source of error is short-term, within-mixed layer repeatability. This conclusion is supported by the manufacturer precision specification for this sensor (± 0.001 pH units), which implies that spatial variability along a section can be resolved to ± 0.001 pH units. Therefore, pH is reported here to the third decimal place.

pH sensor time lag varied seasonally. No shift was necessary for the winter mission, while a 47 second and 30 second shift were applied to the spring mission, a 36 second shift was applied to the summer mission, and a 45 second shift was applied to the fall mission. Spring required two lag corrections because of a shift in the sensor lag between the first third and last two-thirds of deployment, likely due to a shift in water column structure (Saba et al., 2019b).

The magnitude of uncertainty in derived variables varied based on the accuracy of TA estimation and pH. Average absolute differences between discrete TA and estimated TA ranged from 5.5 (winter) to 27.4 $\mu\text{mol kg}^{-1}$ (summer). Average seasonal uncertainty in Ω_{arag} and TA:DIC due to TA offsets ranged from 0.005 to 0.024 and 0.0001 to 0.0003, respectively (Table S2.4). Propagated error in Ω_{arag} and TA:DIC were, at maximum, 0.006 and 0.0007. It is recommended that pH glider operators take discrete water samples during recovery (Saba, Wright-Fairbanks, et al., 2019); if not possible, operators should utilize the maximum offsets determined here.

A full analysis of TA offsets, as well as a list of seasonal TA-salinity regressions, can be found in the supplementary material (Text; Tables S2.4 and S2.5). Full-deployment salinity-derived TA was similar to CANYON-B algorithm estimates of TA, differing at most by a seasonal average of $2.0 \pm 4.3 \mu\text{mol kg}^{-1}$ ($\sim 0.1\%$).

2.4.2 Seasonal and spatial water column dynamics

The winter mission collected 4933 profiles of science data over 19 days, spring collected 6426 profiles over 20 days, summer collected 6948 profiles over 26 days, and fall collected 5333 profiles over 22 days. On average, about 270 profiles were generated per day. Although the four seasonal deployments were not sequential, they highlight stratification and mixing patterns typical of the MAB, revealing seasonal transitions in physical, biological, and chemical characteristics described in detail below.

2.4.2.1 Physical Dynamics

Seasonal changes in stratification occurred in the MAB (Figures 2.2 and 2.3). The winter water column was cold ($<13 \text{ }^\circ\text{C}$) and well-mixed, with no significant MLD ($\text{QI} < 0.5$) and the lowest observed $\text{max}(\text{N}^2)$ ($0.0010 \pm 0.0010 \text{ s}^{-1}$, $n=187$, $p<0.001$). Surface waters were warmer in the spring compared to winter ($p<0.001$), resulting in stronger stratification ($\text{max}(\text{N}^2)=0.0015 \pm 0.0005 \text{ s}^{-1}$, $n=129$, $p<0.001$) and MLD of $14.4 \pm 8.2 \text{ m}$ ($n=129$). Surface temperature peaked in the summer ($23.64 \pm 1.13 \text{ }^\circ\text{C}$, $n=188$, $p<0.001$) while bottom waters remained cold, resulting in continued shoaling of MLD to $10.4 \pm 3.7 \text{ m}$ ($n=188$) and the greatest $\text{max}(\text{N}^2)$ observed seasonally ($0.0082 \pm 0.0025 \text{ s}^{-1}$, $n=188$, $p<0.001$). Strong stratification in the spring and summer trapped a cold ($<12 \text{ }^\circ\text{C}$) water mass below the mixed layer, which was consistent with the well-known summer Cold Pool (Z. Chen et al., 2018; Houghton et al., 1982). Surface waters cooled in the fall,

causing a lower $\max(N^2)$ (0.0011 ± 0.0009 , $n=358$), and a deep MLD (44.7 ± 27.7 m, $n=180$).

Surface and bottom water salinity were significantly lower in the nearshore than at the shelf break in every season ($p<0.001$; Figures 2.3 and 2.4). With the exception of spring (full water column) and summer bottom water, surface and bottom temperature also increased from nearshore to the shelf break in each season ($p<0.004$; Figures 2.3 and 2.4). The lowest salinities were recorded in nearshore summer surface waters ($p<0.001$), averaging 30.06 ± 0.37 PSU ($n=28$). In the summer, midshelf surface waters were also significantly fresher than the other seasons ($p<0.001$), due to heavy rainfall during the mission. The highest salinities were recorded in fall shelf break surface and bottom waters ($p<0.001$), averaging 35.66 ± 0.26 PSU ($n=38$) and 35.37 ± 0.17 PSU ($n=38$).

2.4.2.2 *Biological characteristics*

Phytoplankton biomass varied seasonally as water column structure changed in the MAB (Figures 2.4 and 2.5). The deeply mixed fall water column and the productive spring water column had the highest 35 m-integrated chlorophyll concentrations of 43.39 ± 11.23 mg m⁻² ($n=180$) and 42.82 ± 19.79 mg m⁻² ($n=129$), respectively ($p<0.001$). Fall and spring integrated chlorophyll levels were not significantly different from one another. Winter and summer had significantly lower 35 m-integrated chlorophyll concentrations than the seasons preceding them ($p<0.001$).

In each binned profile, the chlorophyll maximum was identified as the 1 m depth bin with the highest 1 m depth-averaged chlorophyll concentration. Depth-averaged chlorophyll concentrations at the chlorophyll maximum were 1.55 ± 0.48 mg m⁻³

(n=187) in winter, $3.35 \pm 2.16 \text{ mg m}^{-3}$ (n=129) in spring, $2.52 \pm 0.88 \text{ mg m}^{-3}$ (n=188) in summer, and $1.80 \pm 0.58 \text{ mg m}^{-3}$ in fall.

In each season, surface and bottom depth-averaged chlorophyll was highest in the nearshore and lowest at the shelf break ($p < 0.001$), except in fall bottom water which saw no significant spatial change (Figure 2.5). The highest depth-averaged chlorophyll concentrations occurred in nearshore spring bottom water ($2.86 \pm 0.49 \text{ mg m}^{-3}$, n=13, $p < 0.001$), which captured the spring chlorophyll maximum layer. High depth-averaged chlorophyll was also present in spring and summer nearshore surface waters, averaging $2.13 \pm 0.71 \text{ mg m}^{-3}$ (n=13) and $2.30 \pm 0.45 \text{ mg m}^{-3}$ (n=28) respectively.

2.4.2.3 Chemical dynamics

2.4.2.3.1 Oxygen

The chlorophyll-rich, stratified spring and deeply-mixed fall water columns exhibited the highest 35 m integrated DO concentrations of $41.55 \pm 20.12 \text{ g m}^{-2}$ (n=129) and $41.86 \pm 12.46 \text{ g m}^{-2}$ (n=180) ($p < 0.001$; Figures 2.4 and 2.5). Like chlorophyll concentration, winter and summer 35 m integrated oxygen levels were significantly lower than both fall and spring ($p < 0.001$).

In spring, summer, and fall, high depth-averaged DO was observed at the chlorophyll maximum depth (Figure 2.5). Shelf break bottom waters exhibited the lowest depth-averaged DO concentrations in winter, spring, and fall ($p < 0.001$), averaging $6.20 \pm 0.88 \text{ g m}^{-3}$ (n=35), $8.20 \pm 0.49 \text{ g m}^{-3}$ (n=20), and $6.32 \pm 0.36 \text{ g m}^{-3}$ (n=39), respectively. The DO optode malfunctioned shortly after summer deployment, so summer shelf break measurements are not available.

2.4.2.3.2 Carbonate system

Figures 2.6 and 2.7 display seasonal and spatial differences in the carbonate system. Full water column pH ranged from 7.701 to 8.166 throughout all seasons, while Ω_{arag} ranged from 0.83 to 3.72, and TA:DIC ranged from 1.019 to 1.180. Deployment-averaged pH was highest in winter and lowest in summer (Table S2.6). Deployment-averaged Ω_{arag} and TA:DIC were highest in fall and lowest in summer (Table S2.6). Areas that differed from the means were localized in space and time. For example, areas of high pH were associated with the chlorophyll maximum in spring and summer, and areas of high pH, Ω_{arag} , and TA:DIC were found at the shelf break in all seasons (Figure 2.6). Conversely, areas of low pH, Ω_{arag} , and TA:DIC were associated with the nearshore region in spring, summer, and fall, and with shelf bottom waters in the summer (Figure 2.6).

In summer and fall, surface and bottom pH, Ω_{arag} , and TA:DIC were lowest in the nearshore and significantly higher at the shelf break ($p < 0.001$; Figure 2.7). The highest spring pH, Ω_{arag} , and TA:DIC values were also present at the shelf break ($p < 0.005$, Figure 2.7). Winter followed a different spatial pattern, with surface and bottom pH highest in the nearshore and significantly lower at the shelf break ($p < 0.001$). Winter surface Ω_{arag} and TA:DIC were highest in the midshelf region ($p < 0.05$), while bottom Ω_{arag} and TA:DIC increased from nearshore to shelf break ($p < 0.002$).

In the nearshore, surface and bottom pH were highest in winter, averaging 8.124 ± 0.007 ($n=31$) and 8.080 ± 0.014 ($n=31$) respectively ($p < 0.005$; Figures 2.6 and 2.7). The lowest nearshore pH occurred in summer bottom waters ($p < 0.001$), averaging 7.827 ± 0.029 ($n=28$). Bottom waters also reached a minimum in Ω_{arag} and TA:DIC in summer ($p < 0.03$), averaging 1.29 ± 0.11 and 1.048 ± 0.007 respectively ($n=28$). Contrary to

seasonal patterns in pH, nearshore surface water saw the highest Ω_{arag} and TA:DIC in the summer/fall and lowest in the winter/spring ($p < 0.001$).

In the midshelf, the highest seasonal pH occurred in well-mixed, cold winter surface water ($p < 0.002$; Figures 2.3, 2.6, and 2.7). Average winter midshelf surface pH was 8.107 ± 0.013 ($n=121$). Conversely, winter midshelf surface waters had low Ω_{arag} and TA:DIC, averaging 1.84 ± 0.09 and 1.082 ± 0.004 , respectively ($n=121$). The lowest midshelf pH occurred in summer surface and bottom water, averaging 7.934 ± 0.016 in the surface and 7.922 ± 0.053 in the bottom ($p < 0.001$, $n=120$). Low pH summer bottom water was associated with the Cold Pool bottom water mass, and also exhibited the lowest Ω_{arag} and TA:DIC in the midshelf (1.47 ± 0.15 and 1.059 ± 0.009 , respectively; $p < 0.001$; $n=120$). While summer midshelf bottom water had the lowest seasonal Ω_{arag} and TA:DIC, summer midshelf surface water had the highest values in the region, averaging 2.30 ± 0.18 and 1.101 ± 0.008 respectively ($p < 0.001$, $n=120$), though these values were not significantly different than fall.

At the shelf break, a warm, salty water mass persisted throughout all four seasons (Figure 2.3). The highest shelf break Ω_{arag} and TA:DIC occurred in fall ($p < 0.001$), when this water mass mixed into the surface layer (Figure 2.6). There, Ω_{arag} averaged 3.13 ± 0.12 ($n=39$) and TA:DIC averaged 1.138 ± 0.006 ($n=39$). The lowest shelf break Ω_{arag} and TA:DIC occurred in winter surface waters ($p < 0.05$), averaging 1.73 ± 0.06 and 1.075 ± 0.003 ($n=35$), respectively. The lowest seasonal shelf break pH occurred in summer surface waters ($p < 0.001$), averaging 7.969 ± 0.014 ($n=39$).

2.5 Discussion

High-resolution data resulting from deployments of a glider equipped with novel pH sensor technology highlight seasonal and spatial carbonate chemistry dynamics in the MAB for the first time. Results underscore the importance of seasonality, water mass mixing, biological production, and freshwater inputs in controlling the carbonate system in the MAB.

2.5.1 Drivers of MAB seasonality

Seasonal glider deployments recorded physical water column changes caused by intense MAB seasonality. Observations aligned with established MAB physical climatology (Castelao et al., 2010; Castelao et al., 2008). Warming of surface waters in the spring and summer, combined with freshening of surface waters, increased the strength of stratification and trapped a Cold Pool water mass below the mixed layer. Cold Pool bottom water generally contains relatively fresh (<34 PSU) and cold (<10 °C) water, with source water likely originating from the Labrador Sea (Z. Chen et al., 2018). Wind- and storm-driven seasonal overturn in the fall caused surface and Cold Pool bottom waters to mix, resulting in a cool, well-mixed water column that persisted through winter.

The occurrence of low surface water Ω_{arag} and TA:DIC in winter and high Ω_{arag} and TA:DIC in summer surface waters supports the findings of Cai et al. (2020) who concluded that surface water Ω_{arag} and DIC are controlled additively by thermodynamic equilibrium and air-sea gas exchange in the MAB. Unlike Ω_{arag} and TA:DIC, shelf surface water pH during glider deployments exhibited a decoupling from the effect of gas exchange, with the highest pH recorded in winter and lowest pH values in summer. This indicated a more complicated system of seasonal surface pH drivers, including freshwater

input (summer) and biological removal of CO₂ (winter), which acted on a timescale faster than gas equilibrium (Cai et al., 2020).

In areas and periods of dense chlorophyll biomass, primary producers remove CO₂ from the water, increasing DO and pH (Kemp et al., 1994). Fall and spring glider missions captured the highest seasonal integrated chlorophyll levels, due to high phytoplankton biomass. High fall integrated chlorophyll supports the findings of Y. Xu et al. (2011), who identified a bi-modal cycle of biological production in the MAB, in which a dominant fall-winter phytoplankton bloom between the 20-60 m isobaths accounts for almost 60% of the region's annual chlorophyll production. This bloom forms when fall overturn injects nutrient-rich bottom water into the surface, promoting phytoplankton production. High productivity captured in the fall deployment led to high integrated DO and increased surface pH in the nearshore and midshelf. The second mode of MAB phytoplankton production described by Y. Xu et al. (2011) indicates a less dominant spring-summer bloom triggered by stratification, which allows phytoplankton to overcome light limitation caused by deep mixing during the winter. Spring and summer glider deployments captured the development of strong seasonal stratification, isolating a chlorophyll maximum just below the mixed layer predominantly in the midshelf region that was co-located with high pH (Figure 2.6).

High depth-integrated chlorophyll and DO in the fall and spring were followed by periods of lower integrated chlorophyll and DO in the winter and summer. In summer, this was likely influenced by Cold Pool bottom water, where respiration of surface-derived particulate carbon produces CO₂ and reduces DO. Once seasonal stratification is set up, the Cold Pool has little ventilation to seawater above the thermocline, and

accumulation of respired CO_2 reduces pH, Ω_{arag} , and buffering capacity for CO_2 (Cai et al., 2011; Cai et al., 2017; Waldbusser & Salisbury, 2014; Wootton et al., 2008). Our summer mission captured the full extent of low bottom water pH, Ω_{arag} , and TA:DIC associated with stratification and the Cold Pool (Figures 2.6 and 2.7).

In summer nearshore surface and bottom waters, high-low-high cycles in pH, Ω_{arag} , and TA:DIC appeared in ~ 20 km increments (Figure 2.8). Cycles observed there align with the glider's average horizontal movement of 20 km day^{-1} , indicating potential diel variability in pH, Ω_{arag} , and TA:DIC. Daily swings in surface water pH were as large as 0.145 pH units, corresponding to swings in surface Ω_{arag} of 0.52 and TA:DIC of 0.033. These pH swings were about half the amplitude of those observed previously in nearby Mid-Atlantic estuaries, which can exhibit swings of up to 0.26 pH units day^{-1} , attributed to high productivity and shallow waters (Baumann & Smith, 2017). The pattern of daily variability was not always consistent (day vs. night), suggesting these complex carbonate chemistry dynamics are likely driven by a combination of biological productivity, temperature swings, fluctuations in salinity, and mixing. For example, pH and Ω_{arag} in nearshore bottom water exhibited strong positive correlations with temperature and chlorophyll (Spearman's $r > 0.75$, $p < 0.001$), and strong negative correlations with salinity (Spearman's $r < -0.67$, $p < 0.001$). In nearshore surface water, these correlations were weaker, and, in one case, the direction of the correlation flipped (Spearman's r between Ω_{arag} and chlorophyll = -0.50 , $p < 0.001$). Therefore, trends in pH and Ω_{arag} cannot be explained by any one driver. Additional observations are needed in order to thoroughly analyze and establish the relative importance of these drivers to diel variability.

2.5.2 Year-round water column features

In every season, nearshore waters experienced the lowest surface salinities, highlighting the influence of freshwater inputs to the coastal system (Castelao et al., 2010). During the summer, freshening extended into the midshelf due to heavy rainfall and typical seasonal freshening due to peak seasonal runoff from the Hudson River (Castelao et al., 2010; Richaud et al., 2016). Freshwater inputs from rivers and storms introduce low TA water into the coastal system, decreasing CO₂ buffering capacity (Siedlecki et al., 2017; Waldbusser & Salisbury, 2014). Spring, summer, and fall exhibited their lowest respective pH, Ω_{arag} , and TA:DIC in nearshore waters compared to the midshelf and shelf break regions. Summer nearshore and midshelf surface waters had the lowest seasonal pH, pointing to freshwater input as a major driver of pH there. However, as discussed in section 2.5.1, summer nearshore and midshelf surface waters had the highest seasonal Ω_{arag} and TA:DIC, indicating that thermodynamic control was a stronger influence on Ω_{arag} and TA:DIC than salinity. These complex carbonate system dynamics indicate that freshwater influence is a complicated but important driver of the carbonate system on the shelf.

Throughout all seasonal deployments, a warm (>12°C), salty (>35 PSU) water mass persisted at the continental shelf break. This slope water mass signified that the glider traveled through a shelf-break front, formally called the MAB shelf-break jet, which is influenced by warm, saline Gulf Stream waters entrained into the MAB by eddies (K. Chen & He, 2010; Fratantoni et al., 2001; Linder & Gawarkiewicz, 1998; Wanninkhof et al., 2015). The front was pushed progressively farther off-shelf with the onset and persistence of seasonal stratification, and infiltrated back onto the shelf during

fall overturn, following MAB shelf-break jet climatology described by Linder and Gawarkiewicz (1998). The deepest water sampled at the shelf break (> 150 m) exhibited the lowest depth-averaged oxygen levels in each deployment, suggesting that this water mass is not well ventilated to the atmosphere, and ongoing respiration there depletes oxygen and adds CO_2 . Despite ongoing respiration, shelf break jet deep water had high Ω_{arag} and TA:DIC, reflecting its Gulf Stream source and consistently high salinity levels. High TA:DIC indicated that this water mass had a high buffering capacity for CO_2 , and therefore had high pH in spring, summer, and fall, regardless of high net respiration.

The intrusion of the highly buffered shelf break jet onto the shelf during fall overturn, along with the high fall phytoplankton biomass and a decrease in freshwater input, resulted in a well-mixed water column with high pH, Ω_{arag} , and TA:DIC. High pH persisted through winter, while thermodynamic interactions led to low winter Ω_{arag} and TA:DIC after the fall bloom. This suggests that seasonal intrusion of the shelf break jet could be an important mitigator of acidification on the MAB shelf during fall.

2.5.3 Potential ecological implications

It is important to consider natural seasonal, spatial, and depth variability when investigating MAB habitat suitability. Surface water pH, Ω_{arag} , and TA:DIC exhibited seasonal differences across the MAB shelf, with Ω_{arag} and TA:DIC diverging to a greater extent at the shelf break (Figure 2.8). Bottom water pH exhibited seasonal swings on the MAB shelf, but values converged at the continental shelf break, while bottom water Ω_{arag} and TA:DIC saw seasonal divergence at the shelf break (Figure 2.9). Seasonality in pH, Ω_{arag} , and TA:DIC across the shelf and shelf break demonstrated seasonal and spatial fluctuations in carbonate system drivers in the MAB.

Shelf water masses, specifically the MAB Cold Pool, have been linked to the distribution and recruitment of economically important fish species, including the calcifying shellfish Atlantic sea scallop (*Placopecten magellanicus*) and Atlantic surfclam (*Spisula solidissima*), which are vulnerable to acidification (Colvocoresses & Musick, 1984; Cooley et al., 2015; Steves et al., 2000; Sullivan et al., 2000; Weinberg, 2005). These organisms are able to survive and reproduce through observed seasonal swings in carbonate chemistry on the MAB shelf, but the extent to which survival and reproduction may be negatively impacted by current levels of pH and Ω_{arag} is unknown. Potential vulnerability of these organisms during late summer/early fall spawning events on the MAB shelf should be a consideration for future fishery management.

2.5.4 Limitations and benefits

While the pH glider has undergone significant field testing for robustness, it is not exempt from limitations common to AUVs and other sensors used in oceanographic field work. Gliders deployed in areas of high productivity are subject to biofouling over time, which can increase offsets between glider and discrete pH measurements (Saba et al., 2019b). Increased offsets from deployment to recovery in winter, summer, and fall might indicate biofouling throughout deployment. Primary production associated with algal biofouling near the sensor intake would remove CO₂ from water in close vicinity to the glider, thereby increasing pH. Additionally, biofouling from barnacles or juvenile bivalves can occur on gliders. Saba et al. (2019b) reported an instance of biofouling by a juvenile clam which settled onto the glider pH sensor intake valve. In that case, respiration would decrease pH around the sensor. Increases in offsets over time can also occur due to pH sensor drift. Sensor drift generally arises due to a lack of full

conditioning to Br^- anion in seawater and is a common issue for autonomous pH monitoring platforms (Johnson et al., 2016).

Seasonal TA-salinity relationships derived from discrete samples perform generally well when compared to the CANYON-B algorithm and discrete sample TA values. Large offsets between discrete and regression-based TA corresponded to a break in the TA-salinity relationship at approximately 30-31 PSU (Figure S2.1). These offsets were particularly large in summer and fall, with discrete and calculated TA differing by up to 51.1 and 87.6 $\mu\text{mol kg}^{-1}$ respectively (Table S2.5). Uncertainty in Ω_{arag} and TA:DIC due to TA uncertainty were as extreme as -0.08 and 0.0013 (Fall; Table S2.4). However, the difference between CANYON-B-estimated TA and salinity-derived TA was quite small, averaging $\sim 0.1\%$. Because of this, we are confident that seasonal TA-salinity regressions are applicable to full glider deployments.

While none of the seasonal deployment pH offsets described here exceeded manufacturer specifications for the sensor, changes in offsets over time underscore the importance of taking discrete samples at each glider deployment and recovery to ensure continued accuracy and data quality. These missions therefore require a vessel with water sampling capabilities, but the data provided during the otherwise automated 30-60 day missions far outweighs the cost to collect data of this resolution during major research cruises (Schofield et al., 2010). Furthermore, gliders have proven their effectiveness for high quality observations in a range of coastal and open ocean environments, including locations that are not conducive to vessel operation or human presence (e.g., polar environments, hurricane seas) (Testor et al., 2019).

2.6 Significance

The work presented here highlights the distinct capability of an autonomous Slocum glider equipped with a deep-ISFET based pH sensor to make highly accurate, high resolution observations of the marine carbonate system. The use of pH glider technology can be scaled up to address regional, national, and global ocean acidification observing needs. Using this glider sensor suite, we have observed seasonal patterns in the carbonate system directly associated with changes in other physical, biological, and chemical properties. While it is beyond the scope of this paper to quantify the relative importance of different carbonate system drivers, these data make clear that several drivers impact the strength of acidification. These include air-sea CO₂ exchange, seasonal stratification, biological activity, and freshwater input, as well as physical mixing of the MAB shelf break front. Importantly, data presented here describe the typical seasonal patterns of carbonate system dynamics in the MAB, but absolute values will change from year-to-year due to differences in regional climate, temperature, precipitation, wind patterns, and storm activity. Continued seasonal glider observation efforts, together with other carbonate monitoring platforms, will assist in developing a mean carbonate chemistry climatology for the MAB. This will help to inform the design of laboratory experiments investigating the response of commercially important species to acidification using realized carbonate system values and variability (Goldsmith et al., 2019; Saba et al., 2019a). Furthermore, ongoing monitoring efforts can be used to identify areas or time periods prone to acidification due to interaction with other potential stressors, and the derivation of synergistic relationships between these variables. Continued simultaneous collection of chemical, physical, and biological metrics will allow the development of

algorithms linking carbonate chemistry to other ocean properties. These quantitative relationships are necessary to develop broader predictive forecast models for the coastal ecosystem, which will ultimately aid in fisheries management planning and mitigation of short-term acidification events in the MAB.

2.7 Acknowledgements

Data supporting the conclusions made in this paper can be obtained at: <http://slocum-data.marine.rutgers.edu/erddap/search/index.html?page=1&itemsPerPage=1000&searchFor=ru30>. We thank Rutgers University Center for Ocean Observing Leadership (RU COOL) glider technicians: David Aragon, Nicole Waite, Chip Haldeman, Laura Nazzaro, and John Kerfoot for their efforts in glider preparation, deployment logistics, fieldwork, mission piloting, and data management. We also thank Rutgers undergraduate alumni Brandon Grosso and Laura Wiltsee for their dedicated work with gliders in the field and lab. We acknowledge RU COOL faculty Oscar Schofield, Scott Glen, Josh Kohut, and RU COOL manager Michael Crowley for facility support. We appreciate Yui Takeshita (Monterey Bay Aquarium Research Institute) for his support on data interpretation. Finally, we thank our colleagues at SeaBird Scientific including Dave Murphy, Cristina Orrico, Vlad Simontov, and Dave Walter, along with Clara Hulburt and Christopher DeCollibus at Teledyne Webb Research for their technical expertise and support. This project was funded by National Science Foundation's Ocean Technology and Interdisciplinary Coordination program (NSF OCE1634520 and OCE1634582). E W-F received support from the Mid-Atlantic Sea Grant/NOAA OAP Graduate Research

Fellowship (NA18OAR4170087) and the Rutgers University School of Environmental and Biological Sciences Excellence Fellowship.

2.8 References

- Baumann, H., & Smith, E. M. (2017). Quantifying Metabolically Driven pH and Oxygen Fluctuations in US Nearshore Habitats at Diel to Interannual Time Scales. *Estuaries and Coasts*, 41(4), 1102-1117. doi:10.1007/s12237-017-0321-3
- Bittig, H. C., Steinhoff, T., Claustre, H., Fiedler, B., Williams, N. L., Sauzède, R., Körtzinger, A., & Gattuso, J.-P. (2018). An Alternative to Static Climatologies: Robust Estimation of Open Ocean CO₂ Variables and Nutrient Concentrations From T, S, and O₂ Data Using Bayesian Neural Networks. *Frontiers in Marine Science*, 5. doi:10.3389/fmars.2018.00328
- Bresnahan, P. J., Martz, T. R., Takeshita, Y., Johnson, K. S., & LaShomb, M. (2014). Best practices for autonomous measurement of seawater pH with the Honeywell Durafet. *Methods in Oceanography*, 9, 44-60. doi:10.1016/j.mio.2014.08.003
- Cai, W.-J., Hu, X., Huang, W.-J., Jiang, L.-Q., Wang, Y., Peng, T.-H., & Zhang, X. (2010). Alkalinity distribution in the western North Atlantic Ocean margins. *Journal of Geophysical Research*, 115(C8). doi:10.1029/2009jc005482
- Cai, W.-J., Hu, X., Huang, W.-J., Murrell, M. C., Lehrter, J. C., Lohrenz, S. E., Chou, W.-C., Zhai, W., Hollibaugh, J. T., Wang, Y., Zhao, P., Guo, X., Gundersen, K., Dai, M., & Gong, G.-C. (2011). Acidification of subsurface coastal waters enhanced by eutrophication. *Nature Geoscience*, 4(11), 766-770. doi:10.1038/ngeo1297
- Cai, W.-J., Huang, W. J., Luther, G. W., 3rd, Pierrot, D., Li, M., Testa, J., Xue, M., Joesoef, A., Mann, R., Brodeur, J., Xu, Y. Y., Chen, B., Hussain, N., Waldbusser, G. G., Cornwell, J., & Kemp, W. M. (2017). Redox reactions and weak buffering capacity lead to acidification in the Chesapeake Bay. *Nat Commun*, 8(1), 369. doi:10.1038/s41467-017-00417-7
- Cai, W.-J., Xu, Y. Y., Feely, R. A., Wanninkhof, R., Jonsson, B., Alin, S. R., Barbero, L., Cross, J. N., Azetsu-Scott, K., Fassbender, A. J., Carter, B. R., Jiang, L. Q., Pepin, P., Chen, B., Hussain, N., Reimer, J. J., Xue, L., Salisbury, J. E., Hernandez-Ayon, J. M., Langdon, C., Li, Q., Sutton, A. J., Chen, C. A., & Gledhill, D. K. (2020). Controls on surface water carbonate chemistry along North American ocean margins. *Nat Commun*, 11(1), 2691. doi:10.1038/s41467-020-16530-z
- Carvalho, F., Kohut, J., Oliver, M. J., & Schofield, O. (2017). Defining the ecologically relevant mixed-layer depth for Antarctica's coastal seas. *Geophysical Research Letters*, 44, 338-345. doi:10.1002/2016GL071205

- Castelao, R., Glenn, S., & Schofield, O. (2010). Temperature, salinity, and density variability in the central Middle Atlantic Bight. *Journal of Geophysical Research*, *115*(C10). doi:10.1029/2009jc006082
- Castelao, R., Glenn, S., Schofield, O., Chant, R., Wilkin, J., & Kohut, J. (2008). Seasonal evolution of hydrographic fields in the central Middle Atlantic Bight from glider observations. *Geophysical Research Letters*, *35*(3). doi:10.1029/2007gl032335
- Chen, B., Cai, W.-J., & Chen, L. (2015). The marine carbonate system of the Arctic Ocean: Assessment of internal consistency and sampling considerations, summer 2010. *Marine Chemistry*, *176*, 174-188. doi:10.1016/j.marchem.2015.09.007
- Chen, K., & He, R. (2010). Numerical Investigation of the Middle Atlantic Bight Shelfbreak Frontal Circulation Using a High-Resolution Ocean Hindcast Model. *Journal of Physical Oceanography*, *40*(5), 949-964. doi:10.1175/2009jpo4262.1
- Chen, Z., Curchitser, E., Chant, R., & Kang, D. (2018). Seasonal Variability of the Cold Pool Over the Mid-Atlantic Bight Continental Shelf. *Journal of Geophysical Research: Oceans*, *123*(11), 8203-8226. doi:10.1029/2018jc014148
- Clayton, T. D., & Byrne, R. H. (1993). Spectrophotometric seawater pH measurements: total hydrogen ion concentration scale calibration of m-cresol purple and at-sea results. *Deep-Sea Research*, *40*(10), 2115-2129.
- Colvocoresses, J. A., & Musick, J. A. (1984). Species Associations and Community Composition of Middle Atlantic Bight Continental Shelf Demersal Fishes. *VIMS Articles*, 625.
- Cooley, S. R., Rheuban, J. E., Hart, D. R., Luu, V., Glover, D. M., Hare, J. A., & Doney, S. C. (2015). An Integrated Assessment Model for Helping the United States Sea Scallop (*Placopecten magellanicus*) Fishery Plan Ahead for Ocean Acidification and Warming. *PLoS One*, *10*(5), e0124145. doi:10.1371/journal.pone.0124145
- DeIvals, T. A., & Dickson, A. G. (1998). The pH of buffers based on 2-amino-2-hydroxymethyl-1,3-propanediol ('tris') in synthetic sea water. *Deep Sea Research*, *45*, 1541-1554.
- Dickson, A. (1990). Standard potential of the reaction: $\text{AgCl(s)} + 1/2\text{H}_2(\text{g}) = \text{Ag(s)} + \text{HCl(aq)}$, and the standard acidity constant of the ion HSO_4^- in synthetic sea water from 273.15 to 318.15 K. *Journal of Chemical Thermodynamics*, *22*, 113-127.
- Dickson, A., & Millero, F. J. (1987). A comparison of the equilibrium constants for the dissociation of carbonic acid in seawater media. *Deep-Sea Research*, *34*(10), 1733-1743.
- Dlugokencky, E., & Tans, P. (2020). Trends in Atmospheric Carbon Dioxide. *NOAA Earth System Research Laboratory*.
- Doney, S. C., Fabry, V. J., Feely, R. A., & Kleypas, J. A. (2009). Ocean acidification: the other CO₂ problem. *Ann Rev Mar Sci*, *1*, 169-192. doi:10.1146/annurev.marine.010908.163834

- Egleston, E. S., Sabine, C. L., & Morel, F. M. M. (2010). Revelle revisited: Buffer factors that quantify the response of ocean chemistry to changes in DIC and alkalinity. *Global Biogeochemical Cycles*, 24(1), n/a-n/a. doi:10.1029/2008gb003407
- Fratantoni, P. S., Pickart, R. S., Torres, D. J., & Scotti, A. (2001). Mean Structure and Dynamics of the Shelfbreak Jet in the Middle Atlantic Bight during Fall and Winter. *Journal of Physical Oceanography*, 31, 2135-2156.
- Friedrich, T., Timmermann, A., Abe-Ouchi, A., Bates, N. R., Chikamoto, M. O., Church, M. J., Dore, J. E., Gledhill, D. K., González-Dávila, M., Heinemann, M., Ilyina, T., JungCLAUS, J. H., McLeod, E., Mouchet, A., & Santana-Casiano, J. M. (2012). Detecting regional anthropogenic trends in ocean acidification against natural variability. *Nature Climate Change*, 2(3), 167-171. doi:10.1038/nclimate1372
- Gattuso, J., -P., Magnan, A., Bille, R., Cheung, W. W. L., Howes, E. L., Joos, F., ALlemand, D., Bopp, L., Cooley, S. R., Eakin, C. M., Hoegh-Guldberg, O., Kelly, R. P., Portner, H. O., Rogers, A. D., Baxter, J. M., Laffoley, D., Osborn, D., Rankovic, A., Rochette, J., Summaila, U. R., Treyer, S., & Turley, C. (2015). Contrasting futures for ocean and society from different anthropogenic CO₂ emissions scenarios. *Science Magazine*, 349(6243). doi:10.1126/10.1126/science.aac4722
- Gazeau, F., Quiblier, C., Jansen, J. M., Gattuso, J.-P., Middelburg, J. J., & Heip, C. H. R. (2007). Impact of elevated CO₂ on shellfish calcification. *Geophysical Research Letters*, 34(7). doi:10.1029/2006gl028554
- Gledhill, D., White, M., Salisbury, J., Thomas, H., Misna, I., Liebman, M., Mook, B., Grear, J., Candelmo, A., Chambers, R. C., Gobler, C., Hunt, C., King, A., Price, N., Signorini, S., Stancioff, E., Stymiest, C., Wahle, R., Waller, J., Rebuck, N., Wang, Z., Capson, T., Morrison, J. R., Cooley, S., & Doney, S. (2015). Ocean and Coastal Acidification off New England and Nova Scotia. *Oceanography*, 25(2), 182-197. doi:10.5670/oceanog.2015.41
- Gobler, C. J., & Talmage, S. C. (2013). Short- and long-term consequences of larval stage exposure to constantly and ephemerally elevated carbon dioxide for marine bivalve populations. *Biogeosciences*, 10(4), 2241-2253. doi:10.5194/bg-10-2241-2013
- Gobler, C. J., & Talmage, S. C. (2014). Physiological response and resilience of early life-stage Eastern oysters (*Crassostrea virginica*) to past, present and future ocean acidification. *Conserv Physiol*, 2(1), cou004. doi:10.1093/conphys/cou004
- Goldsmith, K. A., Lau, S., Poach, M. E., Sakowicz, G. P., Trice, T. M., Ono, C. R., Nye, J., Shadwick, E. H., StLaurent, K. A., & Saba, G. K. (2019). Scientific considerations for acidification monitoring in the U.S. Mid-Atlantic Region. *Estuarine, Coastal and Shelf Science*, 225. doi:10.1016/j.ecss.2019.04.023
- Gruber, N., Clement, D., Carter, B. R., Feely, R. A., van Heuven, S., Hoppema, M., Ishii, M., Key, R. M., Kozyr, A., Lauvset, S. K., Monaco, C. L., Mathis, J., Murata, A., Olsen, A., Perez, F. F., Sabine, C. L., Tanhua, T., & Wannikhof, R. (2019). The oceanic sink for anthropogenic CO₂ from 1994 to 2007. *Science*, 363, 1193-1199.

- Hare, J. A., Morrison, W. E., Nelson, M. W., Stachura, M. M., Teeters, E. J., Griffis, R. B., Alexander, M. A., Scott, J. D., Alade, L., Bell, R. J., Chute, A. S., Curti, K. L., Curtis, T. H., Kircheis, D., Kocik, J. F., Lucey, S. M., McCandless, C. T., Milke, L. M., Richardson, D. E., Robillard, E., Walsh, H. J., McManus, M. C., Marancik, K. E., & Griswold, C. A. (2016). A Vulnerability Assessment of Fish and Invertebrates to Climate Change on the Northeast U.S. Continental Shelf. *PLoS One*, *11*(2), e0146756. doi:10.1371/journal.pone.0146756
- Hettinger, A., Sanford, E., Hill, T. M., Russell, A. D., Sato, K. N. S., Hoey, J., Forsch, M., Page, H. N., & Gaylord, B. (2012). Persistent carry-over effects of planktonic exposure to ocean acidification in the Olympic oyster. *Ecology*, *93*(12), 2758-2768.
- Houghton, R. W., Shlitz, R., Beardsley, R. C., Butman, B., & Chamberlin, J. L. (1982). The Middle Atlantic Bight Cold Pool: Evolution of the Temperature Structure During Summer 1979. *American Meteorological Society*, *12*, 1019-1029.
- Huang, W.-J., Wang, Y., & Cai, W.-J. (2012). Assessment of sample storage techniques for total alkalinity and dissolved inorganic carbon in seawater. *Limnology and Oceanography: Methods*, *10*(9), 711-717. doi:10.4319/lom.2012.10.711
- Huret, M., Bourriau, P., Doray, M., Gohin, F., & Petitgas, P. (2018). Survey timing vs. ecosystem scheduling: Degree-days to underpin observed interannual variability in marine ecosystems. *Progress in Oceanography*, *166*, 30-40. doi:10.1016/j.pocean.2017.07.007
- IOOS. (2019). Manual for Real-Time Quality Control of pH Data Observations: A Guide to Quality Control and Quality Assurance for pH Observations. doi:10.25923/111k-br08
- IPCC. (2019). Summary for Policymakers. *IPCC Special Report on the Ocean and Cryosphere in a Changing Climate*.
- Johnson, K. S., Jannasch, H. W., Coletti, L. J., Elrod, V. A., Martz, T. R., Takeshita, Y., Carlson, R. J., & Connery, J. G. (2016). Deep-Sea DuraFET: A Pressure Tolerant pH Sensor Designed for Global Sensor Networks. *Anal Chem*, *88*(6), 3249-3256. doi:10.1021/acs.analchem.5b04653
- Johnson, K. S., Plant, J. N., & Maurer, T. L. (2017). Processing BGC-Argo pH data at the DAC level. doi:<https://doi.org/10.13155/57195>
- Kemp, P. F., Falkowski, P. G., Flagg, C. N., Phoel, W. C., Smith, S. L., Wallace, D. W. R., & Wirick, C. D. (1994). Modeling vertical oxygen and carbon flux during stratified spring and summer conditions on the continental shelf, Middle Atlantic Bight, eastern U.S.A. *Deep Sea Research*, *41*(2/3), 629-655.
- Kohut, J., Haldeman, C., & Kerfoot, J. (2014). Monitoring Dissolved Oxygen in New Jersey Coastal Waters Using Autonomous Gliders. *Environmental Protection Agency Office of Research and Development*.
- Levin, J., Wilkin, J., Fleming, N., & Zavala-Garay, J. (2018). Mean circulation of the Mid-Atlantic Bight from a climatological data assimilative model. *Ocean Modelling*, *128*, 1-14. doi:10.1016/j.ocemod.2018.05.003

- Lewis, E., & Wallace, D. W. R. (1998). Program Developed for CO₂ System Calculations.
- Linder, C. A., & Gawarkiewicz, G. (1998). A climatology of the shelfbreak front in the Middle Atlantic Bight. *Journal of Geophysical Research: Oceans*, *103*(C9), 18405-18423. doi:10.1029/98jc01438
- Liu, X., Patsavas, M. C., & Byrne, R. H. (2011). Purification and characterization of meta-cresol purple for spectrophotometric seawater pH measurements. *Environ Sci Technol*, *45*(11), 4862-4868. doi:10.1021/es200665d
- Lorbacher, K., Dommenges, D., Niiler, P. P., & Köhl, A. (2006). Ocean mixed layer depth: A subsurface proxy of ocean-atmosphere variability. *Journal of Geophysical Research*, *111*(C7). doi:10.1029/2003jc002157
- Martz, T. R., McLaughlin, K., & Weisberg, S. (2015). Best Practices for autonomous measurement of seawater pH with the Honeywell Durafet pH sensor. *California Current Acidification Network (C-CAN)*.
- Mehrbach, C., Culberson, C. H., Hawley, J. E., & Pytkowicz, R. M. (1973). Measurement of the apparent dissociation constants of carbonic acid in seawater at atmospheric pressure. *Limnology and Oceanography*, *18*(6), 897-907.
- Melzner, F., Mark, F. C., Seibel, B. A., & Tomanek, L. (2019). Ocean Acidification and Coastal Marine Invertebrates: Tracking CO₂ Effects from Seawater to the Cell. *Annual Review of Marine Science*, *12*, 12.11-12.25. doi:10.1146/annurev-marine-010419-
- Miller, A. W., Reynolds, A. C., Sobrino, C., & Riedel, G. F. (2009). Shellfish face uncertain future in high CO₂ world: influence of acidification on oyster larvae calcification and growth in estuaries. *PLoS One*, *4*(5), e5661. doi:10.1371/journal.pone.0005661
- Millero, F. J. (1986). The pH of estuarine waters. *Limnology and Oceanography*, *31*(4), 839-847.
- Musial, W., Elliott, D., Fields, J., Parker, Z., Scott, G., & Draxl, C. (2013). Assessment of Offshore Wind Energy Leasing Areas for the BOEM New Jersey Wind Energy Area. *National Renewable Energy Laboratory Technical Reports*.
- NEFSC. (2020). State of the Ecosystem 2020: Mid-Atlantic. *NOAA Fisheries Reports*.
- NRC. (2010). Ocean Acidification: A National Strategy to Meet the Challenges of a Changing Ocean. *The National Academies Press*. doi:<https://doi.org/10.17226/12904>
- Orr, J. C., Fabry, V. J., Aumont, O., Bopp, L., Doney, S. C., Feely, R. A., Gnanadesikan, A., Gruber, N., Ishida, A., Joos, F., Key, R. M., Lindsay, K., Maier-Reimer, E., Matear, R., Monfray, P., Mouchet, A., Najjar, R. G., Plattner, G. K., Rodgers, K. B., Sabine, C. L., Sarmiento, J. L., Schlitzer, R., Slater, R. D., Totterdell, I. J., Weirig, M. F., Yamanaka, Y., & Yool, A. (2005). Anthropogenic ocean acidification over the twenty-first century and its impact on calcifying organisms. *Nature*, *437*(7059), 681-686. doi:10.1038/nature04095

- Pan, T. C., Applebaum, S. L., & Manahan, D. T. (2015). Experimental ocean acidification alters the allocation of metabolic energy. *Proc Natl Acad Sci U S A*, *112*(15), 4696-4701. doi:10.1073/pnas.1416967112
- Perez, F. F., & Fraga, F. (1987). Association Constant of Fluoride and Hydrogen Ions in Seawater. *Marine Chemistry*, *21*.
- Pimenta, A. R., & Grear, J. S. (2018). Guidelines for Measuring Changes in Seawater pH and Associated Carbonate Chemistry in Coastal Environments of the Eastern United States. *United States Environmental Protection Agency*.
- Richaud, B., Kwon, Y.-O., Joyce, T. M., Fratantoni, P. S., & Lentz, S. J. (2016). Surface and bottom temperature and salinity climatology along the continental shelf off the Canadian and U.S. East Coasts. *Continental Shelf Research*, *124*, 165-181. doi:10.1016/j.csr.2016.06.005
- Rudnick, D. L. (2016). Ocean Research Enabled by Underwater Gliders. *Ann Rev Mar Sci*, *8*, 519-541. doi:10.1146/annurev-marine-122414-033913
- Runcie, J. W., Krause, C., Torres Gabarda, S. A., & Byrne, M. (2018). Technical note: Continuous fluorescence-based monitoring of seawater pH in situ. *Biogeosciences*, *15*(13), 4291-4299. doi:10.5194/bg-15-4291-2018
- Saba, G. K., Goldsmith, K. A., Cooley, S. R., Grosse, D., Meseck, S. L., Miller, A. W., Phelan, B., Poach, M., Rheault, R., St-Laurent, K., Testa, J. M., Weis, J. S., & Zimmerman, R. (2019a). Recommended priorities for research on ecological impacts of ocean and coastal acidification in the U.S. Mid-Atlantic. *Estuarine, Coastal and Shelf Science*, *225*. doi:10.1016/j.ecss.2019.04.022
- Saba, G. K., Wright-Fairbanks, E., Chen, B., Cai, W.-J., Barnard, A. H., Jones, C. P., Branham, C. W., Wang, K., & Miles, T. (2019b). The Development and Validation of a Profiling Glider Deep ISFET-Based pH Sensor for High Resolution Observations of Coastal and Ocean Acidification. *Frontiers in Marine Science*, *6*. doi:10.3389/fmars.2019.00664
- Salisbury, J., Vandemark, D., Jönsson, B., Balch, W., Chakraborty, S., Lohrenz, S., Chapron, B., Hales, B., Mannino, A., Mathis, J., Reul, N., Signorini, S., Wanninkhof, R., & Yates, K. (2015). How Can Present and Future Satellite Missions Support Scientific Studies that Address Ocean Acidification? *Oceanography*, *25*(2), 108-121. doi:10.5670/oceanog.2015.35
- Schofield, O., Kohut, J., Aragon, D., Creed, L., Graver, J., Haldeman, C., Kerfoot, J., Roarty, H., Jones, C., Webb, D., & Glenn, S. (2007). Slocum Gliders: Robust and ready. *Journal of Field Robotics*, *24*(6), 473-485. doi:10.1002/rob.20200
- Schofield, O., Kohut, J., Glenn, S., Morell, J. M., Capella, J., Corredor, J., Orcutt, J., Arrott, M., Kreuger, I., Meisinger, M., Peach, C., Vernon, F., Chave, A., Chao, Y., Chien, S., Thompson, D., Brown, W., Oliver, M. J., & Boicourt, W. (2010). A Regional Slocum Glider Network in the Mid-Atlantic Bight Leverages Broad Community Engagement. *Marine Technology Society Journal*, *44*(6).
- Sharp, J. D., Pierrot, D., Humphreys, M. P., Epitalon, J.-M., Orr, J. C., Lewis, E., & Wallace, D. W. R. (2020). CO2-System-Extd, v3.0, MATLAB (MathWorks).

- Siedlecki, S. A., Pilcher, D. J., Hermann, A. J., Coyle, K., & Mathis, J. (2017). The Important of Freshwater to Spatial Variability of Aragonite Saturation State in the Gulf of Alaska. *Journal of Geophysical Research: Oceans*, 122, 8482-8502. doi:10.1002/
- Steves, B. P., Cowen, R. K., & Malchoff, M. H. (2000). Settlement and nursery habitats for demersal fishes on the continental shelf of the New York Bight. *Fishery Bulletin*, 98(1), 167-188.
- Sullivan, M. C., Cowen, R. K., Able, K. W., & Fahay, M. P. (2000). Spatial scaling of recruitment in four continental shelf fishes. *Marine Ecology Progress Series*, 207, 141-154.
- Sutton, A. J., Sabine, C. L., Feely, R. A., Cai, W.-J., Cronin, M. F., McPhaden, M. J., Morell, J. M., Newton, J. A., Noh, J.-H., Ólafsdóttir, S. R., Salisbury, J. E., Send, U., Vandemark, D. C., & Weller, R. A. (2016). Using present-day observations to detect when anthropogenic change forces surface ocean carbonate chemistry outside preindustrial bounds. *Biogeosciences*, 13(17), 5065-5083. doi:10.5194/bg-13-5065-2016
- Takeshita, Y., Jones, B.D., Johnson, K.S., Chavez, F.P., Rudnick, D.L., Blum, M., Conner, K., Jensen, S., Long, J.S., Maughan, T., Mertz, K.L., Sherman, J.T., and Warren, J.K. (2021). Accurate pH and O₂ Measurements from Spray Underwater Gliders. *Journal of Atmospheric and Oceanic Technoogy*, 38(2), 181-195.
- Talmage, S. C., & Gobler, C. J. (2009). The effects of elevated carbon dioxide concentrations on the metamorphosis, size, and survival of larval hard clams (*Mercenaria mercenaria*), bay scallops (*Argopecten irradians*), and Eastern oysters (*Crassostrea virginica*). *Limnology and Oceanography*, 54(6), 2072-2080.
- Talmage, S. C., & Gobler, C. J. (2010). Effects of past, present, and future ocean carbon dioxide concentrations on the growth and survival of larval shellfish. *Proc Natl Acad Sci U S A*, 107(40), 17246-17251. doi:10.1073/pnas.0913804107
- Testor, P., de Young, B., Rudnick, D. L., Glenn, S., Hayes, D., Lee, C. M., Pattiaratchi, C., Hill, K., Heslop, E., Turpin, V., Alenius, P., Barrera, C., Barth, J. A., Beard, N., Bécu, G., Bosse, A., Bourrin, F., Brearley, J. A., Chao, Y., Chen, S., Chiggiato, J., Coppola, L., Crout, R., Cummings, J., Curry, B., Curry, R., Davis, R., Desai, K., DiMarco, S., Edwards, C., Fielding, S., Fer, I., Frajka-Williams, E., Gildor, H., Goni, G., Gutierrez, D., Haugan, P., Hebert, D., Heiderich, J., Henson, S., Heywood, K., Hogan, P., Houpert, L., Huh, S., E. Inall, M., Ishii, M., Ito, S.-i., Itoh, S., Jan, S., Kaiser, J., Karstensen, J., Kirkpatrick, B., Klymak, J., Kohut, J., Krahmann, G., Krug, M., McClatchie, S., Marin, F., Mauri, E., Mehra, A., P. Meredith, M., Meunier, T., Miles, T., Morell, J. M., Mortier, L., Nicholson, S., O'Callaghan, J., O'Conchubhair, D., Oke, P., Pallàs-Sanz, E., Palmer, M., Park, J., Perivoliotis, L., Poulain, P.-M., Perry, R., Queste, B., Rainville, L., Rehm, E., Roughan, M., Rome, N., Ross, T., Ruiz, S., Saba, G., Schaeffer, A., Schönau, M., Schroeder, K., Shimizu, Y., Sloyan, B. M., Smeed, D., Snowden, D., Song, Y., Swart, S., Tenreiro, M., Thompson, A., Tintore, J., Todd, R. E., Toro, C., Venables, H., Wagawa, T., Waterman, S., Watlington, R. A., & Wilson, D.

- (2019). OceanGliders: A Component of the Integrated GOOS. *Frontiers in Marine Science*, 6. doi:10.3389/fmars.2019.00422
- Uppstrom, L. (1974). The boron/chlorinity ratio of deep-sea water from the Pacific Ocean. *Deep-Sea Research*, 21(2).
- van Heuven, S., Pierrot, D., Rae, J. W. B., Lewis, E., & Wallace, D. W. R. (2011). MATLAB Program Developed for CO₂ System Calculations. *ORNL/CDIAC-105b. Carbon Dioxide Information Analysis Center, Oak Ridge National Laboratory, U.S. Department of Energy, Oak Ridge, Tennessee.*
doi:doi:10.3334/CDIAC/otg.CO2SYS_MATLAB_v1.1
- Waldbusser, G. G., Hales, B., Langdon, C. J., Haley, B. A., Schrader, P., Brunner, E. L., Gray, M. W., Miller, C. A., & Gimenez, I. (2014). Saturation-state sensitivity of marine bivalve larvae to ocean acidification. *Nature Climate Change*, 5(3), 273-280. doi:10.1038/nclimate2479
- Waldbusser, G. G., & Salisbury, J. E. (2014). Ocean acidification in the coastal zone from an organism's perspective: multiple system parameters, frequency domains, and habitats. *Ann Rev Mar Sci*, 6, 221-247. doi:10.1146/annurev-marine-121211-172238
- Wang, H., Hu, X., Cai, W.-J., & Sterba-Boatwright, B. (2017). Decadal fCO₂ trends in global ocean margins and adjacent boundary current-influenced areas. *Geophysical Research Letters*, 44(17), 8962-8970. doi:10.1002/2017gl074724
- Wang, Z. A., Wanninkhof, R., Cai, W.-J., Byrne, R. H., Hu, X., Peng, T.-H., & Huang, W.-J. (2013). The marine inorganic carbon system along the Gulf of Mexico and Atlantic coasts of the United States: Insights from a transregional coastal carbon study. *Limnology and Oceanography*, 58(1), 325-342.
doi:10.4319/lo.2013.58.1.0325
- Wanninkhof, R., Barbero, L., Byrne, R., Cai, W.-J., Huang, W.-J., Zhang, J.-Z., Baringer, M., & Langdon, C. (2015). Ocean acidification along the Gulf Coast and East Coast of the USA. *Continental Shelf Research*, 98, 54-71.
doi:10.1016/j.csr.2015.02.008
- Weinberg, J. R. (2005). Bathymetric shift in the distribution of Atlantic surfclams: response to warmer ocean temperature. *ICES Journal of Marine Science*, 62(7), 1444-1453. doi:10.1016/j.icesjms.2005.04.020
- Wootton, J. T., Pfister, C. A., & Forester, J. D. (2008). Dynamic patterns and ecological impacts of declining ocean pH in a high-resolution multi-year dataset. *Proc Natl Acad Sci U S A*, 105(48), 18848-18853. doi:10.1073/pnas.0810079105
- Xu, Y., Chant, R., Gong, D., Castelao, R., Glenn, S., & Schofield, O. (2011). Seasonal variability of chlorophyll a in the Mid-Atlantic Bight. *Continental Shelf Research*, 31(16), 1640-1650. doi:10.1016/j.csr.2011.05.019
- Xu, Y.-Y., Cai, W.-J., Gao, Y., Wanninkhof, R., Salisbury, J., Chen, B., Reimer, J. J., Gonski, S., & Hussain, N. (2017). Short-term variability of aragonite saturation state in the central Mid-Atlantic Bight. *Journal of Geophysical Research: Oceans*, 122. doi:10.1002/

- Xu, Y. Y., Cai, W. J., Wanninkhof, R., Salisbury, J., Reimer, J., & Chen, B. (2020). Long-Term Changes of Carbonate Chemistry Variables Along the North American East Coast. *Journal of Geophysical Research: Oceans*, 125(7). doi:10.1029/2019jc015982
- Zeebe, R. E. (2012). History of Seawater Carbonate Chemistry, Atmospheric CO₂, and Ocean Acidification. *Annual Review of Earth and Planetary Sciences*, 40(1), 141-165. doi:10.1146/annurev-earth-042711-105521

2.9 Figures

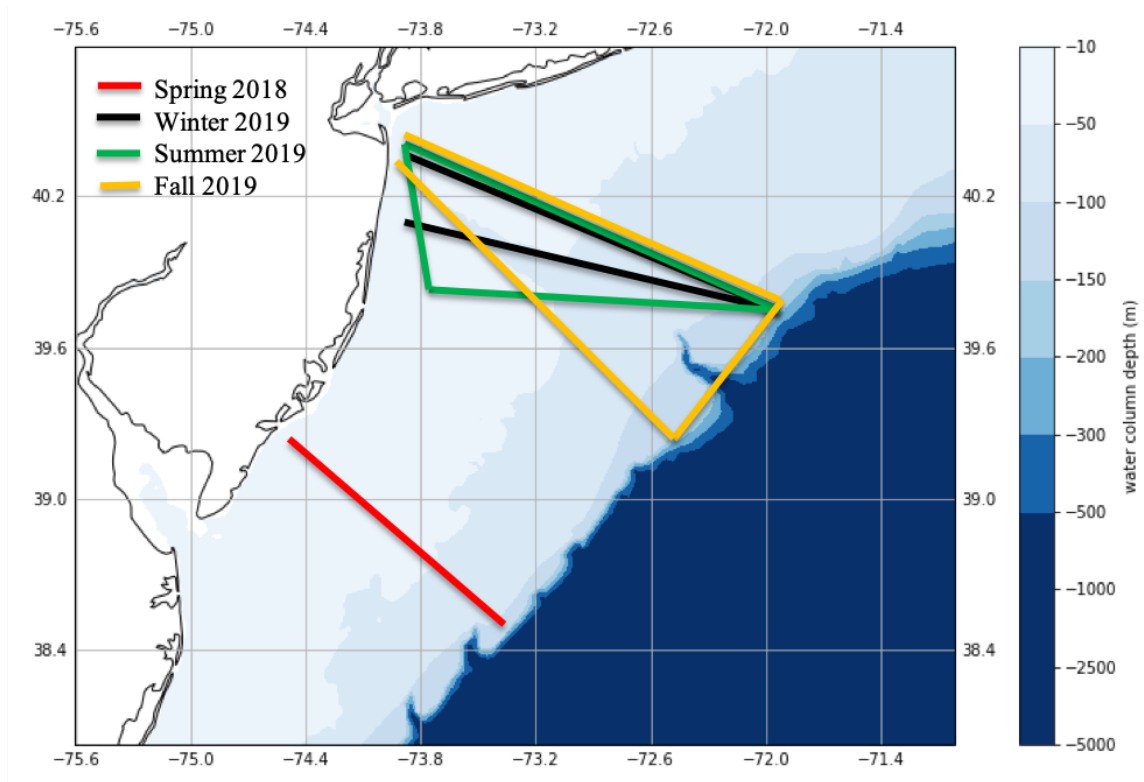


Figure 2.1: Seasonal glider deployments completed between May 2018 and November 2019.

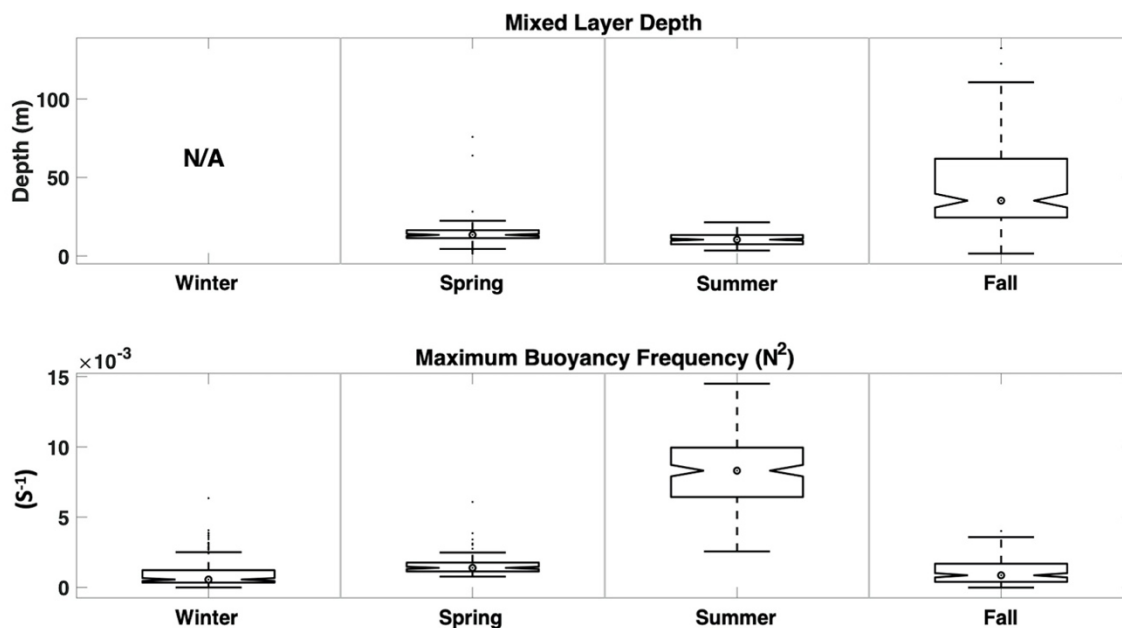


Figure 2.2: Comparisons of mixed layer depth (MLD) and maximum buoyancy frequency ($\max(N^2)$) during seasonal glider deployments. Targets indicate median values, box limits indicate the 25th-75th percentiles, and whiskers represent the full range of data. Data points beyond 1.5 times the interquartile range away from the top or bottom of the box were identified as outliers, and are shown as black dots extending from the whiskers. Notches depict the 95% confidence interval around the median. If notches do not overlap, there is 95% confidence that the medians are different ($p < 0.05$). Winter had a well-mixed water column with insignificant MLD QI values; thus, no data is shown for winter MLD.

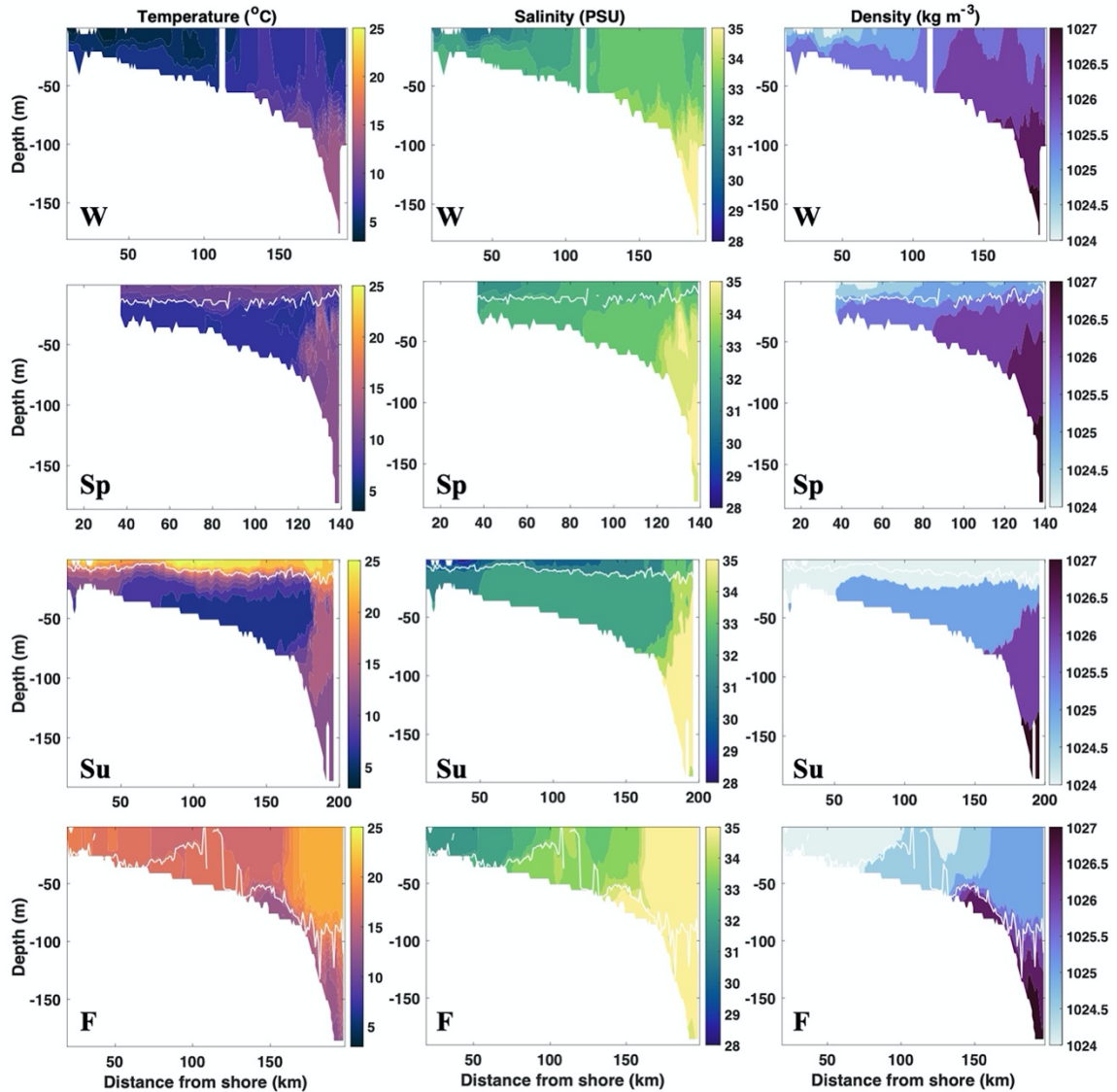


Figure 2.3: Contour plots of temperature, salinity, and density from four seasonal glider deployments in the MAB (W=winter, Sp=spring, Su=summer, F=fall). Data shown are from the first cross-shelf transect of each deployment. Mixed layer depth (MLD) for each binned profile is plotted in white. Winter had no significant mixed layer. The nearshore region was defined as 1-40 km offshore, midshelf was 40-160 km offshore (40-120 km in spring), and the shelf break was >160 km offshore (>120 km offshore in spring).

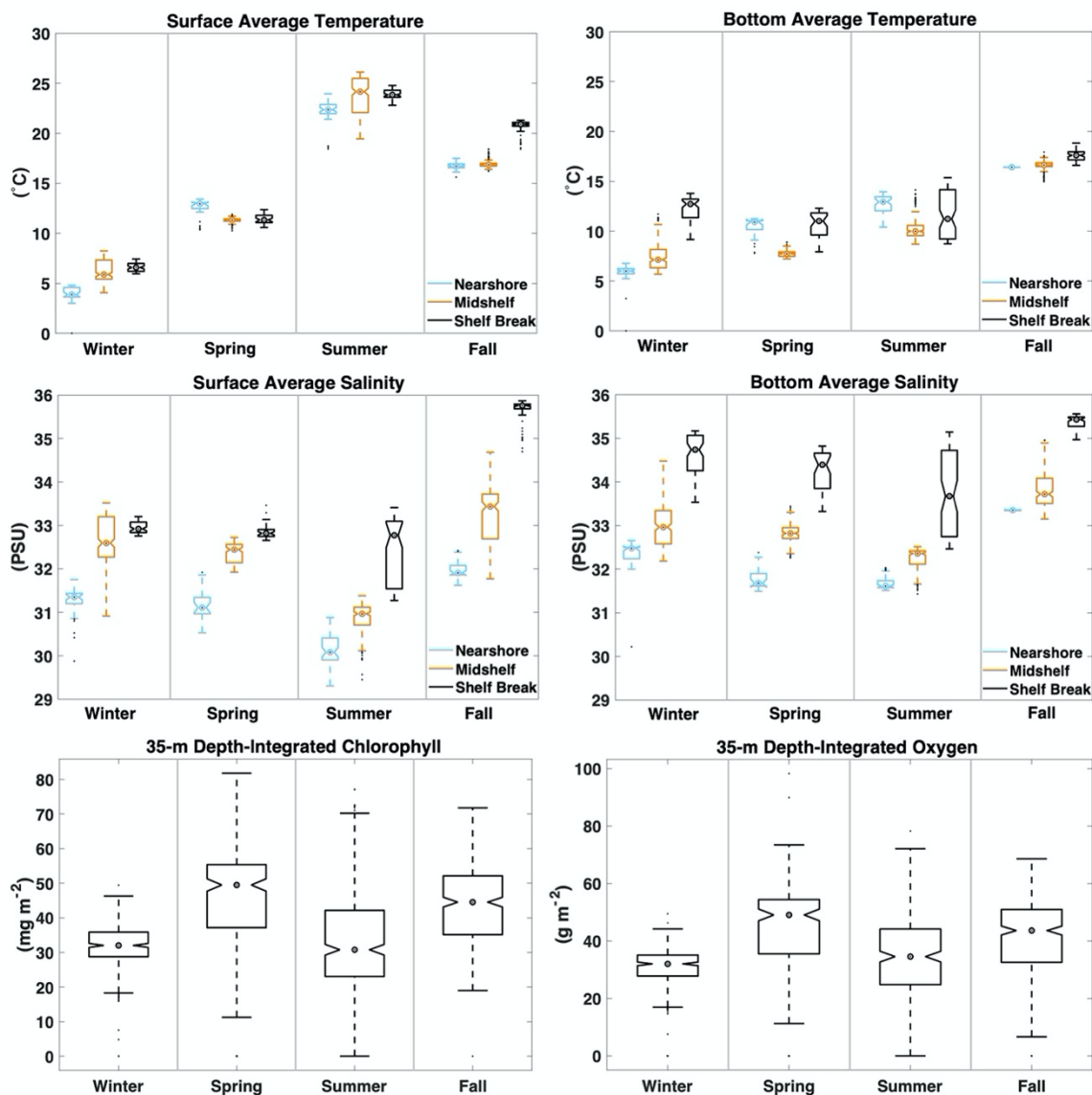


Figure 2.4: Comparisons of physical, biological, and chemical ocean properties during seasonal glider deployments. Targets indicate median values, box limits indicate the 25th-75th percentiles, and whiskers represent the full range of data. Data points beyond 1.5 times the interquartile range away from the top or bottom of the box were identified as outliers, and are shown as black dots extending from the whiskers. Notches depict the 95% confidence interval around the median. If notches do not overlap, there is 95% confidence that the medians are different ($p < 0.05$).

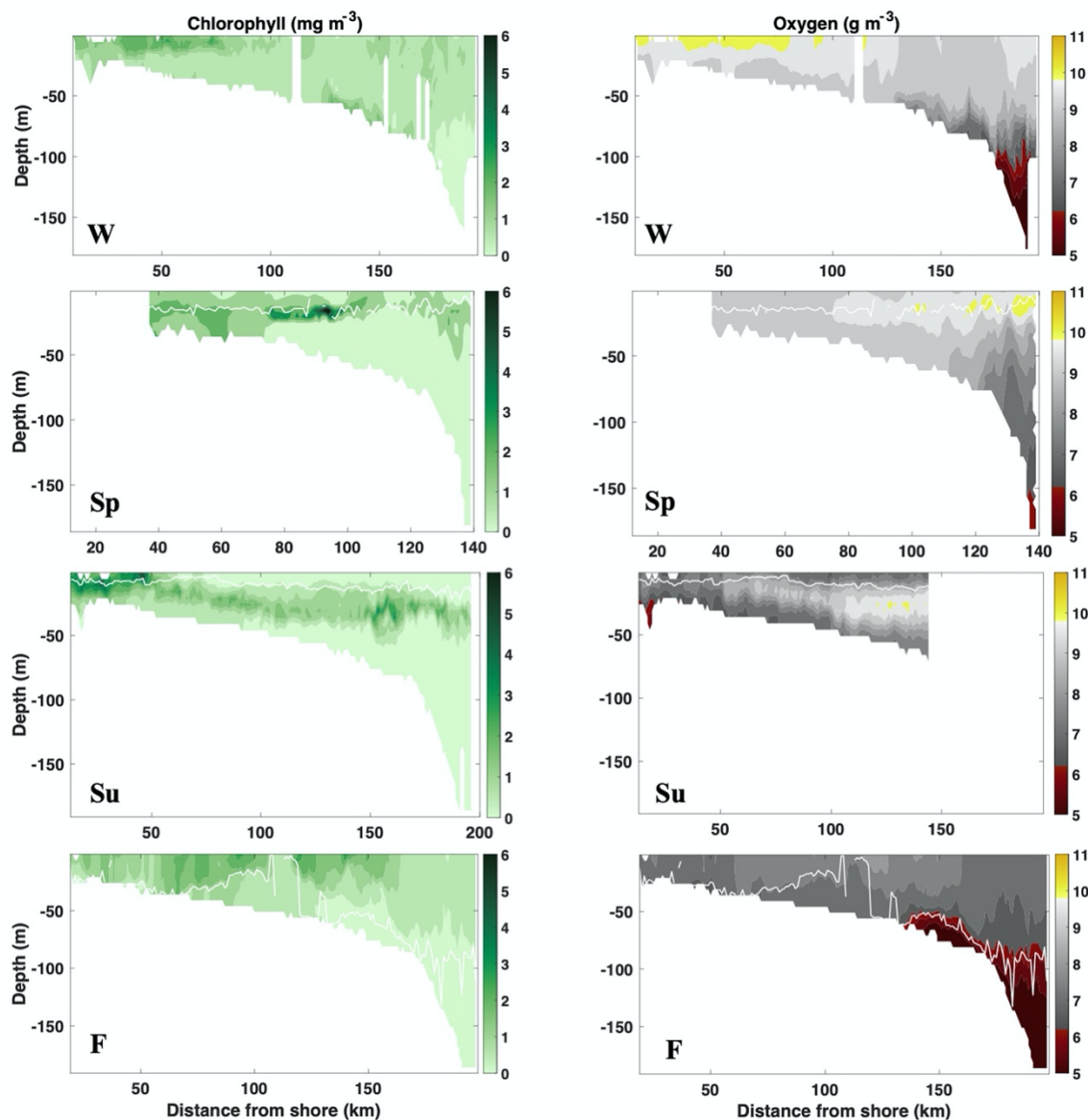


Figure 2.5: Contour plots of depth-averaged chlorophyll and oxygen from four seasonal glider deployments in the MAB (W=winter, Sp=spring, Su=summer, F=fall). Data shown are from the first cross-shelf transect of each deployment. Mixed layer depth (MLD) for each binned profile is plotted in white. Winter had no significant mixed layer. The nearshore region was defined as 1-40 km offshore, midshelf was 40-160 km offshore (40-120 km in spring), and the shelf break was >160 km offshore (>120 km offshore in spring).

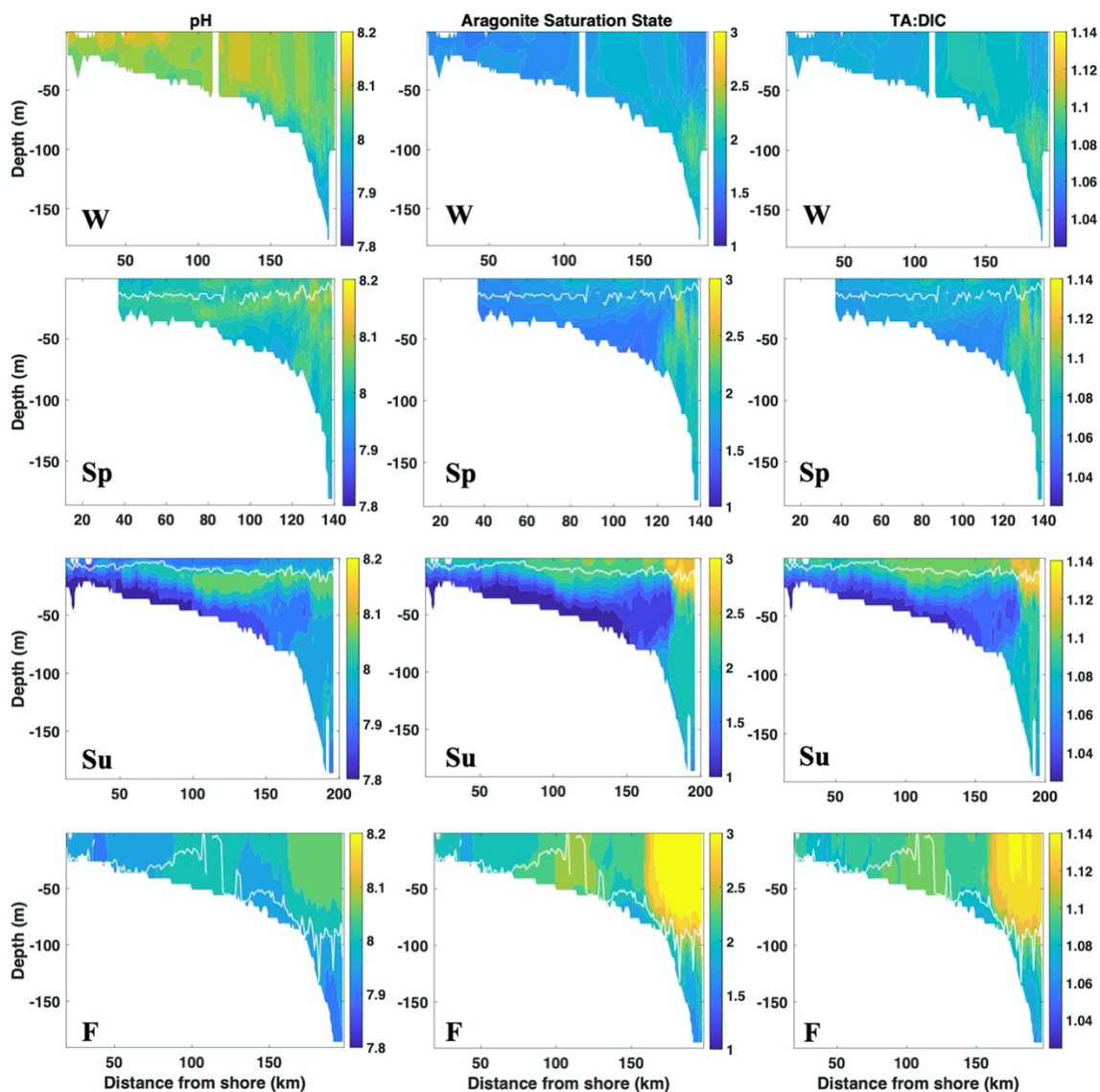


Figure 2.6: Contour plots of *in situ* pH, Ω_{arag} , and TA:DIC from four seasonal glider deployments in the MAB (W=winter, Sp=spring, Su=summer, F=fall). Data shown are from the first cross-shelf transect of each deployment. Mixed layer depth (MLD) for each binned profile is plotted in white. Winter had no significant mixed layer. The nearshore region was defined as 1-40 km offshore, midshelf was 40-160 km offshore (40-120 km in spring), and the shelf break was >160 km offshore (>120 km offshore in spring).

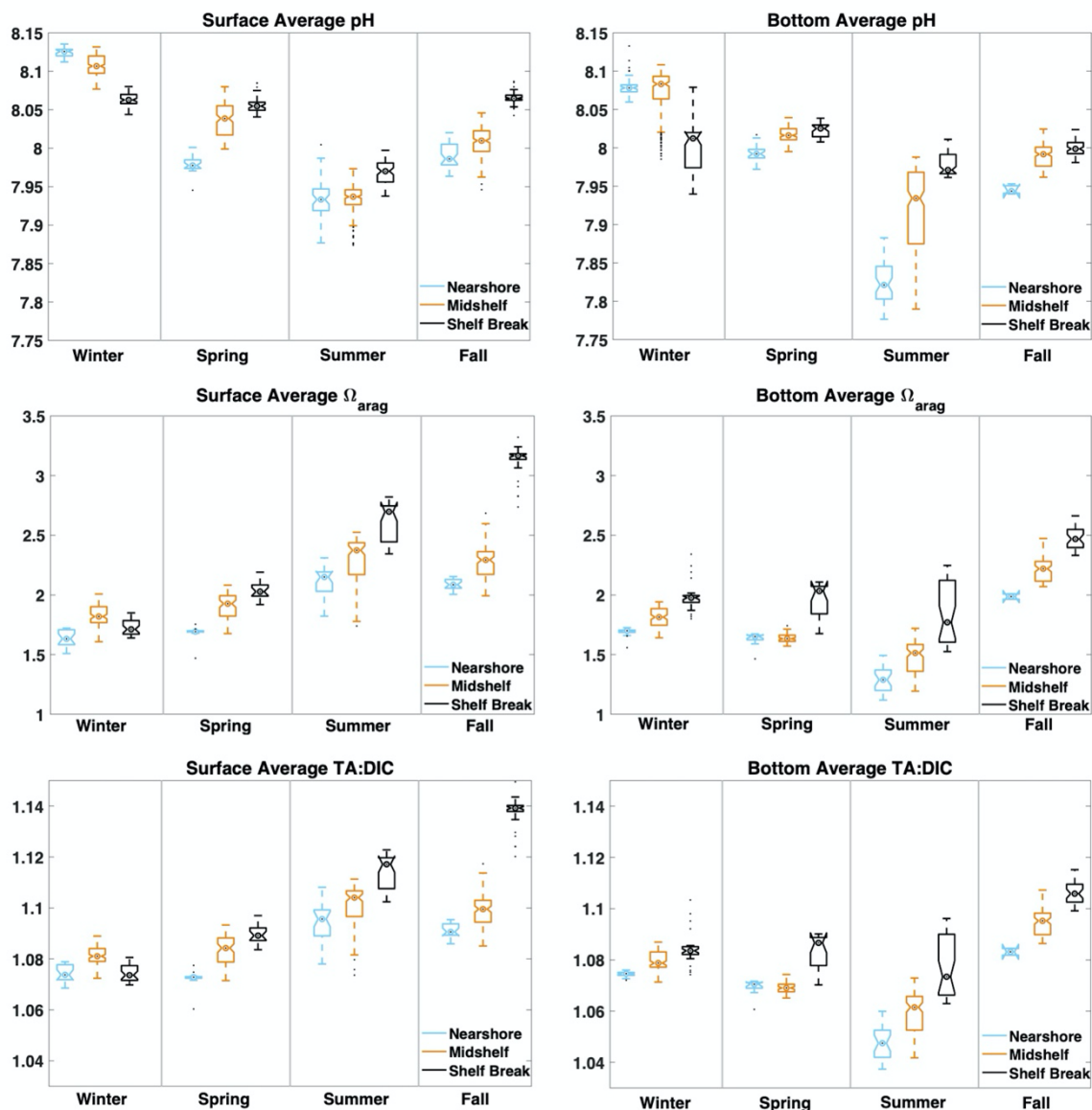


Figure 2.7: Comparisons of carbonate system parameters measured during and derived from seasonal glider deployments. Targets indicate median values, box limits indicate the 25th-75th percentiles, and whiskers represent the full range of data. Data points beyond 1.5 times the interquartile range away from the top or bottom of the box were identified as outliers, and are shown as black dots extending from the whiskers. Notches depict the 95% confidence interval around the median. If notches do not overlap, there is 95% confidence that the medians are different ($p < 0.05$).

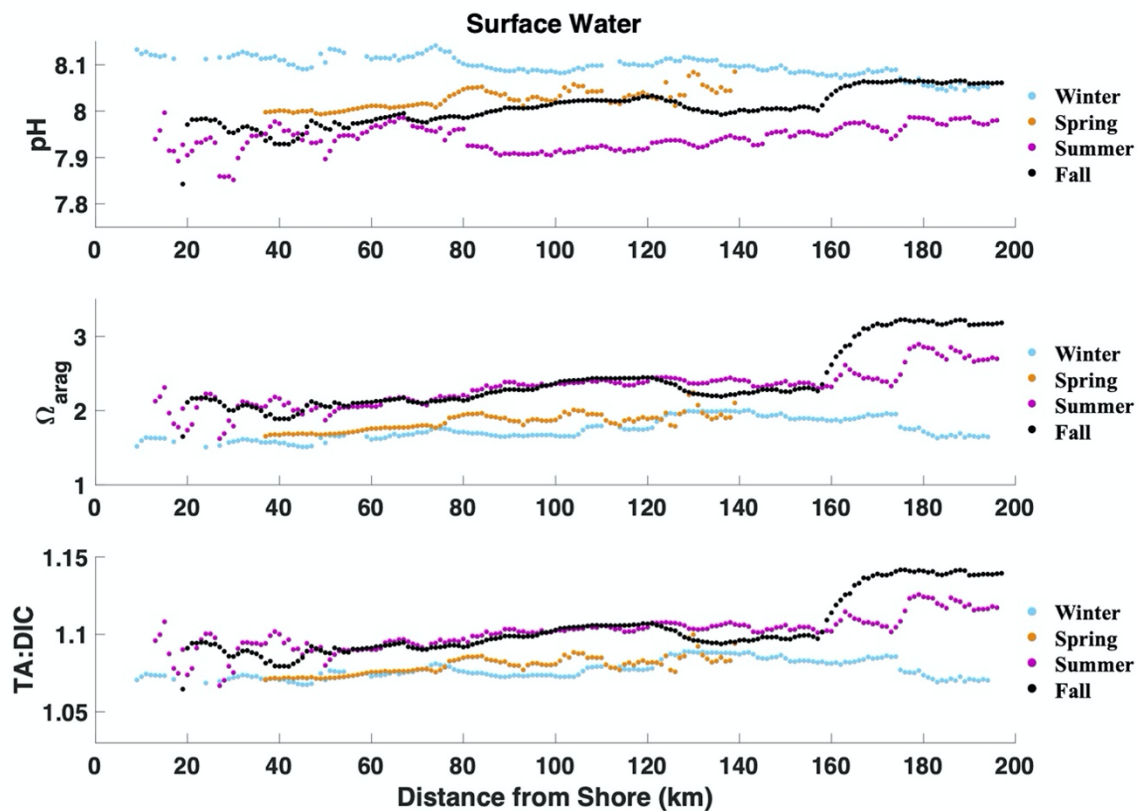


Figure 2.8: Seasonal differences in surface water pH (top), Ω_{arag} (middle), and TA:DIC (bottom) expressed as a function of distance from shore. Surface water is defined as above MLD in spring, summer, and fall, and as the top 5 m in winter. Data presented are from the entire deployment and are 1 m depth- and 1 km distance-binned.

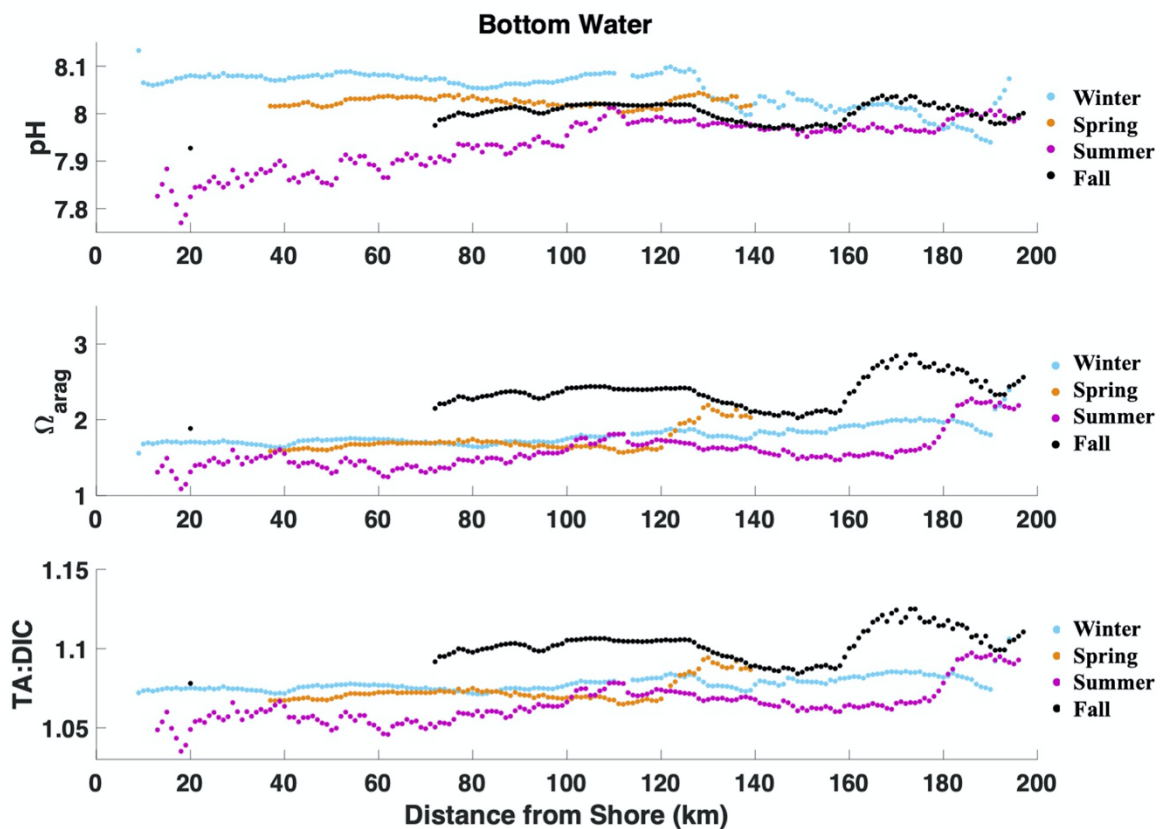


Figure 2.9: Seasonal differences in bottom water pH (top), Ω_{arag} (middle), and TA:DIC (bottom) expressed as a function of distance from shore. Bottom water is defined as below MLD in spring, summer, and fall, and as the bottom 5 m in winter. Data presented are from the entire deployment and are 1 m depth- and 1 km distance-binned.

2.10 Supplemental Text

For each seasonal deployment, a TA-salinity relationship was derived by taking a linear regression of salinity vs. TA as measured in discrete samples from glider deployment and/or recovery, and from the Mid-Atlantic sampling lines of the 2015 ECOA-1 cruise. Cruise samples taken at depths below 200 m were excluded. Analyzing samples from glider missions as well as the ECOA-1 cruise ensured that the regression accounted for the wide range of salinities seen in the nearshore and on the MAB shelf. Discrete sample values and regression lines can be found in figure S1. Uncertainty estimates for slope and intercept were calculated as the square root of the diagonal of the covariance matrix of the slope and intercept. The derived equations and corresponding uncertainties are as follows:

$$\text{Winter: TA} = 50.8010 \pm 0.4747 * \text{Salinity} + 539.7881 \pm 15.9347 \quad (1)$$

$$\text{Spring: TA} = 49.9494 \pm 0.4537 * \text{Salinity} + 572.5738 \pm 15.1615 \quad (2)$$

$$\text{Summer: TA} = 53.0125 \pm 0.6334 * \text{Salinity} + 463.2730 \pm 21.1890 \quad (3)$$

$$\text{Fall: TA} = 46.1700 \pm 0.7933 * \text{Salinity} + 698.0040 \pm 26.4727 \quad (4)$$

2.11 Supplemental Figures

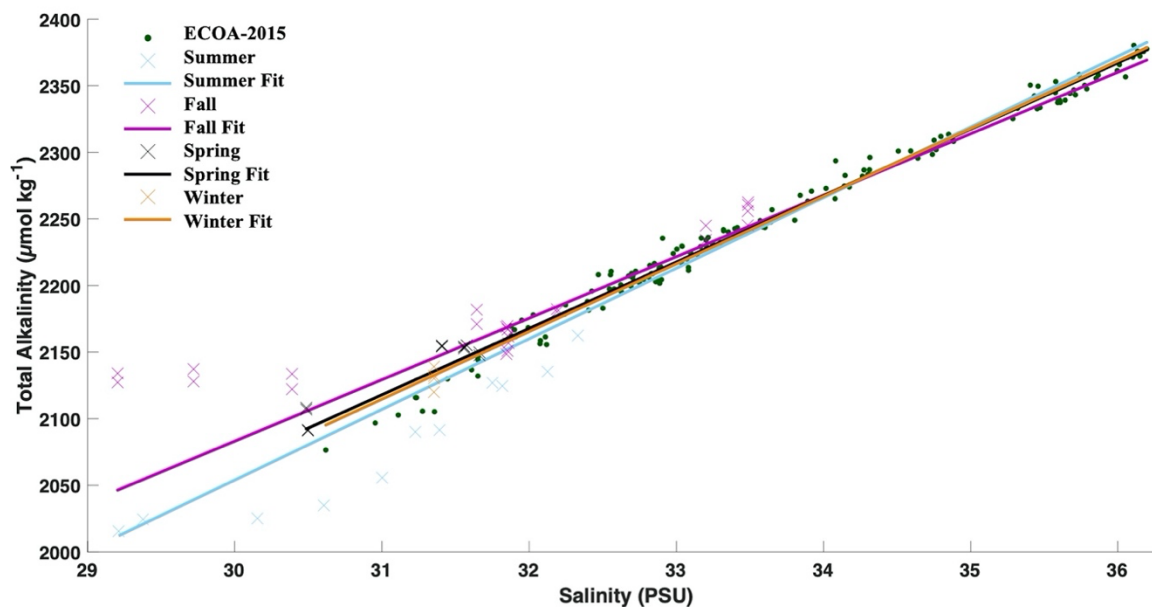


Figure S2.1 Discrete sample salinity vs. total alkalinity from the 2015 ECOA cruise and four seasonal glider deployments. ECOA-2015 samples were collected at a maximum of 200 m depth across the Mid-Atlantic shelf. Glider deployment samples were collected in the nearshore region during glider deployment and/or recovery in each season.

2.12 Supplemental Tables

Table S2.1 Average values of glider-measured and -derived variables, split up by deployment region and depth, from four seasonal missions. Values are shown as mean \pm one standard deviation. Surface water is defined as above MLD in spring, summer, and fall, and defined as the top 5 m in winter. Bottom water is defined as below MLD in spring, summer, and fall, and defined as the bottom 5 m in winter. The nearshore region stretches from 1-40 km offshore, while midshelf is 40-160 km offshore (40-120 km in spring), and the shelf break is >160 km offshore (>120 km offshore in spring).

Season, Region, and Depth	Temperature (°C)	Salinity (PSU)	Depth-Averaged Chlorophyll (mg m ⁻³)	Depth-Averaged Oxygen (g m ⁻³)	pH	Ω_{arag}	TA:DIC
Winter Nearshore Surface	3.98 \pm 0.51	31.14 \pm 0.43	1.36 \pm 0.28	10.37 \pm 0.07	8.124 \pm 0.007	1.64 \pm 0.07	1.075 \pm 0.003
Winter Nearshore Bottom	5.94 \pm 0.65	32.33 \pm 0.45	1 \pm 0.27	9.53 \pm 0.20	8.080 \pm 0.014	1.69 \pm 0.03	1.075 \pm 0.001
Winter Midshelf Surface	6.25 \pm 1.08	32.66 \pm 0.57	0.93 \pm 0.14	9.88 \pm 0.37	8.107 \pm 0.013	1.84 \pm 0.09	1.082 \pm 0.004
Winter Midshelf Bottom	7.47 \pm 1.54	33.03 \pm 0.53	0.9 \pm 0.13	8.86 \pm 0.78	8.072 \pm 0.030	1.81 \pm 0.08	1.080 \pm 0.004
Winter Shelf Break Surface	6.61 \pm 0.41	32.95 \pm 0.13	0.86 \pm 0.31	9.56 \pm 0.12	8.063 \pm 0.008	1.73 \pm 0.06	1.075 \pm 0.003
Winter Shelf Break Bottom	12.48 \pm 0.87	34.72 \pm 0.36	0.5 \pm 0.40	6.20 \pm 0.88	7.997 \pm 0.031	1.99 \pm 0.11	1.084 \pm 0.006
Spring Nearshore Surface	12.52 \pm 0.97	31.18 \pm 0.41	2.13 \pm 0.71	8.74 \pm 0.31	7.982 \pm 0.010	1.70 \pm 0.02	1.073 \pm 0.002

Table S2.1 Continued

Spring Nearshore Bottom	10.29 ± 1.19	31.80 ± 0.28	2.86 ± 0.49	8.83 ± 0.29	7.995 ± 0.010	1.65 ± 0.03	1.070 ± 0.001
Spring Midshelf Surface	11.33 ± 0.20	32.35 ± 0.24	1.20 ± 0.30	9.32 ± 0.30	8.037 ± 0.023	1.91 ± 0.10	1.084 ± 0.006
Spring Midshelf Bottom	7.73 ± 0.30	32.84 ± 0.25	1.40 ± 0.47	9.39 ± 0.08	8.018 ± 0.009	1.64 ± 0.04	1.069 ± 0.002
Spring Shelf Break Surface	11.42 ± 0.47	32.86 ± 0.17	0.84 ± 0.22	9.67 ± 0.20	8.058 ± 0.011	2.04 ± 0.07	1.090 ± 0.004
Spring Shelf Break Bottom	10.77 ± 1.30	34.29 ± 0.46	0.63 ± 0.15	8.20 ± 0.49	8.022 ± 0.007	1.96 ± 0.13	1.083 ± 0.006
Summer Nearshore Surface	22.42 ± 0.90	30.06 ± 0.37	2.30 ± 0.45	8.02 ± 0.44	7.933 ± 0.026	2.11 ± 0.12	1.094 ± 0.007
Summer Nearshore Bottom	12.53 ± 1.16	31.70 ± 0.17	1.43 ± 0.48	6.87 ± 0.29	7.827 ± 0.029	1.29 ± 0.11	1.048 ± 0.007
Summer Midshelf Surface	23.84 ± 1.79	30.87 ± 0.36	0.85 ± 0.95	7.82 ± 0.57	7.934 ± 0.016	2.30 ± 0.18	1.101 ± 0.008
Summer Midshelf Bottom	10.19 ± 1.05	32.27 ± 0.23	0.86 ± 0.23	8.24 ± 0.67	7.922 ± 0.053	1.47 ± 0.15	1.059 ± 0.009
Summer Shelf Break Surface	23.93 ± 0.45	32.45 ± 0.74	0.11 ± 0.04	N/A	7.969 ± 0.014	2.61 ± 0.16	1.114 ± 0.007
Summer Shelf Break Bottom	11.84 ± 2.31	33.80 ± 0.93	0.49 ± 0.19	N/A	7.979 ± 0.014	1.85 ± 0.26	1.078 ± 0.012
Fall Nearshore Surface	16.70 ± 0.28	31.99 ± 0.19	1.36 ± 0.26	7.32 ± 0.07	7.991 ± 0.014	2.09 ± 0.04	1.091 ± 0.003
Fall Nearshore Bottom	16.41 ± 0.00	33.35 ± 0.01	0.40 ± 0.02	6.71 ± 0.0	7.948 ± 0.008	1.99 ± 0.03	1.083 ± 0.002

Table S2.1 Continued

Fall Midshelf Surface	16.94 ± 0.32	33.29 ± 0.65	1.39 ± 0.19	7.55 ± 0.18	8.009 ± 0.016	2.29 ± 0.13	1.099 ± 0.006
Fall Midshelf Bottom	16.60 ± 0.47	33.86 ± 0.48	0.68 ± 0.23	7.06 ± 0.50	7.991 ± 0.014	2.22 ± 0.10	1.095 ± 0.005
Fall Shelf Break Surface	20.68 ± 0.70	35.66 ± 0.26	0.87 ± 0.18	7.08 ± 0.13	8.066 ± 0.006	3.13 ± 0.12	1.138 ± 0.006
Fall Shelf Break Bottom	17.57 ± 0.50	35.37 ± 0.17	0.33 ± 0.06	6.32 ± 0.36	8.000 ± 0.009	2.48 ± 0.09	1.107 ± 0.004

Table S2.2 Glider pH sensor agreement and field uncertainty (within-mixed-layer variability) during four seasonal deployments. Deployment agreement is the average absolute offset from discrete water samples taken at deployment and recovery and analyzed spectrophotometrically. Glider field uncertainty is calculated as the standard deviation of glider pH in surface waters during groundtruthing sample collection. Manufacturer specifications for this sensor are 0.05 accuracy (agreement) and 0.001 precision (uncertainty).

Season	Deployment Agreement	Deployment Uncertainty	Recovery Agreement	Recovery Uncertainty
Winter	0.005	0.007	0.010	0.001
Spring	0.016	0.005	0.012	0.001
Summer	0.027	0.022	0.039	0.027
Fall	0.026	0.011	0.042	0.001

Table S2.3 pH glider offsets at deployment and recovery during four seasonal deployments. Offsets are calculated as glider pH – discrete pH.

Date and Time (EST)	Depth (m)	Glider pH	Discrete pH	pH Offset (Glider-Discrete)
May 2, 2018, 10:15	0.5	7.945	7.977	-0.032
May 2, 2018, 10:18	0.5	7.945	7.975	-0.030
May 2, 2018, 10:20	0.5	7.945	7.976	-0.031
May 2, 2018, 10:34	11	7.947	7.938	0.009
May 2, 2018, 10:45	11	7.947	7.941	0.006
May 2, 2018, 10:52	11	7.947	7.942	0.005
May 2, 2018, 11:09	15	7.973	7.958	0.015
May 2, 2018, 11:15	15	7.973	7.972	0.001
May 2, 2018, 11:22	14	7.972	7.955	0.017
May 22, 2018, 09:48	0.5	8.010	8.026	-0.016
May 22, 2018, 09:52	0.5	8.010	8.024	-0.014
May 22, 2018, 10:02	9	7.988	8.001	-0.013
May 22, 2018, 10:04	9	7.988	8.002	-0.014
May 22, 2018, 10:12	23	7.987	7.998	-0.011
May 22, 2018, 10:15	23	7.987	7.993	-0.006
February 1, 2019, 11:55	1	8.131	8.127	0.004
February 1, 2019, 11:55	1	8.131	8.122	0.009
February 1, 2019, 11:55	1	8.131	8.135	-0.004
February 1, 2019, 11:55	1	8.131	8.130	0.001
February 19, 2019, 14:00	1	8.141	8.134	0.007
February 19, 2019, 14:00	1	8.141	8.129	0.012
February 19, 2019, 14:00	1	8.141	8.131	0.010
February 19, 2019, 14:00	1	8.141	8.129	0.012
February 19, 2019, 14:00	1	8.141	8.130	0.011
July 17, 2019, 11:06	1.07	7.968	7.987	-0.019

Table S2.3 Continued

July 17, 2019, 11:06	6.75	7.965	7.961	0.004
July 17, 2019, 11:05	13.62	7.980	8.022	-0.042
July 17, 2019, 11:05	20.59	7.819	7.823	-0.004
July 17, 2019, 11:05	25.40	7.774	7.751	0.023
July 17, 2019, 11:05	26.58	7.774	7.752	0.022
July 17, 2019, 14:13	0.61	7.969	7.991	-0.022
July 17, 2019, 14:13	6.98	7.944	8.010	-0.066
July 17, 2019, 14:13	9.67	7.905	7.870	0.035
July 17, 2019, 14:13	13.61	7.901	7.872	0.029
July 17, 2019, 14:13	20.62	7.795	7.757	0.038
July 17, 2019, 14:12	24.83	7.746	7.725	0.021
August 12, 2019, 12:13	1.05	7.993	8.040	-0.047
August 12, 2019, 12:13	6.65	7.960	7.993	-0.033
August 12, 2019, 12:12	9.56	7.911	7.974	-0.063
August 12, 2019, 12:12	13.51	7.905	7.908	0.003
August 12, 2019, 12:11	21.22	7.840	7.820	0.020
August 12, 2019, 12:10	27.61	7.836	7.771	0.065
October 15, 2019, 12:49	1.04	7.958	7.986	-0.028
October 15, 2019, 12:49	3.54	7.959	7.987	-0.028
October 15, 2019, 12:49	5.22	7.957	7.986	-0.029
October 15, 2019, 12:49	12.33	7.952	7.977	-0.025
October 15, 2019, 12:49	24.23	7.944	7.979	-0.035
October 15, 2019, 12:49	39.38	7.926	7.936	-0.010
November 6, 2019, 13:45	1.07	8.036	8.039	-0.003
November 6, 2019, 13:45	4.66	8.040	8.048	-0.008
November 6, 2019, 13:45	8.72	8.037	8.045	0.008
November 6, 2019, 13:45	14.54	8.025	7.994	0.031

Table S2.3 Continued

November 6, 2019, 13:45	20.02	8.008	7.907	0.101
November 6, 2019, 13:45	22.45	8.005	7.905	0.100

Table S2.4 Uncertainty in Ω_{arag} and TA:DIC measurements due to salinity-derived TA offsets. Ω_{arag} and TA:DIC were calculated using measured and predicted TA values for each discrete sample, and uncertainty was calculated as the difference between the two. The range of uncertainty in Ω_{arag} and TA:DIC due to TA offset is presented here along with the absolute average in uncertainty for each seasonal mission.

Metric	Winter	Spring	Summer	Fall
Absolute average of hybrid equation TA offsets ($\mu\text{mol kg}^{-1}$)	5.5	7.5	27.4	21.6
Ω_{arag} uncertainty due to TA offsets (range (absolute average))	-0.005 – 0.011 (0.005)	-0.011 – 0.005 (0.006)	-0.004 – 0.057 (0.024)	-0.083 – 0.020 (0.021)
TA:DIC uncertainty due to TA offsets (range (absolute average))	-0.0002 – 0.0001 (0.0001)	-0.0001 – 0.0002 (0.0001)	-0.0009 – 0.0001 (0.0004)	-0.0003 – 0.0013 (0.0003)

Table S2.5 A comparison of discrete sample TA and TA derived from a seasonal regression analysis of TA-salinity relationships. An equation was derived for each season individually by deriving a linear regression of salinity vs. TA as measured in discrete samples taken at glider deployment and/or recovery, and during the 2015 ECOA-1 cruise. Combining seasonal glider data with ECOA cruise data ensures that both nearshore and shelf TA-salinity relationships are represented, and that seasonal changes in the TA-salinity relationship are accounted for. Offsets are calculated as derived TA – discrete TA.

Season - Sample #	Depth (m)	Salinity (PSU)	Discrete TA ($\mu\text{mol kg}^{-1}$)	Hybrid Equation TA ($\mu\text{mol kg}^{-1}$)	TA Offset ($\mu\text{mol kg}^{-1}$)
Winter - 01	1	31.354	2139.0	2132.6	-6.4
Winter - 02	1	31.354	2119.9	2132.6	12.7
Winter - 03	1	31.354	2132.1	2132.6	0.5
Winter - 04	1	31.354	2130.2	2132.6	2.4
Spring - 01	0.5	31.663	2149.7	2154.1	4.4
Spring - 02	0.5	31.663	2149.8	2154.1	4.3
Spring - 03	0.5	31.663	2147.6	2154.1	6.5
Spring - 04	11	31.408	2154.3	2141.4	-12.9
Spring - 05	11	31.408	2154.1	2141.4	-12.7
Spring - 06	11	31.408	2155.0	2141.4	-13.6
Spring - 07	15	31.559	2153.8	2148.9	-4.9
Spring - 08	15	31.559	2154.1	2148.9	-5.2
Spring - 09	14	31.559	2152.7	2148.9	-3.8

Table S2.5 Continued

Spring - 10	0.5	30.498	2091.7	2095.9	4.2
Spring - 11	0.5	30.498	2091.0	2095.9	4.9
Spring - 12	9	30.487	2108.2	2095.4	-12.8
Spring - 13	9	30.487	2106.9	2095.4	-11.5
Spring - 14	23	31.577	2155.0	2149.8	-5.2
Spring - 15	23	31.577	2155.1	2149.8	-5.3
Summer - 01	1.07	29.211	2015.5	2011.8	-3.7
Summer - 02	6.75	29.377	2024.4	2020.6	-3.8
Summer - 03	13.62	31.228	2090.1	2118.7	28.6
Summer - 04	25.41	31.751	2126.9	2146.5	19.6
Summer - 05	26.58	31.819	2124.5	2150.1	25.6
Summer - 06	1.05	30.154	2025.1	2061.8	36.7
Summer - 07	6.65	30.606	2034.9	2085.8	50.9
Summer - 08	9.56	31.002	2055.7	2106.8	51.1
Summer - 09	13.51	31.392	2091.5	2127.4	35.9
Summer - 10	21.22	32.125	2135.3	2166.3	31.0
Summer - 11	27.61	32.331	2162.4	2177.2	14.8
Fall - 01	1.04	31.854	2150.9	2168.7	17.8
Fall - 02	1.04	31.854	2169.6	2168.7	-0.9
Fall - 03	3.54	31.855	2162.2	2168.7	6.5
Fall - 04	3.54	31.855	2167.0	2168.7	1.7
Fall - 05	5.22	31.846	2168.8	2168.3	-0.5
Fall - 06	5.22	31.846	2148.5	2168.3	19.8

Table S2.5 Continued

Fall - 07	12.33	31.860	2156.7	2169.0	12.3
Fall - 08	12.33	31.860	2161.5	2169.0	7.5
Fall - 09	24.23	32.189	2182.2	2184.2	2.0
Fall - 10	24.23	32.189	2180.3	2184.2	3.9
Fall - 11	39.38	33.200	2234.2	2230.8	-3.4
Fall - 12	39.38	33.200	2244.9	2230.8	-14.1
Fall - 13	1.07	29.205	2127.2	2046.4	-80.8
Fall - 14	1.07	29.205	2134.0	2046.4	-87.6
Fall - 15	4.66	29.721	2127.9	2070.2	-57.7
Fall - 16	4.66	29.721	2137.2	2070.2	-67.0
Fall - 17	9.72	30.389	2133.6	2101.1	-32.5
Fall - 18	9.72	30.389	2122.1	2101.1	-21.0
Fall - 19	14.54	31.645	2181.8	2159.1	-22.7
Fall - 20	14.54	31.645	2171.0	2159.1	-11.9
Fall - 21	20.02	33.485	2255.8	2244.0	-11.8
Fall - 22	20.02	33.485	2245.2	2244.0	-1.2
Fall - 23	22.45	33.487	2260.6	2244.1	-16.5
Fall - 24	22.45	33.487	2262.5	2244.1	-18.4

Table S2.6 Full water column glider-measured and -derived carbonate system parameters from four seasonal missions. Maximums, minimums, and averages were calculated over the entire course of deployment. Averages are reported as mean value \pm one standard deviation.

Metric	Winter	Spring	Summer	Fall
Maximum pH	8.138	8.144	8.104	8.166
Minimum pH	7.939	7.928	7.701	7.889
Average pH	8.088 \pm 0.009	8.018 \pm 0.012	7.927 \pm 0.016	8.004 \pm 0.015
Maximum Ω_{arag}	2.40	2.34	3.17	3.72
Minimum Ω_{arag}	1.47	1.43	0.83	1.70
Average Ω_{arag}	1.81 \pm 0.05	1.75 \pm 0.06	1.68 \pm 0.08	2.32 \pm 0.17
Maximum TA:DIC	1.107	1.114	1.142	1.180
Minimum TA:DIC	1.068	1.058	1.019	1.069
Average TA:DIC	1.080 \pm 0.002	1.075 \pm 0.003	1.069 \pm 0.004	1.100 \pm 0.009

CHAPTER 3: Quantification of the Dominant Drivers of Acidification in the Coastal
Mid-Atlantic Bight*

* This Chapter is in preparation for submission to the Journal of Geophysical Research: Oceans as “Wright-Fairbanks, E.K. and Saba, G.K. Quantification of the Dominant Drivers of Acidification in the Coastal Mid-Atlantic Bight.”

3.1 Abstract

In shallow coastal shelves like the Mid-Atlantic Bight (MAB), ocean acidification due to increased atmospheric CO₂ is compounded by highly variable coastal processes including riverine freshwater inputs, nutrient loading, biogeochemical influence, coastal currents and water mass mixing, and seasonal transitions in physical parameters. Past deconstructions of carbonate system drivers in the MAB have focused on nearshore zones or single season data, and thus lack the spatial and temporal resolution required to assess impacts to important species occupying the shelf. Deconstructing highly resolved data collected during four seasonal Slocum glider deployments in the MAB, this study uses a Taylor Series decomposition to quantify the influence of temperature, salinity, biogeochemical activity, and water mass mixing on pH and aragonite saturation state from sea surface to bottom. Results show that water mass mixing and biogeochemical activity were the most significant drivers of the carbonate system in the MAB. Nearshore water was more acidic year-round due to riverine freshwater input, but photosynthesis reduced acidity at certain depths and times. Intense stratification and respiration of organic material increased acidity in bottom water on the shelf, particularly in summer. Gulf Stream intrusions at the shelf break during fall acted to mitigate acidification on the shelf in habitats occupied by carbonate-bearing organisms. The relationships quantified here can be used to improve biogeochemical forecast models and determine habitat suitability for commercially important fin and shellfish species residing in the MAB.

3.2 Introduction

Ocean acidification, caused by increasing levels of anthropogenic CO₂ in the atmosphere, is a complex chemical issue that alters the marine carbonate system (Doney et al., 2009; Orr et al., 2005) and threatens calcifying and non-calcifying organisms (Doney et al., 2020; Doney et al., 2009; Kroeker et al., 2013; Saba et al., 2019a). Ocean acidification has caused measured declines in global ocean pH and the saturation state of aragonite, Ω_{arag} , the soluble form of calcium carbonate used by many marine calcifying organisms. Global open ocean surface pH has decreased by 0.05-0.08 over the last 3 decades (Gledhill et al., 2015; IPCC, 2019) and is projected to continue declining by up to 0.29 pH units over the course of the 21st century (IPCC, 2019; RCP8.5). Global open ocean Ω_{arag} is decreasing at unprecedented rates, and variability in Ω_{arag} is outside the bounds of natural variability, indicating that anthropogenic activity is driving this change (Sutton et al., 2016).

The focus area in this study is the Mid-Atlantic Bight (MAB), which is located within the U.S. Northeast Shelf Large Marine Ecosystem. The MAB has been identified as a net CO₂ sink, meaning it absorbs CO₂ on an annual basis and is therefore subject to acidification patterns observed globally (DeGrandpre et al., 2002). In coastal shelves like the MAB, ocean acidification is influenced by coastal processes such as riverine freshwater input, biological growth and decay, upwelling, changes in temperature and water column structure, and interactions between coastal currents (Cai et al., 2020; Gledhill et al., 2015; Saba et al., 2019a; Samantha A. Siedlecki et al., 2021; S. A. Siedlecki et al., 2021; Wootton et al., 2008). These processes affect acidification on timescales from minutes to years (Runcie et al., 2018; Xu et al., 2017; Xu et al., 2020).

Riverine and estuarine waters feeding into the MAB shelf are lower in salinity and total alkalinity (TA) than seawater, and therefore are more acidic (Kwiatkowski & Orr, 2018). Consequently, surface water where rivers meet the ocean have lower pH and Ω_{arag} than surface seawater further offshore (Cai et al., 2020; Saba et al., 2019b; Wright-Fairbanks et al., 2020). Rivers also deliver nutrients to the coastal zone, supporting phytoplankton blooms that lead to uptake of CO₂ and increased pH in the surface ocean, followed by the release of CO₂ and decreased pH in bottom waters when biological material sinks and is respired (Cai et al., 2011; Wright-Fairbanks et al., 2020). Seasonal stratification in the MAB is significant and traps a subsurface water mass (the Cold Pool) on the shelf in the spring and summer (Chen et al., 2018; Houghton et al., 1982; Saba et al., 2019b; Wright-Fairbanks et al., 2020). Lack of ventilation between the Cold Pool and the atmosphere during seasonal stratification likely traps respired CO₂ in this subsurface water, contributing to a decline in pH and Ω_{arag} from spring through summer. Wright-Fairbanks et al. (2020) reported seasonal changes in the MAB carbonate system, suggesting potential links to seasonal stratification in the spring and summer, thermodynamic equilibrium and air-sea gas exchange in near-surface waters, seasonal subsurface phytoplankton blooms, freshwater riverine inputs and precipitation in the nearshore, and the influence of slope water at the shelf break. However, these relationships were not quantitatively evaluated.

Drivers of the carbonate system have been investigated at various resolutions in the MAB and nearby Gulf of Maine, but due to a lack of sufficient data, none have quantified drivers over highly resolved space on a seasonal scale. On a decadal scale, interactions between the northward-flowing Gulf Stream and southward-flowing

Labrador Current have been shown to influence MAB shelf water properties, including the carbonate system, as they intersect offshore (Grotsky et al., 2017; Saba et al., 2016; Salisbury & Jonsson, 2018; Wanninkhof et al., 2015). The Gulf Stream is warm, salty, and characterized by high pH and Ω_{arag} , while the Labrador Current is cold, fresher, and has lower pH and Ω_{arag} (Grotsky et al., 2017; Saba et al., 2016; Salisbury & Jonsson, 2018; Wanninkhof et al., 2015). Additionally, seasonal temperature and salinity cycles in the MAB can influence regional pH and Ω_{arag} (Cai et al., 2020; Richaud et al., 2016). Monthly sampling programs along shelf and embayment transects have provided physical, biological, and chemical data in surface, bottom, and mid-depth water (10-50 m resolution) (Boehme et al., 1998; Rheuban et al., 2019; Wang et al., 2016). These sampling programs have high temporal resolution, capturing all seasons over multiple years, but lack spatial resolution across the shelf. Conversely, multiple major cruise campaigns (GOMECC-1, 2, ECOA-1, 2) have conducted carbonate chemistry sampling on cross-shelf transects in the MAB from sea surface to the bottom (10-100 m resolution) (Cai et al., 2020; Xu et al., 2017; Xu et al., 2020), but occur every few years and most often in the summer, therefore lacking critical seasonal resolution.

In this study, we quantified the drivers of pH and Ω_{arag} from sea surface to bottom using data from four seasonal deployments of a Teledyne-Webb Slocum G2 glider. The glider is an autonomous underwater vehicle (AUV), equipped with a recently developed ISFET-based pH sensor. Along with pH, the glider collects high resolution measurements of salinity, temperature, depth, dissolved oxygen, and optical properties (e.g., chlorophyll *a* and backscatter), allowing the quantification of carbonate system drivers as they vary seasonally and over space and depth. It is imperative to understand

the interactions between drivers of the coastal marine carbonate system in order to accurately predict and mitigate the effects of acidification on coastal ecosystems. High resolution data is necessary to detect fine-scale changes in the carbonate system that occur due to biogeochemical and physical influence, especially in the highly dynamic coastal shelf.

3.3 Materials and Methods

3.3.1 Dataset Description

Data were obtained from four seasonal glider missions throughout the New Jersey coastal shelf over the course of two years (spring 2018, summer 2019, fall 2019, and winter 2019; Figure 3.1; data available at: <http://slocum-data.marine.rutgers.edu/erddap/search/index.html?page=1&itemsPerPage=1000&searchFor=ru30>). During each deployment, the glider was equipped with a deep ISFET-based pH sensor integrated into a pumped CTD port located in the glider's science bay (Saba et al., 2019b). Additional sensors included an Aanderaa oxygen optode and a Sea-Bird Scientific BB2FL ECO puck used to measure chlorophyll fluorescence, CDOM, and optical backscatter. Concurrent measurements from the glider sensors provided high temporal (0.5 Hz sampling) and spatial (<1 m depth, ~270 profiles over 20 km per day) resolution measurements of biological, physical, and chemical ocean properties over four seasons. Efforts taken to ensure glider sensor data quality were described by Wright-Fairbanks et al. (2020). pH sensor accuracy and field uncertainty were better than ± 0.05 pH units and ± 0.001 pH units, respectively, for these deployments (Wright-Fairbanks et al., 2020).

Gliders-measured variables were used to resolve the marine carbonate system. pH on the total scale was calculated using glider-measured pH reference voltage, temperature, salinity, and pressure. TA was calculated from measured salinity based on season-specific linear relationships between TA and salinity in the Mid-Atlantic Bight (Wright-Fairbanks et al., 2020). Discrete samples used to derive TA-salinity relationships spanned depths from 0-200 m along the MAB shelf, which is the space covered by these glider deployments. Seasonal TA-salinity regressions were:

$$\text{Winter: TA} = 50.8010 \pm 0.4747 * \text{Salinity} + 539.7881 \pm 15.9347 \quad (1)$$

$$\text{Spring: TA} = 49.9494 \pm 0.4537 * \text{Salinity} + 572.5738 \pm 15.1615 \quad (2)$$

$$\text{Summer: TA} = 53.0125 \pm 0.6334 * \text{Salinity} + 463.2730 \pm 21.1890 \quad (3)$$

$$\text{Fall: TA} = 46.1700 \pm 0.7933 * \text{Salinity} + 698.0040 \pm 26.4727 \quad (4)$$

These seasonal TA-salinity regressions are comparable to previously derived regressions. Hunt et al. (2021) derived winter, spring, and summer TA-salinity equations using surface samples from eight cruises in 2017 and 2018 that were equipped with an underway TA analyzer. Their equations had lower slopes (winter: 40.8, spring: 44.1, summer: 14.5) and higher endmember TA values (winter: 880, spring: 763, summer: 1726) than those used here. Cai et al. (2010) derived a MAB TA-salinity relationship using full water column samples from GOMECC and OMP cruise campaigns, which resulted in a slope of 46.6 and endmember TA of 767.6. Brodeur et al. (2019) utilized a TA-salinity relationship from ECOA-1 data, similar to the equations derived here, with a slope of 47.69 and endmember TA value of 640.77. Endmember TA values used in this study are slightly lower than previous studies, likely reflecting samples taken near the Raritan and Hudson River outflows, which are an important component of the study area.

pH and TA were used as inputs into CO2SYS for MATLAB (v3.0); Lewis and Wallace, 1998; Orr et al., 2018; van Heuven et al., 2011), along with glider temperature, salinity, and pressure, K1 and K2 constants (Mehrbach et al., 1973) with refits (Dickson & Millero, 1987), KSO_4 constant (Dickson, 1990), KHF dissociation constant (Perez & Fraga, 1987), and borate-to-salinity ratio (Uppstrom, 1974). Variables derived from the CO2SYS program and used in this study were Ω_{arag} , hydrogen ion concentration ($[\text{H}^+]$), and DIC.

3.3.2 Definition of Spatial and Depth Regions

Each seasonal deployment was divided into three spatial and two or three depth regions. Spatial regions were determined based on the distance of the glider from a shore point near the deployment location. In winter, summer, and fall, the shore point was Sandy Hook, New Jersey and in spring, the shore point was Atlantic City, New Jersey. The nearshore region was defined as 0-40 km from the shore point, midshelf was defined as 40-160 km from shore (40-120 km in spring), and the shelf break was defined as >160 km from shore (>120 km in spring), which is beyond the continental shelf. Depth regions were defined as near-surface, subsurface, and deep. Near-surface water was considered to be above the mixed-layer depth, while subsurface water was below the mixed-layer. In winter, which exhibited a well-mixed water column, pseudo-surface and -bottom regions were defined as the top 5 and bottom 5 meters of the water column. Defining these regions in winter allowed consistent analyses of all seasons.

Deep water was identified based on the relationship between depth and sensitivity of carbonate system parameters to changes in driver variables. In a season, all drivers exhibited a change in this relationship at similar depths, indicating differential driver

influence beginning at that depth (Supplemental Figure S3.1). Breaks in the slope of these relationships are indicative of deep water mass influence and occurred most often in the deepest water in the midshelf or shelf break in spring, summer, and fall. Additionally, deep water had distinctively different temperature (colder) and salinity (saltier) than subsurface and near-surface water. Overall, 29 seasonal, spatial, and depth regions were defined (Table 3.1).

3.3.3 First-Order Taylor Series Decomposition of Ω_{arag} and pH

The mathematical influence of four driver variables (temperature (T), salinity (S), TA, and dissolved inorganic carbon (DIC)) on two output variables (Ω_{arag} and pH) was demonstrated using a first-order Taylor Series Decomposition, which has been used previously for similar data sets (Kwiatkowski & Orr, 2018; Rheuban et al., 2019; Wang et al., 2016; Xu et al., 2020). The Taylor Series method is applicable to ocean water, where metrics like DIC, pCO_2 , and carbonate saturation sensitivity aren't affected by low salinity extremes (Cai et al., 2021).

Anomalies in output variables Y (ΔY) were calculated for each sample compared to a reference value Y_0 .

$$\Delta Y = Y - Y_0 \quad (5)$$

where

$$Y_0 = Y(\bar{T}, \bar{S}, \bar{TA}, \bar{DIC}) \quad (6)$$

and \bar{X} represents the mean value of input variables X in the reference condition (X_{ref}).

Here, two analyses are run with different X_{ref} definitions. Analysis 1 defines \bar{X} in one depth region throughout a deployment's full spatial extent (e.g., mean TA in fall near-surface water). Analysis 2 defines \bar{X} in one depth/spatial region throughout all

seasonal deployments (e.g., annual mean TA in nearshore near-surface water). Analysis 1 allows for quantification of spatial variability in carbonate system drivers in each season, while Analysis 2 quantifies the relative importance of drivers over an annual cycle.

A first-order Taylor Series defines the anomaly of an output variable as the sum of driver variable anomalies multiplied by the sensitivity of the output variable Y to changes in each driver variable X .

$$\Delta Y = \sum \frac{\partial Y}{\partial X} \Delta X \quad (7)$$

ΔX is computed as $X - X_{ref}$, where X is the sample value and X_{ref} is calculated using Analysis 1 or Analysis 2, as described above. Sensitivities are multiplied by ΔX , then summed (Equations 8 and 9).

$$\Delta pH = \frac{\partial pH}{\partial T} \Delta T + \frac{\partial pH}{\partial S} \Delta S + \frac{\partial pH}{\partial TA} \Delta TA + \frac{\partial pH}{\partial DIC} \Delta DIC + \epsilon \quad (8)$$

$$\Delta \Omega_{arag} = \frac{\partial \Omega_{arag}}{\partial T} \Delta T + \frac{\partial \Omega_{arag}}{\partial S} \Delta S + \frac{\partial \Omega_{arag}}{\partial TA} \Delta TA + \frac{\partial \Omega_{arag}}{\partial DIC} \Delta DIC + \epsilon \quad (9)$$

The sensitivities of Ω_{arag} and H^+ to temperature, salinity, TA, and DIC

($\frac{\partial Y}{\partial T}$, $\frac{\partial Y}{\partial S}$, $\frac{\partial Y}{\partial TA}$, and $\frac{\partial Y}{\partial DIC}$) were derived explicitly using the `derivnum.m` subroutine of CO2SYS (v.3.0) (Lewis & Wallace, 1998; Orr et al., 2018; Sharp et al., 2020; van Heuven et al., 2011). The `derivnum.m` subroutine calculates partial derivatives of output variables to two carbonate inputs (here, TA and DIC), temperature, salinity, nutrients, ammonium, hydrogen sulfide, dissociation constants, and total boron by introducing a small perturbation in one input variable and determining the change in each output variable as calculated using CO2SYS. H^+ sensitivities were used to calculate pH anomalies according the established relationship between the two variables (Equation 10). Error propagation through CO2SYS caused error in Ω_{arag} of ~ 0.1 and error in H^+ of

~0.001, but this error should not affect the relative magnitude of each driver in the sensitivity analysis.

$$pH = -\log[H^+] \quad (10)$$

Results from this analysis are reported as the numerical influence of each driver variable on each output variable (i.e., the value of $\frac{\partial Y}{\partial X} \Delta X$). For example, the influence of temperature on pH ($\frac{\partial pH}{\partial T} \Delta T$) is discussed as ΔpH_T and the influence of salinity on $\Delta \Omega_{arag}$ ($\frac{\partial \Omega_{arag}}{\partial S} \Delta S$) is discussed as $\Delta \Omega_S$. These terms allow a comparison of the relative influence of each driver on each output variable. A negative ΔY_X indicates that X acts to decrease Y relative to the mean and a positive ΔY_X indicates that X increases Y.

Marine TA and DIC are altered by biogeochemical processes such as photosynthesis, respiration, CaCO_3 dissolution and precipitation, physical mixing of water masses, and air-sea gas exchange (DIC only). The influence of air-sea gas exchange in each season was assessed by simulating changes in mixed layer $p\text{CO}_2$ and DIC assuming air-sea flux was the only driver of change. Disequilibrium in $p\text{CO}_2$ between the sea surface and atmosphere was calculated using seasonal average sea surface temperature, salinity, and $p\text{CO}_2$ as measured or estimated in glider deployments, mixed layer depth in each season, and an estimate of atmospheric $p\text{CO}_2$ (403 ppm). $p\text{CO}_2$ disequilibrium and seasonal average wind speed were used to quantify the changes in $p\text{CO}_2$ and DIC caused by gas exchange and the half-life of equilibrium time. The half-life of equilibration time is determined as the time it takes to reach the halfway point between air and sea $p\text{CO}_2$. Full equilibration time, or the time it takes to reach equilibrium between atmospheric and sea surface $p\text{CO}_2$, is represented by an asymptotic function and is therefore difficult to quantify.

In spring and fall, changes in $p\text{CO}_2$ and DIC were small ($<3 \mu\text{atm}$ and $<2 \mu\text{mol/kg}$), therefore air-sea gas exchange was minor. In winter, $p\text{CO}_2$ and DIC changed significantly but the half-life of equilibration time was 146 days, indicating that gas exchange was minor at a seasonal time scale. Summer showed significant changes in $p\text{CO}_2$ and DIC at a seasonal scale (half-life of equilibration = 46 days), indicating significant air-sea exchange. Therefore, gas exchange is considered in the analysis of summer surface water but excluded in the remaining seasons and regions.

The sensitivity of output variables to biogeochemical (BGC), mixing (MIX), and gas exchange influence were calculated based on changes in TA and DIC. Along the western Atlantic coast, TA is dominated by two-endmember mixing between riverine inputs and coastal seawater (Cai et al., 2010; Jiang et al., 2014). Non-mixing factors that might also influence TA include carbonate dissolution, calcification, and denitrification. There was little evidence of carbonate dissolution or calcification in any season (Figure 3.2). Denitrification in sediments has been shown to occur in the MAB, altering TA and therefore air-sea gas exchange (Fennel et al., 2008; Seitzinger, 1998; Seitzinger & Giblin, 1996). The seasonal glider data sets do not include nutrient measurements, so it is difficult to identify areas of potential denitrification. However, air-sea gas exchange was minimal in all seasons except summer, and therefore denitrification likely had little effect on the system via changes in TA. Any changes would have to disperse throughout the entire water column, dampening their effects. Additionally, conditions in the water column were not optimal for denitrification due to sufficient oxygen levels. Thus, changes in TA (ΔTA) were attributed solely to water mass mixing.

In order to separate changes in DIC due to biogeochemistry, air-sea gas exchange, and mixing, DIC was normalized following the method of Friis et al. (2003),

$$nDIC = \frac{DIC_{spl} - DIC_{Sal=0}}{Sal_{spl}} * Sal_{ref} + DIC_{Sal=0} \quad (11)$$

where Sal_{spl} is the sample salinity, Sal_{ref} is the reference salinity as calculated in equation 6, and $DIC_{Sal=0}$ is DIC in the freshwater endmember. The value of DIC at the freshwater endmember was the y-intercept of the TA-salinity equation derived for each season, under the assumption that $TA \approx DIC$ at zero salinity (Zeebe & Wolf-Gladrow, 2001). While a DIC-salinity regression was derived, the endmember values for each season had greater error than those of the TA-salinity regression. Normalizing DIC using the TA endmember changed nDIC by a maximum of 0.4% compared to nDIC calculated using the DIC endmember. TA-salinity equations incorporated data from 0-200 m, so they were used to calculate nDIC for surface, bottom, and deep water.

Normalization to a reference salinity removes the effect of conservative mixing from DIC, meaning $\Delta nDIC$ represents the change in DIC due to biogeochemical factors. The BGC term also includes the effects of air-sea gas exchange in summer surface water, but is referred to as BGC for continuity. The sensitivity of output variables to BGC was determined explicitly as $\frac{\partial Y}{\partial nDIC}$ using the `derivnum.m` subroutine of CO2SYS.

$$\Delta Y_{BGC} = \frac{\partial Y}{\partial nDIC} \Delta nDIC \quad (12)$$

$$\text{Summer: } \Delta Y_{BGC+air-sea} = \frac{\partial Y}{\partial nDIC} \Delta nDIC \quad (13)$$

The change in output variables due to water mass mixing altering DIC was then calculated as:

$$\Delta Y_{DIC_{MIX}} + \varepsilon = \Delta Y - \Delta Y_T - \Delta Y_S - \Delta Y_{BGC} - \Delta Y_{TA} \quad (14)$$

and $\Delta Y_{DIC_{MIX}} + \varepsilon$ were added to ΔY_{TA} to determine the overall change in output variables caused by water mass mixing.

$$\Delta Y_{MIX} + \varepsilon = \Delta Y_{TA} + \Delta Y_{DIC_{MIX}} + \varepsilon \quad (15)$$

In this deconvolution, ε accounts for non-linear effects on the carbonate system and other unidentified processes. The cumulative error of non-linear effects by allowing only one input to vary at a time was less than 0.005 in Ω_{arag} and less than 0.01 in pH in each season, meaning ε is likely inconsequential.

Final algorithms to calculate output variable anomalies were as follows:

$$\Delta pH_{tot} = \Delta pH_T + \Delta pH_S + \Delta pH_{BGC} + \Delta pH_{MIX} + \varepsilon \quad (16)$$

$$\Delta \Omega_{tot} = \Delta \Omega_T + \Delta \Omega_S + \Delta \Omega_{BGC} + \Delta \Omega_{MIX} + \varepsilon \quad (17)$$

To assess the significance of drivers, we discuss the driver influence using three definitions: minor influence ($|\Delta \Omega_X| \leq 0.05$ and $|\Delta pH_X| \leq 0.03$), moderate influence ($|\Delta \Omega_X| = 0.05 - 0.50$ and $|\Delta pH_X| = 0.03 - 0.15$), and major influence ($|\Delta \Omega_X| > 0.50$ and $|\Delta pH_X| > 0.15$). Driver values were non-normally distributed (Shapiro-Wilks test; visual examination of quantile-quantile plot). Therefore, these bounds were set using percentiles, where minor influence was below the 50th percentile, moderate influence was between the 50st and 90th percentile, and major influence was 90th percentile or above.

3.4 Results

Glider data exhibited seasonal, spatial, and depth variability in biological, physical, and chemical ocean properties. Likewise, physical and biological drivers of the carbonate system varied spatially and seasonally. Sensitivities of each response variable

to the various drivers and property anomalies from seasonal and annual means are reported (Supplemental Tables S3.1-S3.3).

3.4.1 Analysis 1: Season-Specific Spatial Variability in Drivers

Carbonate system drivers varied in influence between the nearshore, midshelf, and shelf break in each depth region and season (Supplemental Figures S3.2-S3.5; Supplemental Table S3.2). We describe results from Analysis 1 below.

Winter near-surface water displayed little variation in Ω_{arag} or pH over the spatial extent of deployment. The influences of water mass mixing and biogeochemistry on Ω_{arag} and pH were moderate to major but opposite in sign, canceling each other out. Temperature and salinity had minor influence on surface Ω_{arag} ($-0.02 - 0.02$ in all regions), and minor to moderate ($-0.01 - 0.04$ in all regions) influence on pH.

Winter subsurface Ω_{arag} and pH varied spatially, with shelf break Ω_{arag} more positive and pH more negative than the shelf regions. Positive subsurface $\Delta\Omega_{tot}$ at the shelf break was driven by major positive mixing influence (0.78 ± 0.03 , $n=34$). Negative ΔpH_{tot} at the shelf break was driven by major negative biogeochemical (-0.17 ± 0.03 , $n=34$), moderate negative temperature (-0.08 ± 0.02 , $n=34$), and minor negative salinity influences (-0.03 ± 0.01 , $n=34$), which offset major positive ΔpH_{MIX} (0.22 ± 0.01 , $n=34$).

Spring, summer, and fall near-surface and sub-surface $\Delta\Omega_{tot}$ were negative in the nearshore and positive at the shelf break, and the midshelf often acted as a transition zone between the two. This pattern followed the sign of $\Delta\Omega_{MIX}$, indicating that mixing was the most important driver of Ω_{arag} spatial variability. As such, spring, summer, and fall were influenced by mixing of a low- Ω_{arag} water mass in the nearshore and high- Ω_{arag} mixing at the shelf break. Finer-scale variability in $\Delta\Omega_{tot}$ corresponded to changes in

biogeochemistry or gas exchange (summer only). For instance, a positive BGC/gas exchange influence from 100-160 km offshore in summer caused positive $\Delta\Omega_{tot}$, deviating from mixing influence.

Spring and fall near-surface and sub-surface pH experienced little spatial variability. In all regions, mixing was balanced by a combination of opposite biogeochemical, temperature, and/or salinity influence. Summer surface pH anomalies were also minor or moderate (-0.04 – 0.01), driven by the balance between biogeochemistry/air-sea gas exchange and mixing. Summer subsurface pH anomaly was moderately negative from shore to 100 km offshore, driven by mixing and biogeochemistry. Further than 100 km from shore, summer ΔpH_{tot} was positive, driven by biogeochemistry in the midshelf and mixing at the shelf break.

A deep-water mass was identified in spring (midshelf and shelf break), summer (nearshore, midshelf, and shelf break), and fall (shelf break). In spring and summer, shelf break deep water exhibited a positive Ω_{arag} anomaly compared to other spatial regions due to major positive $\Delta\Omega_{MIX}$ (spring: 0.73 ± 0.01 , n=18; summer: 1.06 ± 0.01 , n=18). Both seasons exhibited negative $\Delta\Omega_{BGC}$ in shelf break deep water and positive $\Delta\Omega_{BGC}$ in the midshelf. Spring and summer deep water showed little evidence of carbonate dissolution or precipitation, meaning biogeochemical influence can be attributed to photosynthesis and respiration (Figure 3.2). Positive $\Delta\Omega_{BGC}$ in the midshelf indicated the relative importance of deep water photosynthesis and negative $\Delta\Omega_{BGC}$ at the shelf break indicated deep water respiration. Spring and summer deep water pH also experienced major positive influence of mixing at the shelf break (spring: 0.17 ± 0.00 , n=82; summer: 0.26 ± 0.00 , n=39).

A deep-water mass was also identified at the shelf break in fall, which exhibited a minor negative ΔpH_{tot} (-0.03 ± 0.01 , $n=39$). Though fall deep water only occurred in one spatial region, a pH anomaly can appear because anomalies were calculated using reference values (Equation 6) instead of mean pH values, reflecting the non-linear nature of thermodynamic equations (Rheuban et al., 2019).

3.4.2 Analysis 2: Seasonal Variability in Drivers

Analysis 2 revealed that carbonate system drivers varied between seasons in the MAB (Supplemental Table S3.3). Rather than compare each space/depth region throughout an annual cycle, here we highlight seasonal changes in water column features that influence the carbonate system.

Analysis 1 revealed that nearshore near-surface water in every season had negative Ω_{arag} and pH anomalies driven mainly by low-salinity water mass mixing. Analysis 2 showed that of all seasons, summer nearshore near-surface water was most influenced by mixing, as it exhibited the most negative $\Delta\Omega_{MIX}$ (-0.83 ± 0.26 , $n=28$; Supplemental Table S3.3; Figure 3.4) and ΔpH_{MIX} (-0.32 ± 0.11 , $n=28$; Supplemental Table S3.3; Figure 3.3). Conversely, fall nearshore near-surface water had the most positive $\Delta\Omega_{MIX}$ (0.61 ± 0.02 , $n=21$; Supplemental Table S3.3; Figure 3.3) and ΔpH_{MIX} (0.16 ± 0.01 , $n=21$; Supplemental Table S3.3; Figure 3.3).

Negative $\Delta\Omega_{tot}$ compared to an annual mean is characteristic of the Cold Pool and was evident in the midshelf region in spring (deep) and summer (subsurface and deep) (Figure 3.4). Summer subsurface and deep waters also exhibited a negative pH anomaly in the midshelf (subsurface: -0.09 ± 0.06 , $n=120$; deep: -0.11 ± 0.03 , $n=120$). In summer, these anomalies were driven by negative $\Delta\Omega_{MIX}$ ($-0.97 - -0.40$) and ΔpH_{MIX} (-

0.14 - -0.12) while biogeochemical influence caused deviations of ΔY_{tot} from ΔY_{MIX} (Figure 3.5). The negative Ω_{arag} anomaly in spring deep water was driven by mixing (Figure 3.6).

The sensitivity analysis in this study showed positive surface ΔpH_{tot} in winter (0.07 ± 0.04 , n=187) and negative surface ΔpH_{tot} in summer (-0.05 ± 0.02 , n=188) when compared to an annual mean (Figure 3.7). On the other hand, surface $\Delta \Omega_{tot}$ was negative in winter (-0.28 ± 0.24 , n=187) and positive in summer (0.26 ± 0.19 , n=188). Drivers influencing these differential patterns are shown in Figure 3.8. Summer $\Delta \Omega_{tot}$ was driven by the balance between major biogeochemical/air-sea gas exchange and mixing influences. In winter, the Ω_{arag} anomaly was negative or near-zero. Positive ΔpH_{tot} in winter was driven by moderate to major temperature influence, while negative ΔpH_{tot} in summer was driven by mixing and counteracted by BGC/air-sea gas exchange.

3.5 Discussion

This analysis of carbonate system drivers identified distinct oceanographic features influencing seasonal and spatial dynamics of acidification in the MAB (Figure 3.9). Water mass mixing was the primary driver of variability in Ω_{arag} and pH, while biogeochemical activity often had a finer scale influence on the response variables. Temperature and salinity influence were, more often than not, small in magnitude and equal-but-opposite, meaning the effect of one canceled out the effect of the other. Quantitative deductions of spatial and seasonal variability in complex carbonate system drivers allow the identification of important ocean properties, processes, and source waters that influence the location and timing of acidification in this system.

3.5.1 Water Mass Mixing

Multiple modes of water mass mixing likely played a role in seasonal and spatial variability in the carbonate system. The nearshore MAB experiences upwelling, downwelling, and cross-shelf flow regimes due to sustained along-shore southwest winds in the summer, northwest winds in the winter, and southwest, northwest, and northeast winds in both spring and fall (Gong et al., 2010). In the nearshore, tidal action and river runoff have a potential mixing influence year-round. At the shelf break, water mass mixing may be driven by eddy interactions with the shelf break jet or internal wave action. Submarine canyons in the MAB experience upwelling of slope water due to wind stress and eddy action, which can lead to the formation of dense slope water plumes along the shelf (Wang, 2021). Lastly, storms influence water column mixing seasonally with tropical storms affecting the MAB in summer and extra-tropical cyclones (nor'easters) more prominent in fall, winter, and early spring. Taken together, these modes of mixing can greatly influence MAB chemistry. The major water mass interactions observed during this study (freshwater endmember mixing, slope water mixing, and cold pool stagnation) are discussed in detail below (sections 3.5.1.1 – 3.5.1.3).

3.5.1.1 Freshwater Influence

In the nearshore, all seasons exhibited lower-than-seasonal-average Ω_{arag} driven by water mass mixing, indicating that a low-alkalinity water mass was influencing the system. This water likely originated from riverine inputs to the system. Sandy Hook, New Jersey, the shore point in winter, summer, and fall, is located near the intersection of the Raritan Bay and Lower New York Bay, two major freshwater influences in the coastal

MAB (Figure 1). The spring shore point, Atlantic City, New Jersey, is adjacent to Great Bay and Great Egg Harbor, and ~70 km northeast of the Delaware Bay mouth (Figure 1). Proximity to these bays allows mixing of low-alkalinity freshwater into nearshore coastal near-surface water, decreasing Ω_{arag} and pH. Freshwater mixing influence was partially counteracted by nearshore photosynthesis in each season which removed CO₂ from the water column, in turn increasing Ω_{arag} and pH. The acidifying effects of freshwater mixing nearshore extended into the subsurface in spring, summer, and fall.

Coastal ocean mixing with freshwater sources in the nearshore was most influential in the summer. Historically, rivers draining into the MAB exhibit peak outflow during spring, and coastal waters have the lowest salinity in summer, when the cumulative influence of seasonal runoff and precipitation are greatest (Manning, 1991; Whitney, 2010). During the summer glider deployment, multiple large precipitation events caused higher than average rainfall while the glider was in the nearshore and midshelf (July 17-22, 2019; https://weather.gov/marfc/precipitation_departures/). High levels of rainfall caused salinity to decrease to ~29 PSU, which is lower than average climatology levels for the 30-m isobath off coastal New Jersey (30-32 PSU; Fleming, 2016). Low salinity was linked to low total alkalinity, Ω_{arag} , and pH in surface waters (Wright-Fairbanks et al., 2020). The negative pH and Ω_{arag} anomalies in summer nearshore surface water demonstrate that high-precipitation events in the MAB can directly influence coastal buffering capacity for CO₂. It is important to note that salinity in these deployments was, on average, no less than 29 PSU, meaning carbonate

sensitivity to salinity was not as extreme as it would be in an estuarine environment (Cai et al., 2021).

3.5.1.2 *The Shelf Break Front*

The Gulf Stream carries warm, high-salinity water from the equatorial region northward along the U.S. East Coast. Though the Gulf Stream doesn't interact directly with the MAB coastal shelf, it does influence the slope sea via the shelf break front, which acts as a heat source for the shelf via eddy heat flux (Chen & He, 2010). The Gulf Stream also periodically delivers heat and salt to the MAB shelf via warm core rings that break off of meanders north and west of the Gulf Stream deflection point near Cape Hatteras, North Carolina (Andres, 2016). When warm core rings hit the MAB shelf, salt and heat are transferred onto the shelf at a magnitude 6-9x larger than long-term average exchange (Chen et al., 2014).

The influence of the Gulf Stream was especially important at the shelf-slope boundary in our study, as evidenced by high Ω_{arag} and pH in spring, summer, and fall near-surface and subsurface shelf break zones compared to the rest of the shelf (Figure 3.10). While mixing of shelf water with high- Ω_{arag} slope water influenced the shelf break carbonate system relative to other coastal processes in spring, summer, and fall, that mixing was most impactful in fall (Figure 3.11). A Gulf Stream intrusion onto the shelf was visible in satellite sea surface temperature observations when the glider was at the shelf break during this time (Figure 3.12). This intrusion brought water with salinity >35 PSU to the 60 m isobath on the shelf, exceeding the climatological average of shelf break front intrusion for summer in the MAB (~75 m; Linder & Gawarkiewicz, 1998). The salinity of this intrusion was higher than average for MAB shelf break waters in

summer (33.5 PSU; Fleming, 2016). The identification of this feature provided a direct link between Gulf Stream intrusion and delivery of high Ω_{arag} water to the MAB shelf.

Changes in carbonate chemistry due to Gulf Stream influence in the northeast U.S. have been recorded previously. From 2005-2015, a northward shift in the Gulf Stream related to wind variability and moderately influenced by North Atlantic Oscillation caused an increase in sea surface salinity in the Northwest Atlantic (Grotsky et al., 2017). This brought high TA water to the MAB shelf, which counteracted DIC increases and caused a slowdown in the decades-long decline of Ω_{arag} (Xu et al., 2020). Salisbury and Jonsson (2018) recorded an extreme warming ($0.2\text{ }^{\circ}\text{C yr}^{-1}$) and increased salinity ($\sim 0.2\text{ PSU yr}^{-1}$) event in the Gulf of Maine from 2005-2014, which was linked to the weakening of AMOC. During that time period, warming and increasing salinity exhibited a 2.5x stronger effect on Ω_{arag} than ocean acidification, mitigating the effects of acidification despite a 40+ year trend of decreasing pH and Ω_{arag} due to increased $p\text{CO}_2$ and decreased TA. Based on our sensitivity analysis and links between the Labrador Current, Gulf Stream, and the MAB, a similar event structure could occur in the MAB.

Interestingly, shelf water mixing with slope water did not lead to a major positive pH anomaly in any season because it was counterbalanced by biogeochemical activity and/or temperature. Though mixing of the shelf break jet caused high Ω_{arag} at the edge of the shelf, respiration and temperature had a greater impact on pH compared to the near shore and midshelf regions. Differences in drivers of pH and Ω_{arag} are discussed further in section 3.5.2.

At the shelf break, a deep water mass was identified in spring, summer, and fall. This water mass aligns with a deep coastal current identified by Wanninkhof et al. (2015), which originates north of the MAB and has high DIC due to remineralization and a lack of ventilation to the atmosphere. The high pH and Ω_{arag} Gulf Stream influenced the carbonate system of MAB slope water to depths of ~ 100 m, and the deep coastal current caused lower pH and Ω_{arag} below 100 m in spring and fall. In summer, shelf break deep water was more well-mixed with slope water, so it did not exhibit the same characteristic low pH and Ω_{arag} as in spring and fall.

3.5.1.3 Cold Pool Carbonate Chemistry Drivers

The MAB Cold Pool forms due to the onset of stratification in the spring and persists throughout summer (Castelao et al., 2008; Chen et al., 2018; Houghton et al., 1982). Midshelf subsurface and deep water in the spring and summer exhibited lower-than-average Ω_{arag} and pH compared to the annual mean. These anomalies align with the general understanding of the Cold Pool, which has little ventilation to the atmosphere due to strong seasonal stratification at its full extent and therefore accumulates CO_2 from respiration, which decreases pH and Ω_{arag} .

Given that understanding, one might extrapolate that biological respiration is the main driver behind low Ω_{arag} and pH in the Cold Pool. That assumption holds in the spring, which saw low midshelf Ω_{arag} and pH driven by a combination of biogeochemistry and mixing. However, water mass mixing, specifically the lack thereof, was the primary driver causing low Ω_{arag} and pH in Cold Pool water in the summer, and biogeochemistry drove finer-scale change. This indicates that a transition in the drivers of Cold Pool carbonate chemistry occurred between spring and summer. In the spring,

seasonal stratification began but there was still some surface-subsurface mixing, which allowed ventilation of the Cold Pool to the atmosphere. Therefore, mixing had a lesser effect on springtime low Ω_{arag} and pH. In summer, stratification was at its greatest extent, and the lack of mixing between Cold Pool and surface water became the primary driver of the carbonate system in subsurface water. An alternative theory holds that the Cold Pool forms and persists due to the intrusion of water from north of the MAB, primarily the Georges Bank and the Gulf of Maine regions (originating from as far north as the Labrador Sea) (Castelao et al. 2008, Brown et al. 2015, Chen et al. 2018). This source water has low Ω_{arag} compared the MAB and therefore could be mixing into MAB shelf water and causing low Ω_{arag} and pH in the Cold Pool subsurface water during summer.

3.5.2 Decoupling of Ω_{arag} and pH Drivers

In the MAB, surface water Ω_{arag} and pH are driven by a combination of thermodynamics, air-sea gas exchange, and biological activity (Cai et al., 2020). In an open system, pH and Ω_{arag} experience two temperature-dependent responses, namely gas exchange and internal shifts in thermodynamic equilibrium due to changes in dissociation constants K_1 and K_2 . These two temperature-dependent responses counteract each other in terms of their effect on pH, but enhance one another in terms of their effect on $[CO_3^{2-}]$, and as such, Ω_{arag} . (Cai et al., 2020; Qi et al., 2020). In a closed system with no air-sea gas exchange, the opposite occurs, whereby pH is largely driven by temperature (cooling = higher pH), and Ω_{arag} is minimally affected by temperature. Though Cai et al. (2020) applied this concept to a spatial analysis of the carbonate system along a latitude gradient, the underlying principles can be applied to our seasonal dataset.

The seasonal deployments showed little effect of gas exchange in winter, spring, and fall (Section 3.3.3), meaning they represent a closed system, while summer surface water is governed by the principles of an open system. Surface water had higher-than-average Ω_{arag} in summer and lower-than-average Ω_{arag} in winter, but lower pH in summer and higher pH in winter. This decoupling is expected in a closed system where pH is driven by seasonal temperature swings and Ω_{arag} is driven by faster, local processes. Our driver analyses supported this, showing that surface Ω_{arag} in summer and winter was mainly driven by local mixing and biogeochemical activity, and winter surface pH was driven by temperature (Figure 3.8). However, in a deviation from the closed system ideal, summer surface pH was mainly driven by BGC and mixing.

The BGC influence on pH in summer likely reflects air-sea gas exchange that was identified as a contributing driver in summer surface water (Section 3.3.3). pH is more sensitive to changes in DIC caused by air-sea gas exchange than Ω_{arag} (Cai et al., 2021), which might explain why the influence of gas exchange was only reflected in pH. Additionally, the importance of mixing might reflect an overwhelming freshwater influence in surface water during the summer deployment (Section 3.5.1).

Because the glider data set covers only one deployment in each season, it is not possible to account for interannual differences in the importance of temperature here. Continued high-resolution monitoring of seasonal changes in the carbonate system will allow for analysis of interannual change and development of a regional carbonate system climatology for the MAB that will better identify long-term trends.

3.5.3 Comparison of Results to Past Studies

The results from our sensitivity analysis align well with previous studies of carbonate system drivers focused in localized regions within the NES or single season, single depth studies in the MAB. Xu et al. (2017) investigated short-term changes in surface carbonate chemistry along the U.S. East Coast using data from the summer ECOA-1 cruise in 2015. Similar to the results presented here, they found that Ω_{arag} increased from shore to shelf, driven mainly by physical mixing of slope water, though biological activity could alter this pattern on a shorter time scale. Xu et al. (2020) investigated long-term change in surface Ω_{arag} along the U.S. East Coast, and concluded that TA and DIC are the dominant controls of Ω_{arag} on an interannual and decadal scale. Rheuban et al. (2019) conducted a monthly discrete sampling program in Buzzard's Bay, off the coast of Massachusetts, to investigate the influence of fresh water and nutrient inputs on surface carbonate chemistry. Akin to our study and Xu et al. (2017), they concluded that freshwater input is a strong local driver of carbonate chemistry in the inner shelf. Rheuban et al. (2019) also observed an important biogeochemical influence, which was linked to eutrophication based on total nitrogen measurements. Similarly, Wang et al. (2016) sampled 6 stations in Wilkinson Bay (Gulf of Maine) at 10-50 m depth resolution and found that Ω_{arag} was most strongly driven by seasonal cycles of photosynthesis and respiration, though mixing of low salinity water did impact Ω_{arag} in the nearshore. Common observations in past studies and the present study emphasize the

importance of local processes of daily, seasonal, interannual, and decadal timescales on controlling the coastal carbonate system.

Glider data analyzed here allowed the identification of important local controls on the carbonate system in higher spatial resolution than previous studies. Drivers were resolved at <1 m in depth and <1 km in distance over four seasons. This allowed the clear differentiation of carbonate parameters and their driving forces in surface and subsurface waters. The seasonal evolution and extent of acidified subsurface water in the MAB is necessary to understand in high resolution due to its importance to economically important fin- and shellfisheries.

In addition to providing high-resolution data, gliders have the unique ability to observe in areas that are difficult to access in discrete sampling programs, such as the continental shelf break. Cross-shelf glider deployments revealed the changing seasonal extent of Gulf Stream intrusions onto the shelf, which mitigated acidified conditions based on its presence. Continued tracking of Gulf Stream-influenced slope water intrusions will allow a better understanding of ecological impacts of acidification for organisms inhabiting the shelf break.

Furthermore, glider missions provide continuous data streams that can show how changes in environmental conditions over the course of deployment effect changes in the system. For example, heavy rainfall during the summer deployment was linked to short-term decreases in surface pH in summer (section 3.5.1.1), which may not have been captured with discrete sampling. While past studies have identified depth and distance

related carbonate system changes, they have not been able to clarify the extent of driving forces at the scale allowed by glider technology.

3.6 Conclusions

This study decomposed the drivers of the carbonate system in the Mid-Atlantic Bight based on temporally and spatially high-resolution data. High-resolution data were used to identify areas of the shelf and transition points into times of year that are most susceptible to acidification in the MAB. Sensitivity of Ω_{arag} and pH to water mass mixing, biogeochemical activity, temperature, and salinity, and varied over a spatial dimension in each season, as well as between seasons compared to an annual mean. Water mass mixing and biogeochemical changes were consistently major drivers of change in the carbonate system, while seasonal temperature changes caused further deviation. Given these major drivers, future studies should focus on the potential impacts of projected changes in freshwater runoff and precipitation in the nearshore, and Gulf Stream intrusions at the shelf break, on the carbonate system on the shelf. These processes may cause opposing acidification regimes in the nearshore and at the shelf break with implications for the ecology of the region.

The sensitivity values derived here define how ocean properties determine the carbonate system, which can be used to improve coastal biogeochemical forecast models. These deployments cover one instance of each season, serving as a base understanding of seasonal carbonate system changes in the MAB. Continued seasonal monitoring will allow the derivation of a carbonate system climatology for the region and further investigation of interannual variability in dynamic carbonate system drivers like the

extent of Gulf Stream intrusion. Continued monitoring may also capture dynamic events not seen in the deployments analyzed here, like upwelling of cold, low- Ω_{arag} water due to seasonal wind shifts.. This information will be valuable in fine-tuning habitat suitability studies and designing environmentally relevant laboratory experiments investigating the impact of acidification on commercially important species susceptible to acidification.

3.7 Acknowledgments

We thank the Rutgers University Center for Ocean Observing Leadership (RUCOOL) faculty for facility support. We thank RUCOOL glider and software technicians (David Aragon, Nicole Waite, Chip Haldeman, Laura Nazzaro, and John Kerfoot) for their efforts in glider preparation, logistics, fieldwork, and mission piloting. We thank our colleagues at Sea-Bird Scientific (Andrew Barnard, Cristina Orrico, Charles Branham, Dave Murphy, Vlad Simontov, and Dave Walter), as well as colleagues at Teledyne Webb Research (Clayton Jones, Clara Hulburt, and Christopher DeCollibus) for their technical expertise and collaboration. We thank Joe Salisbury for his guidance and expertise in complex coastal carbonate system principles. Glider development, deployments, and carbonate chemistry laboratory work were funded by National Science Foundation's Ocean Technology and Interdisciplinary Coordination program (National Science Foundation OCE1634520 and OCE1634582). E.W.F. received support from the Mid-Atlantic Sea Grant/NOAA Ocean Acidification Program Graduate Research Fellowship #NA19OAR4170087 and the Rutgers University School of Environmental and Biological Sciences Excellence Fellowship.

3.8 References

- Andres, M. (2016). On the recent destabilization of the Gulf Stream path downstream of Cape Hatteras. *Geophysical Research Letters*, *43*, 9836-9842. doi:10.1002/
- Boehme, S. E., Sabine, C. L., & Reimers, C. E. (1998). CO₂ fluxes from a coastal transect: a time-series approach. *Marine Chemistry*, *63*, 49-67.
- Brodeur, J. R., Chen, B., Su, J., Xu, Y.-Y., Hussain, N., Scaboo, K. M., Zhang, Y., Testa, J. M., & Cai, W.-J. (2019). Chesapeake Bay Inorganic Carbon: Spatial Distribution and Seasonal Variability. *Frontiers in Marine Science*, *6*. doi:10.3389/fmars.2019.00099
- Cai, W.-J., Hu, X., Huang, W.-J., Jiang, L.-Q., Wang, Y., Peng, T.-H., & Zhang, X. (2010). Alkalinity distribution in the western North Atlantic Ocean margins. *Journal of Geophysical Research*, *115*(C8). doi:10.1029/2009jc005482
- Cai, W.-J., Hu, X., Huang, W.-J., Murrell, M. C., Lehrter, J. C., Lohrenz, S. E., Chou, W.-C., Zhai, W., Hollibaugh, J. T., Wang, Y., Zhao, P., Guo, X., Gundersen, K., Dai, M., & Gong, G.-C. (2011). Acidification of subsurface coastal waters enhanced by eutrophication. *Nature Geoscience*, *4*(11), 766-770. doi:10.1038/ngeo1297
- Cai, W.-J., Xu, Y. Y., Feely, R. A., Wanninkhof, R., Jonsson, B., Alin, S. R., Barbero, L., Cross, J. N., Azetsu-Scott, K., Fassbender, A. J., Carter, B. R., Jiang, L. Q., Pepin, P., Chen, B., Hussain, N., Reimer, J. J., Xue, L., Salisbury, J. E., Hernandez-Ayon, J. M., Langdon, C., Li, Q., Sutton, A. J., Chen, C. A., & Gledhill, D. K. (2020). Controls on surface water carbonate chemistry along North American ocean margins. *Nat Commun*, *11*(1), 2691. doi:10.1038/s41467-020-16530-z
- Cai, W. J., Feely, R. A., Testa, J. M., Li, M., Evans, W., Alin, S. R., Xu, Y. Y., Pelletier, G., Ahmed, A., Greeley, D. J., Newton, J. A., & Bednarsek, N. (2021). Natural and Anthropogenic Drivers of Acidification in Large Estuaries. *Ann Rev Mar Sci*, *13*, 23-55. doi:10.1146/annurev-marine-010419-011004
- Castelao, R., Glenn, S., Schofield, O., Chant, R., Wilkin, J., & Kohut, J. (2008). Seasonal evolution of hydrographic fields in the central Middle Atlantic Bight from glider observations. *Geophysical Research Letters*, *35*(3). doi:10.1029/2007gl032335
- Chen, K., & He, R. (2010). Numerical Investigation of the Middle Atlantic Bight Shelfbreak Frontal Circulation Using a High-Resolution Ocean Hindcast Model. *Journal of Physical Oceanography*, *40*(5), 949-964. doi:10.1175/2009jpo4262.1
- Chen, K., He, R., Powell, B. S., Gawarkiewicz, G. G., Moore, A. M., & Arango, H. G. (2014). Data assimilative modeling investigation of Gulf Stream Warm Core Ring interaction with continental shelf and slope circulation. *Journal of Geophysical Research: Oceans*, *119*(9), 5968-5991. doi:10.1002/2014jc009898
- Chen, Z., Curchitser, E., Chant, R., & Kang, D. (2018). Seasonal Variability of the Cold Pool Over the Mid-Atlantic Bight Continental Shelf. *Journal of Geophysical Research: Oceans*, *123*(11), 8203-8226. doi:10.1029/2018jc014148

- DeGrandpre, M. D., Olbu, G. J., Beatty, C. M., & Hammar, T. R. (2002). Air-sea CO₂ fluxes on the US Middle Atlantic Bight. *Deep Sea Research*, 49.
- Dickson, A. (1990). Standard potential of the reaction: $\text{AgCl(s)} + 1/2\text{H}_2(\text{g}) = \text{Ag(s)} + \text{HCl(aq)}$, and the standard acidity constant of the ion HSO_4^- in synthetic sea water from 273.15 to 318.15 K. *Journal of Chemical Thermodynamics*, 22, 113-127.
- Dickson, A., & Millero, F. J. (1987). A comparison of the equilibrium constants for the dissociation of carbonic acid in seawater media. *Deep-Sea Research*, 34(10), 1733-1743.
- Doney, S. C., Busch, D. S., Cooley, S. R., & Kroeker, K. J. (2020). The Impacts of Ocean Acidification on Marine Ecosystems and Reliant Human Communities. *Annual Review of Environment and Resources*, 13(8). doi:10.1146/annurev-environ-012320-
- Doney, S. C., Fabry, V. J., Feely, R. A., & Kleypas, J. A. (2009). Ocean acidification: the other CO₂ problem. *Ann Rev Mar Sci*, 1, 169-192. doi:10.1146/annurev.marine.010908.163834
- Fennel, K., Wilkin, J., Previdi, M., & Najjar, R. (2008). Denitrification effects on air-sea CO₂ flux in the coastal ocean: Simulations for the northwest North Atlantic. *Geophysical Research Letters*, 35(24). doi:10.1029/2008gl036147
- Fleming, N. (2016). Seasonal and Spatial Variability in Temperature, Salinity, and Circulation of the Middle Atlantic Bight. *Rutgers University Ph.D. Dissertation*.
- Friis, K., Körtzinger, A., & Wallace, D. W. R. (2003). The salinity normalization of marine inorganic carbon chemistry data. *Geophysical Research Letters*, 30(2). doi:10.1029/2002gl015898
- Gledhill, D., White, M., Salisbury, J., Thomas, H., Misna, I., Liebman, M., Mook, B., Grear, J., Candelmo, A., Chambers, R. C., Gobler, C., Hunt, C., King, A., Price, N., Signorini, S., Stancioff, E., Stymiest, C., Wahle, R., Waller, J., Rebeck, N., Wang, Z., Capson, T., Morrison, J. R., Cooley, S., & Doney, S. (2015). Ocean and Coastal Acidification off New England and Nova Scotia. *Oceanography*, 25(2), 182-197. doi:10.5670/oceanog.2015.41
- Gong, D., Kohut, J. T., & Glenn, S. M. (2010). Seasonal climatology of wind-driven circulation on the New Jersey Shelf. *Journal of Geophysical Research*, 115(C4). doi:10.1029/2009jc005520
- Grodsky, S. A., Reul, N., Chapron, B., Carton, J. A., & Bryan, F. O. (2017). Interannual surface salinity on Northwest Atlantic shelf. *Journal of Geophysical Research: Oceans*, 122(5), 3638-3659. doi:10.1002/2016jc012580
- Houghton, R. W., Shlitz, R., Beardsley, R. C., Butman, B., & Chamberlin, J. L. (1982). The Middle Atlantic Bight Cold Pool: Evolution of the Temperature Structure During Summer 1979. *American Meteorological Society*, 12, 1019-1029.
- Hunt, C. W., Salisbury, J. E., Vandemark, D., Abmann, S., Fietzek, P., Melrose, C., Wanninkhof, R., & Azetsu-Scott, K. (2021). Variability of USA East Coast

- surface total alkalinity distributions revealed by automated instrument measurements. *Marine Chemistry*, 232. doi:10.1016/j.marchem.2021.103960
- IPCC. (2019). Summary for Policymakers. *IPCC Special Report on the Ocean and Cryosphere in a Changing Climate*.
- Jiang, Z.-P., Tyrrell, T., Hydes, D. J., Dai, M., & Hartman, S. E. (2014). Variability of alkalinity and the alkalinity-salinity relationship in the tropical and subtropical surface ocean. *Global Biogeochemical Cycles*, 28(7), 729-742. doi:10.1002/2013gb004678
- Kroeker, K. J., Kordas, R. L., Crim, R., Hendriks, I. E., Ramajo, L., Singh, G. S., Duarte, C. M., & Gattuso, J. P. (2013). Impacts of ocean acidification on marine organisms: quantifying sensitivities and interaction with warming. *Glob Chang Biol*, 19(6), 1884-1896. doi:10.1111/gcb.12179
- Kwiatkowski, L., & Orr, J. C. (2018). Diverging seasonal extremes for ocean acidification during the twenty-first century. *Nature Climate Change*, 8(2), 141-145. doi:10.1038/s41558-017-0054-0
- Lewis, E., & Wallace, D. W. R. (1998). Program Developed for CO₂ System Calculations.
- Linder, C. A., & Gawarkiewicz, G. (1998). A climatology of the shelfbreak front in the Middle Atlantic Bight. *Journal of Geophysical Research: Oceans*, 103(C9), 18405-18423. doi:10.1029/98jc01438
- Manning, J. (1991). Middle Atlantic Bight salinity: interannual variability. *Continental Shelf Research*, 11(2), 123-137.
- Mehrbach, C., Culberson, C. H., Hawley, J. E., & Pytkowicz, R. M. (1973). Measurement of the apparent dissociation constants of carbonic acid in seawater at atmospheric pressure. *Limnology and Oceanography*, 18(6), 897-907.
- Orr, J. C., Epitalon, J.-M., Dickson, A. G., & Gattuso, J.-P. (2018). Routine uncertainty propagation for the marine carbon dioxide system. *Marine Chemistry*, 207, 84-107. doi:10.1016/j.marchem.2018.10.006
- Orr, J. C., Fabry, V. J., Aumont, O., Bopp, L., Doney, S. C., Feely, R. A., Gnanadesikan, A., Gruber, N., Ishida, A., Joos, F., Key, R. M., Lindsay, K., Maier-Reimer, E., Matear, R., Monfray, P., Mouchet, A., Najjar, R. G., Plattner, G. K., Rodgers, K. B., Sabine, C. L., Sarmiento, J. L., Schlitzer, R., Slater, R. D., Totterdell, I. J., Weirig, M. F., Yamanaka, Y., & Yool, A. (2005). Anthropogenic ocean acidification over the twenty-first century and its impact on calcifying organisms. *Nature*, 437(7059), 681-686. doi:10.1038/nature04095
- Perez, F. F., & Fraga, F. (1987). Association Constant of Fluoride and Hydrogen Ions in Seawater. *Marine Chemistry*, 21.
- Qi, D., Chen, B., Chen, L., Lin, H., Gao, Z., Sun, H., Zhang, Y., Sun, X., & Cai, W.-J. (2020). Coastal acidification induced by biogeochemical processes driven by sea-ice melt in the western Arctic ocean. *Polar Science*. doi:10.1016/j.polar.2020.100504

- Rheuban, J. E., Doney, S. C., McCorkle, D. C., & Jakuba, R. W. (2019). Quantifying the effects of nutrient enrichment and freshwater mixing on coastal ocean acidification. *Journal of Geophysical Research: Oceans*. doi:10.1029/2019jc015556
- Richaud, B., Kwon, Y.-O., Joyce, T. M., Fratantoni, P. S., & Lentz, S. J. (2016). Surface and bottom temperature and salinity climatology along the continental shelf off the Canadian and U.S. East Coasts. *Continental Shelf Research*, *124*, 165-181. doi:10.1016/j.csr.2016.06.005
- Runcie, J. W., Krause, C., Torres Gabarda, S. A., & Byrne, M. (2018). Technical note: Continuous fluorescence-based monitoring of seawater pH in situ. *Biogeosciences*, *15*(13), 4291-4299. doi:10.5194/bg-15-4291-2018
- Saba, G. K., Goldsmith, K. A., Cooley, S. R., Grosse, D., Meseck, S. L., Miller, A. W., Phelan, B., Poach, M., Rheault, R., St-Laurent, K., Testa, J. M., Weis, J. S., & Zimmerman, R. (2019a). Recommended priorities for research on ecological impacts of ocean and coastal acidification in the U.S. Mid-Atlantic. *Estuarine, Coastal and Shelf Science*, *225*. doi:10.1016/j.ecss.2019.04.022
- Saba, G. K., Wright-Fairbanks, E., Chen, B., Cai, W.-J., Barnard, A. H., Jones, C. P., Branham, C. W., Wang, K., & Miles, T. (2019b). The Development and Validation of a Profiling Glider Deep ISFET-Based pH Sensor for High Resolution Observations of Coastal and Ocean Acidification. *Frontiers in Marine Science*, *6*. doi:10.3389/fmars.2019.00664
- Saba, V. S., Griffies, S. M., Anderson, W. G., Winton, M., Alexander, M. A., Delworth, T. L., Hare, J. A., Harrison, M. J., Rosati, A., Vecchi, G. A., & Zhang, R. (2016). Enhanced warming of the Northwest Atlantic Ocean under climate change. *Journal of Geophysical Research: Oceans*, *121*(1), 118-132. doi:10.1002/2015jc011346
- Salisbury, J., & Jonsson, B. F. (2018). Rapid warming and salinity changes in the Gulf of Maine alter surface ocean carbonate parameters and hide ocean acidification. *Biogeochemistry*, *141*(3), 401-418. doi:10.1007/s10533-018-0505-3
- Seitzinger, S. P. (1988). Denitrification in freshwater and coastal marine ecosystems: Ecological and geochemical significance. *Limnology and Oceanography*, *33*(4, part 2), 702-724.
- Seitzinger, S. P., & Giblin, A. E. (1996). Estimating Denitrification in North Atlantic Continental Shelf Sediments. *Biogeochemistry*, *35*, 235-260.
- Sharp, J. D., Pierrot, D., Humphreys, M. P., Epitalon, J.-M., Orr, J. C., Lewis, E., & Wallace, D. W. R. (2020). CO2-System-Extd, v3.0, MATLAB (MathWorks).
- Siedlecki, S. A., Pilcher, D., Howard, E. M., Deutsch, C., MacCready, P., Norton, E. L., Frenzel, H., Newton, J., Feely, R. A., Alin, S. R., & Klinger, T. (2021). Coastal processes modify projections of some climate-driven stressors in the California Current System. *Biogeosciences*, *18*(9), 2871-2890. doi:10.5194/bg-18-2871-2021
- Siedlecki, S. A., Salisbury, J., Gledhill, D. K., Bastidas, C., Meseck, S., McGarry, K., Hunt, C. W., Alexander, M., Lavoie, D., Wang, Z. A., Scott, J., Brady, D. C.,

- Mlsna, I., Azetsu-Scott, K., Liberti, C. M., Melrose, D. C., White, M. M., Pershing, A., Vandemark, D., Townsend, D. W., Chen, C., Mook, W., & Morrison, R. (2021). Projecting ocean acidification impacts for the Gulf of Maine to 2050. *Elementa: Science of the Anthropocene*, 9(1). doi:10.1525/elementa.2020.00062
- Sutton, A. J., Sabine, C. L., Feely, R. A., Cai, W.-J., Cronin, M. F., McPhaden, M. J., Morell, J. M., Newton, J. A., Noh, J.-H., Ólafsdóttir, S. R., Salisbury, J. E., Send, U., Vandemark, D. C., & Weller, R. A. (2016). Using present-day observations to detect when anthropogenic change forces surface ocean carbonate chemistry outside preindustrial bounds. *Biogeosciences*, 13(17), 5065-5083. doi:10.5194/bg-13-5065-2016
- Uppstrom, L. (1974). The boron/chlorinity ratio of deep-sea water from the Pacific Ocean. *Deep-Sea Research*, 21(2).
- van Heuven, S., Pierrot, D., Rae, J. W. B., Lewis, E., & Wallace, D. W. R. (2011). MATLAB Program Developed for CO₂ System Calculations. *ORNL/CDIAC-105b. Carbon Dioxide Information Analysis Center, Oak Ridge National Laboratory, U.S. Department of Energy, Oak Ridge, Tennessee*. doi:10.3334/CDIAC/otg.CO2SYS_MATLAB_v1.1
- Wang, H. (2021). Impact of Canyon Upwelling and Downwelling in the Mid-Atlantic Bight. *Ph.D. Dissertation at The College of William & Mary*.
- Wang, Z., Lawson, G. L., Pilskain, C. H., & Maas, A. E. (2016). Seasonal controls of aragonite saturation state in the Gulf of Maine. *Journal of Geophysical Research: Oceans*(122), 372-389. doi:10.1002/
- Wanninkhof, R., Barbero, L., Byrne, R., Cai, W.-J., Huang, W.-J., Zhang, J.-Z., Baringer, M., & Langdon, C. (2015). Ocean acidification along the Gulf Coast and East Coast of the USA. *Continental Shelf Research*, 98, 54-71. doi:10.1016/j.csr.2015.02.008
- Whitney, M. M. (2010). A study on river discharge and salinity variability in the Middle Atlantic Bight and Long Island Sound. *Continental Shelf Research*, 30(3-4), 305-318. doi:10.1016/j.csr.2009.11.011
- Wootton, J. T., Pfister, C. A., & Forester, J. D. (2008). Dynamic patterns and ecological impacts of declining ocean pH in a high-resolution multi-year dataset. *Proc Natl Acad Sci U S A*, 105(48), 18848-18853. doi:10.1073/pnas.0810079105
- Wright-Fairbanks, E. K., Miles, T. N., Cai, W. J., Chen, B., & Saba, G. K. (2020). Autonomous Observation of Seasonal Carbonate Chemistry Dynamics in the Mid-Atlantic Bight. *Journal of Geophysical Research: Oceans*. doi:10.1029/2020jc016505
- Xu, Y. Y., Cai, W.-J., Gao, Y., Wanninkhof, R., Salisbury, J., Chen, B., Reimer, J. J., Gonski, S., & Hussain, N. (2017). Short-term variability of aragonite saturation state in the central Mid-Atlantic Bight. *Journal of Geophysical Research: Oceans*, 122. doi:10.1002/

- Xu, Y. Y., Cai, W.-J., Wanninkhof, R., Salisbury, J., Reimer, J., & Chen, B. (2020). Long-Term Changes of Carbonate Chemistry Variables Along the North American East Coast. *Journal of Geophysical Research: Oceans*, 125(7). doi:10.1029/2019jc015982
- Zeebe, R. E., & Wolf-Gladrow, D. A. (2001). CO₂ in Seawater: Equilibrium, Kinetics, Isotopes. . *Elsevier*, 1-84.

3.9 Figures

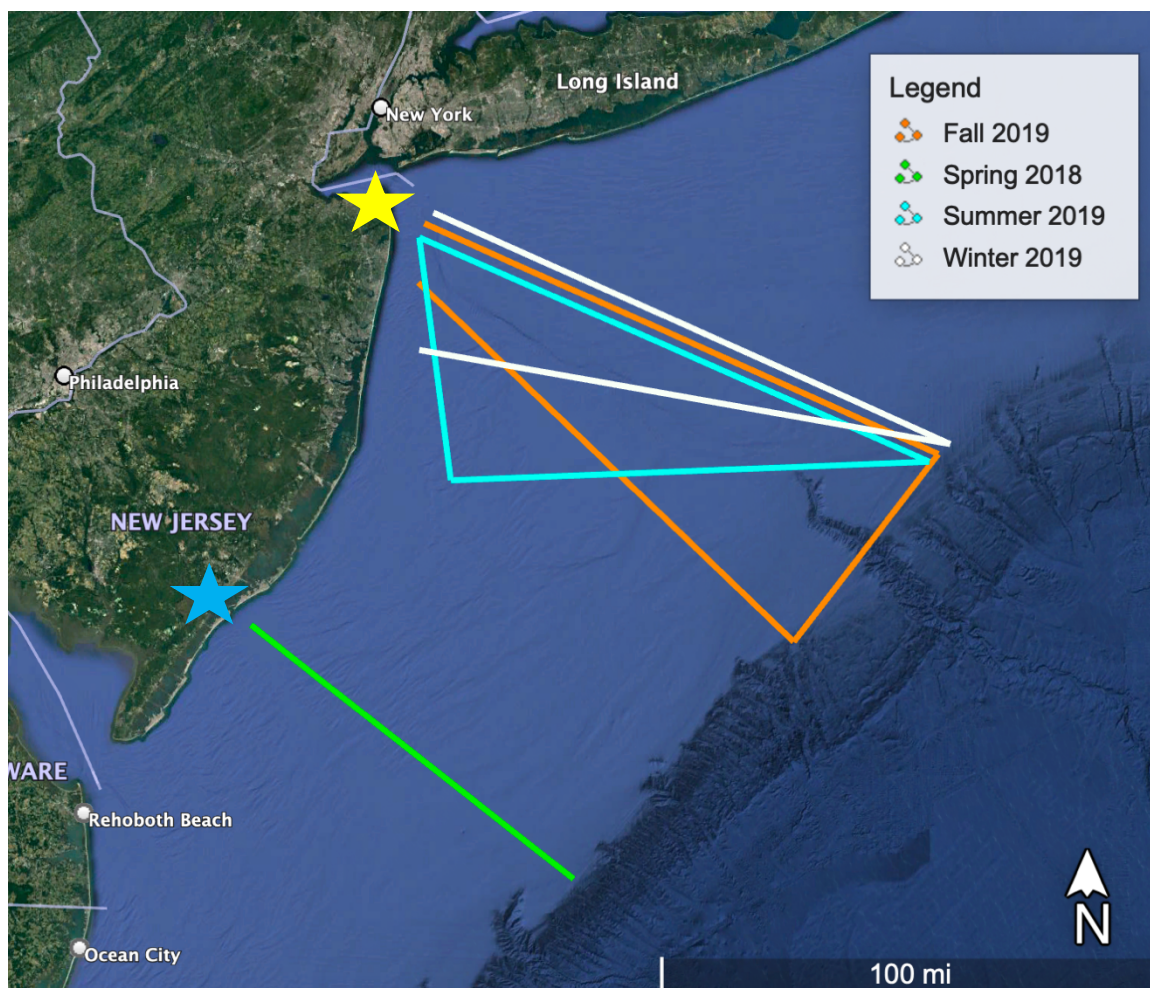


Figure 3.1: Map of pH glider deployment tracks in the Mid-Atlantic Bight, 2018-2019. A yellow star marks the winter, summer, and fall shore point (Sandy Hook, NJ) and a blue star marks the spring shore point (Atlantic City, New Jersey). Produced using Google Earth, with data from SIO, NOAA, U.S. Navy, NGA, and GEBCO, and imaging from Landsat/Copernicus.

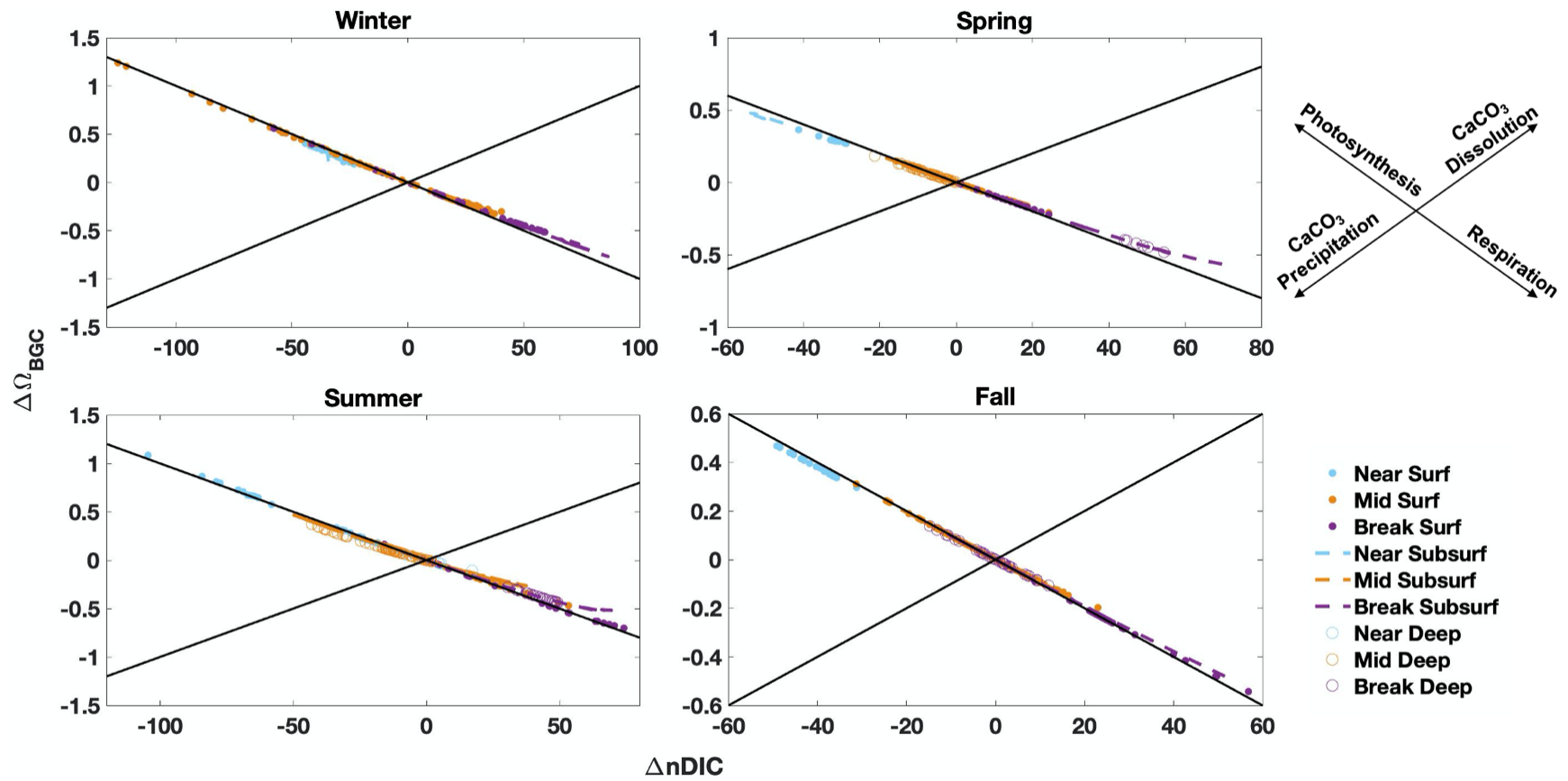


Figure 3.2: $\Delta nDIC$ vs. $\Delta \Omega_{BGC}$ in all four seasons. Black lines represent the theoretical relationship between $\Delta nDIC$ and $\Delta \Omega_{BGC}$ if only photosynthesis/respiration and/or $CaCO_3$ dissolution/precipitation occur. Deviations from the photosynthesis-respiration line are minor in shelf break subsurface water (all seasons) and nearshore surface water (spring).

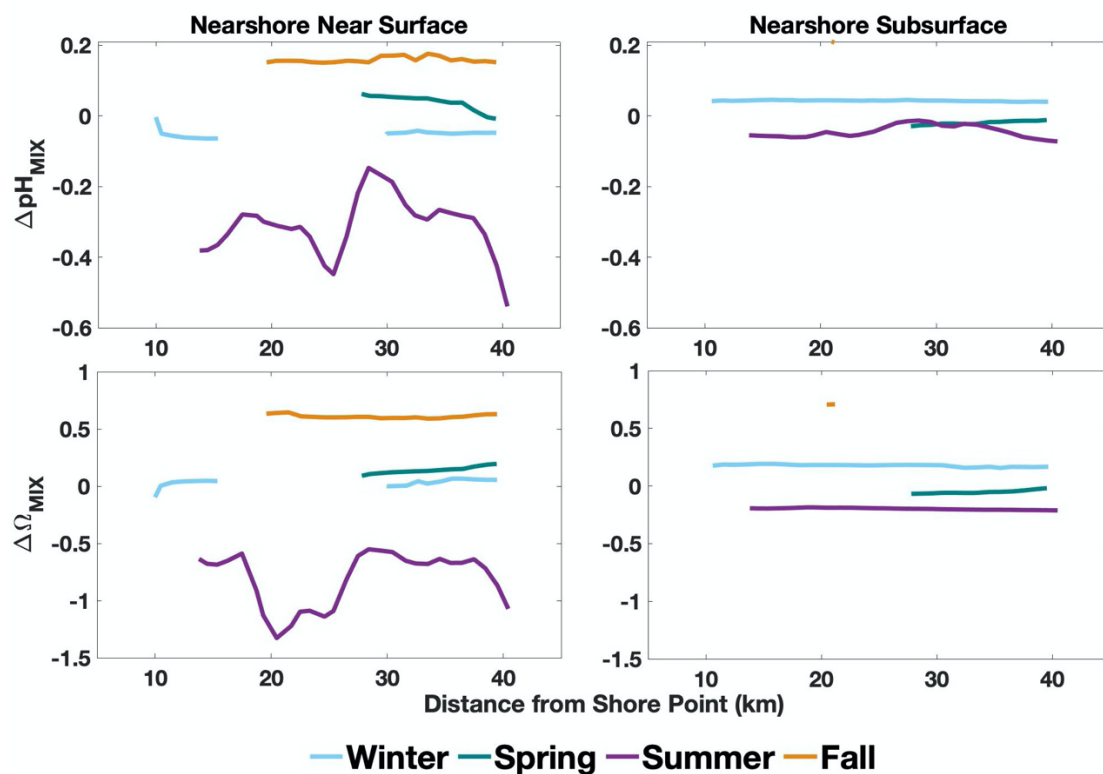


Figure 3.3: Relative influence of water mass mixing on Ω_{arag} and pH in the nearshore region in four seasons. ΔY_{MIX} was calculated as the difference from an annual mean value in the nearshore surface and/or bottom water (Analysis 2). A robust loess smoothing filter, spanning 10% of the data points, was applied for visualization purposes.

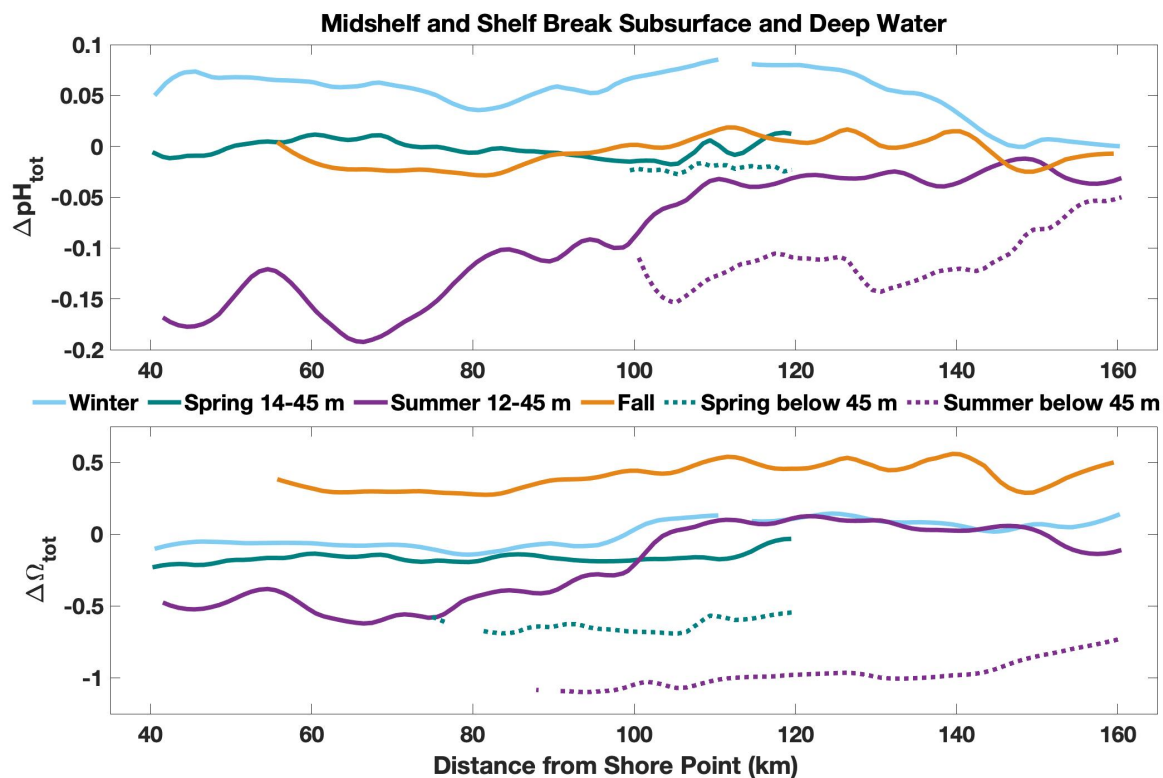


Figure 3.4: Patterns of change in Ω_{arag} and pH in Cold Pool-area water, defined as midshelf sub-surface and/or deep water. Negative $\Delta\Omega_{tot}$ and positive ΔpH_{tot} are characteristic of Cold Pool carbonate chemistry patterns. ΔY_{tot} is the resulting sum of all driver influences, and is reported relative to the annual mean (Analysis 2). A robust loess smoothing filter, spanning 10% of the data points, was applied for visualization purposes.

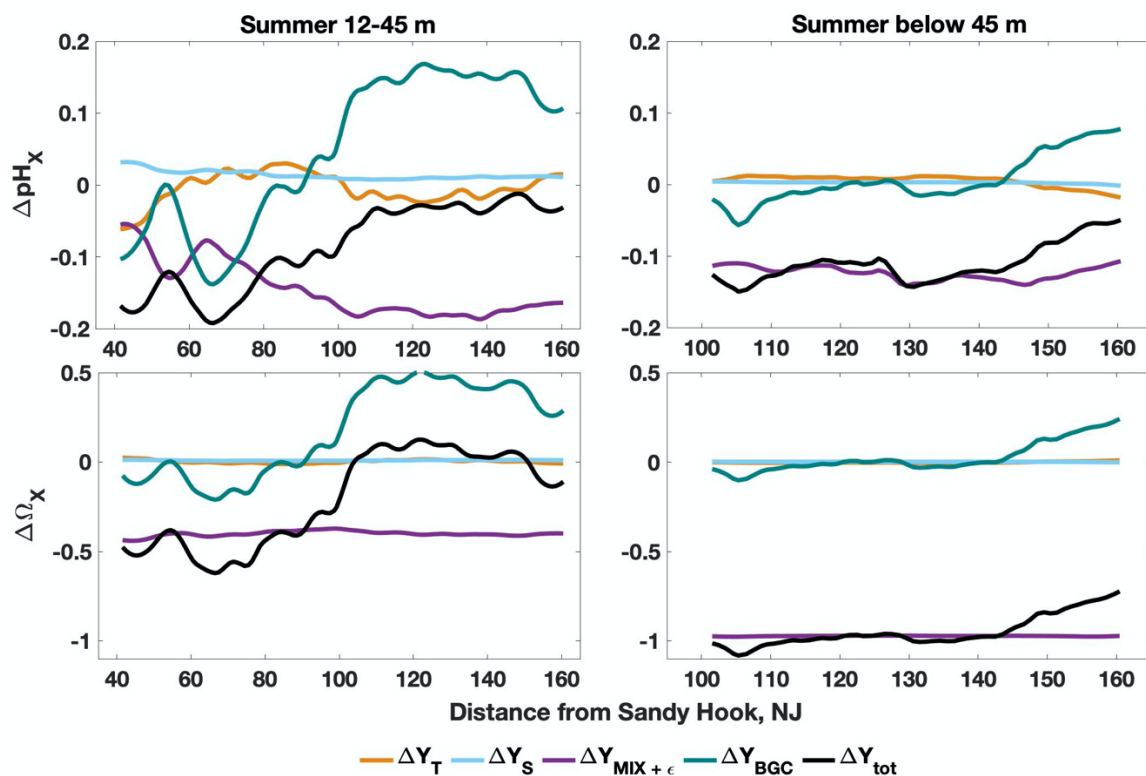


Figure 3.5: Drivers of change in Ω_{arag} and pH in summer 2019 Cold Pool water. ΔY_x is reported relative to the annual mean (Analysis 2). ΔY_{tot} is the resulting sum of all driver influences. A robust loess smoothing filter, spanning 10% of the data points, was applied for visualization purposes.

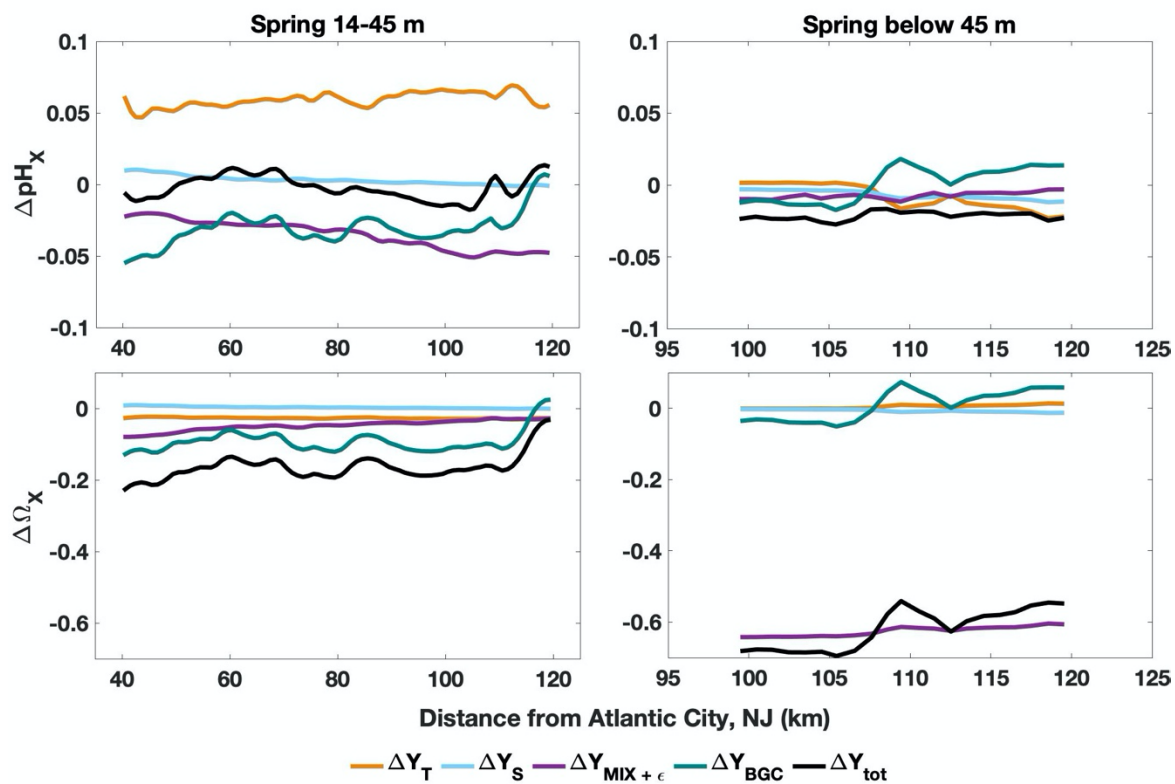


Figure 3.6: Drivers of change in Ω_{arag} and pH in spring 2018 Cold Pool water. ΔY_X is reported relative to the annual mean (Analysis 2). ΔY_{tot} is the resulting sum of all driver influences. A robust loess smoothing filter, spanning 10% of the data points, was applied for visualization purposes.

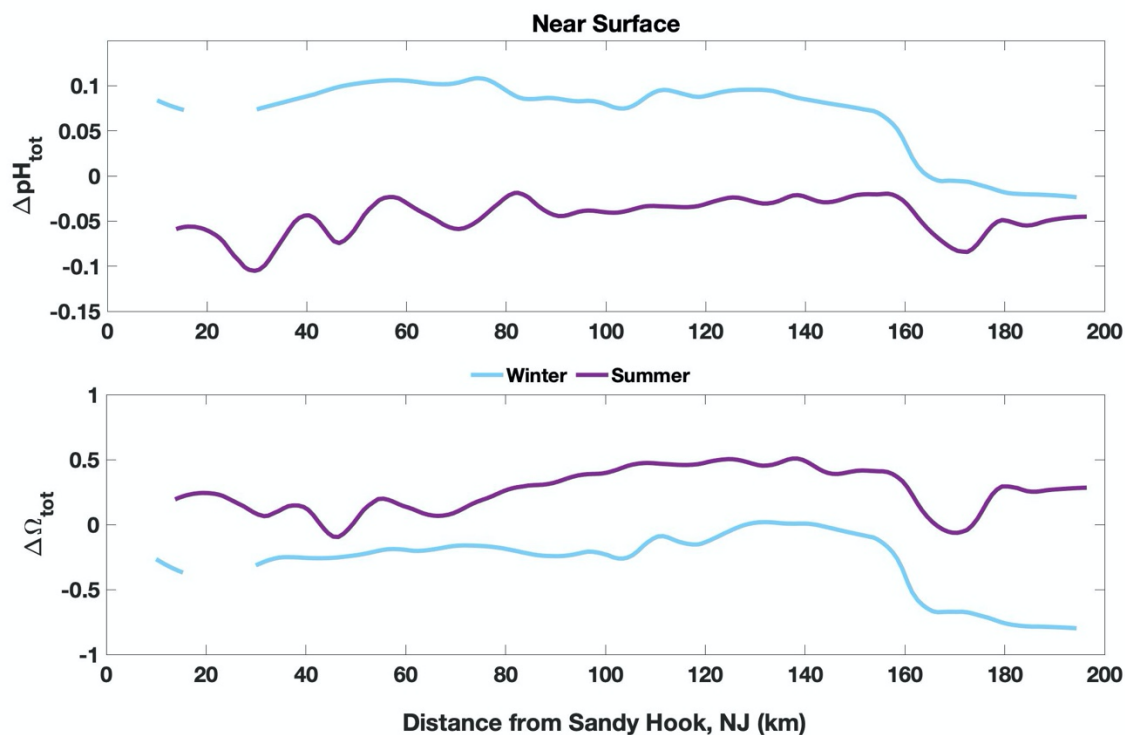


Figure 3.7: Differences in $\Delta\Omega_{\text{tot}}$ and $\Delta\text{pH}_{\text{tot}}$ in surface water between winter and summer 2019. ΔY_X is reported relative to the annual mean (Analysis 2). ΔY_{tot} is the resulting sum of all driver influences. A robust loess smoothing filter, spanning 10% of the data points, was applied for visualization purposes.

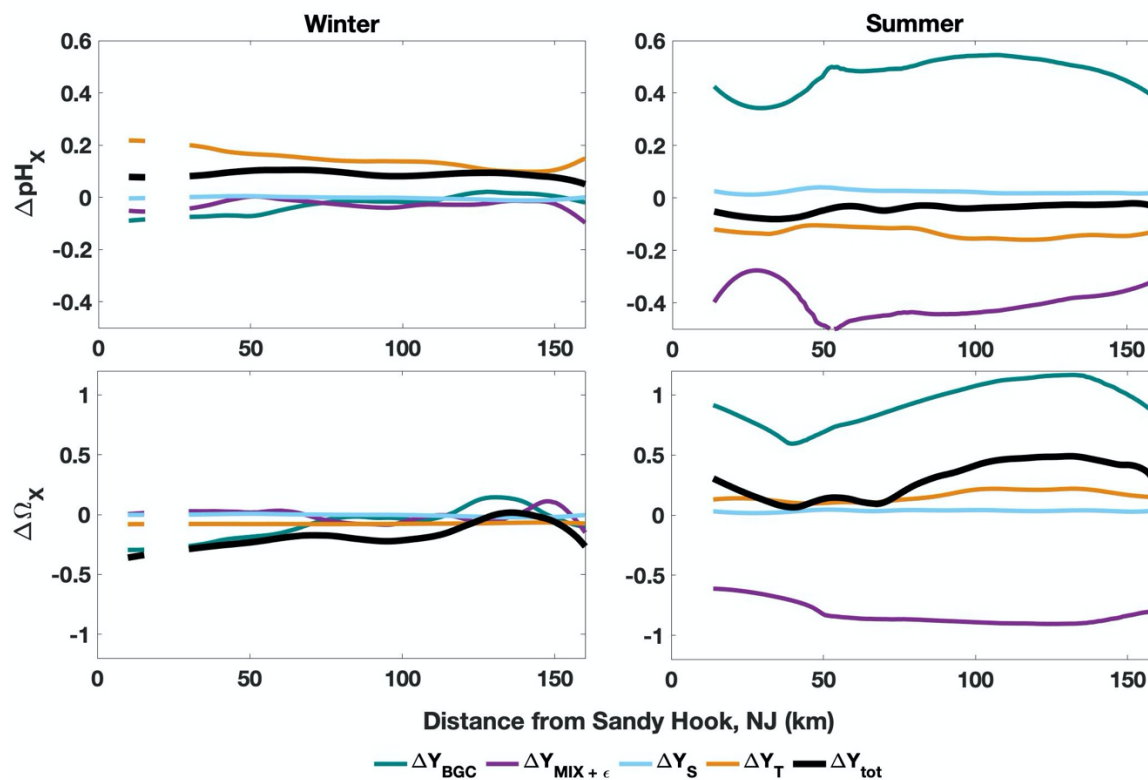


Figure 3.8: Drivers of change in Ω_{arag} and pH in shelf surface water in winter and summer 2019. ΔY_{tot} is the resulting sum of all driver influences. A robust loess smoothing filter, spanning 10% of the data points, was applied for visualization purposes.

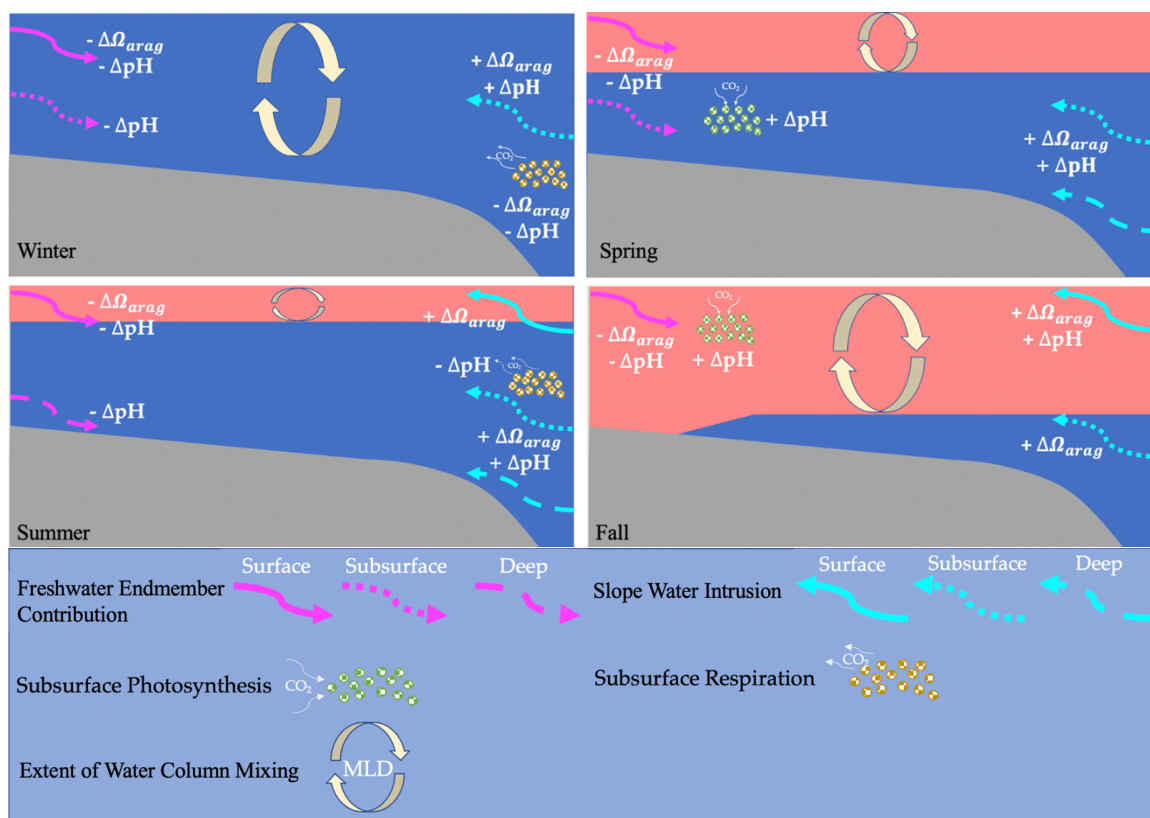


Figure 3.9: Schematic depiction of the major drivers of Ω_{arag} and pH in each season.

Major drivers were identified as those which changed $\Delta\Omega_{arag} > 0.50$ and $\Delta\text{pH} > 0.15$ (90th percentile; see Section 3.3.3). Red indicates the approximate surface mixed-layer depth in each season.

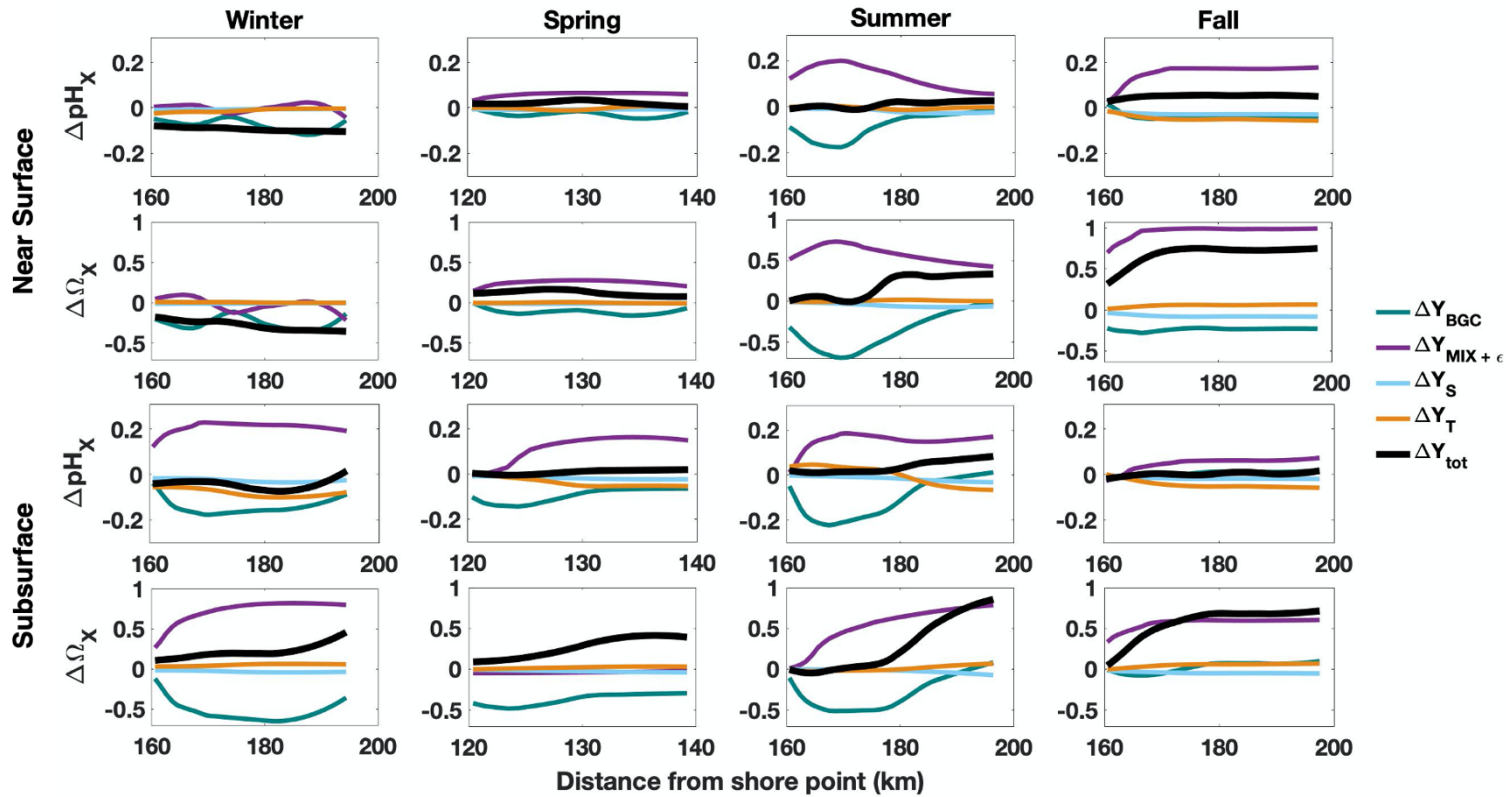


Figure 3.10: Drivers of change in pH and Ω_{arag} in shelf break surface and subsurface water. Values shown are comparisons to the seasonal mean (Analysis 1). Elevated pH and Ω_{arag} were present at the shelf break in spring, summer, and fall, largely due to the influence of the Gulf Stream influenced shelf break jet. A robust loess smoothing filter, spanning 10% of the data points, was applied for visualization purposes.

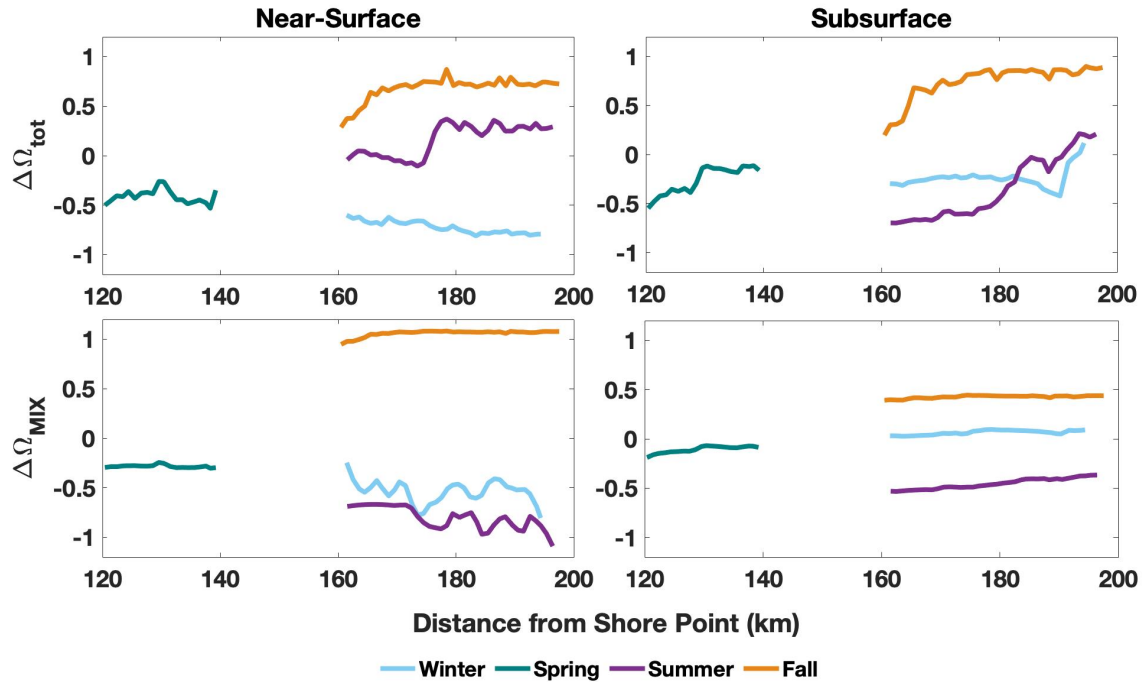


Figure 3.11: Relative change in Ω_{arag} at the shelf break in each season, compared to an annual mean (Analysis 2). Top panels indicate the total resulting sum of all driver influences, and bottom panels show the influence of mixing on Ω_{arag} . Mixing of the high- Ω_{arag} shelf break jet water had the most influence during the fall deployment. A robust loess smoothing filter, spanning 10% of the data points, was applied for visualization purposes.

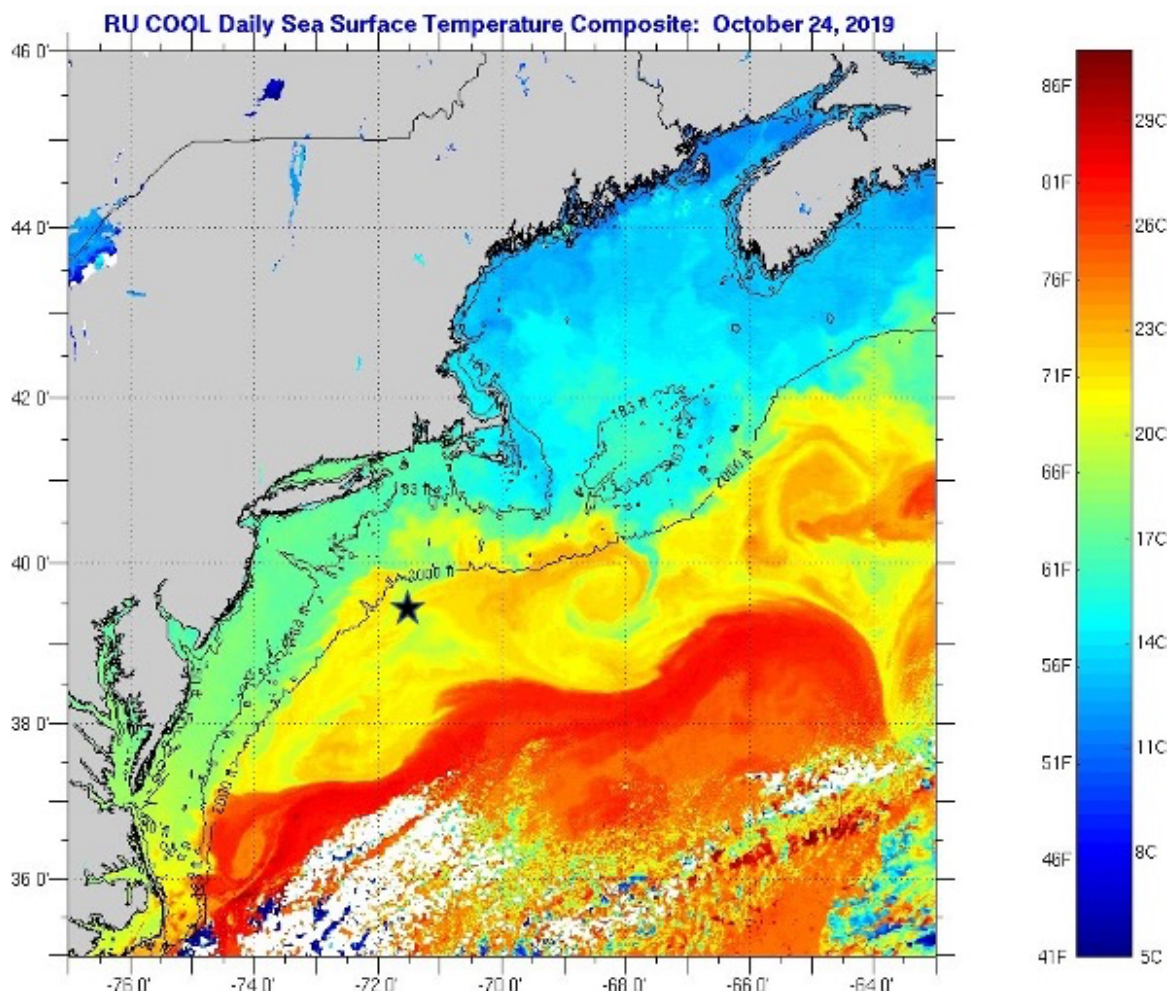


Figure 3.12: Mid-Atlantic sea surface temperature observations on October 24, 2019 (fall glider deployment). Glider data showed an intrusion of Gulf Stream-influenced water onto the shelf, which was linked to high Ω_{arag} and pH. Glider location on October 24 is marked with a star. Map credit: Rutgers Coastal Ocean Observation Lab (https://marine.rutgers.edu/cool/sat_data/).

3.10 Tables

Table 3.1: Regional and depth definitions used in this analysis.

	Winter	Spring	Summer	Fall
Nearshore				
<i>Near-Surface</i>	Top 5 m	Above 13 m	Above 11 m	Above 42 m
<i>Subsurface</i>	Bottom 5 m	Below 13 m	11-38 m	Below 42 m
<i>Deep Water</i>	<i>N/A</i>	<i>N/A</i>	Below 39 m	<i>N/A</i>
Midshelf				
<i>Near-Surface</i>	Top 5 m	Above 13 m	Above 11 m	Above 42 m
<i>Subsurface</i>	Bottom 5 m	13-45 m	11-45 m	Below 42 m
<i>Deep Water</i>	<i>N/A</i>	Below 56 m	Below 45 m	<i>N/A</i>
Shelf Break				
<i>Near-Surface</i>	Top 5 m	Above 13 m	Above 11 m	Above 42 m
<i>Subsurface</i>	Bottom 5 m	13-120 m	11-100 m	42-80 m
<i>Deep Water</i>	<i>N/A</i>	Below 120 m	Below 100 m	Below 88 m

3.11 Supplemental Figures

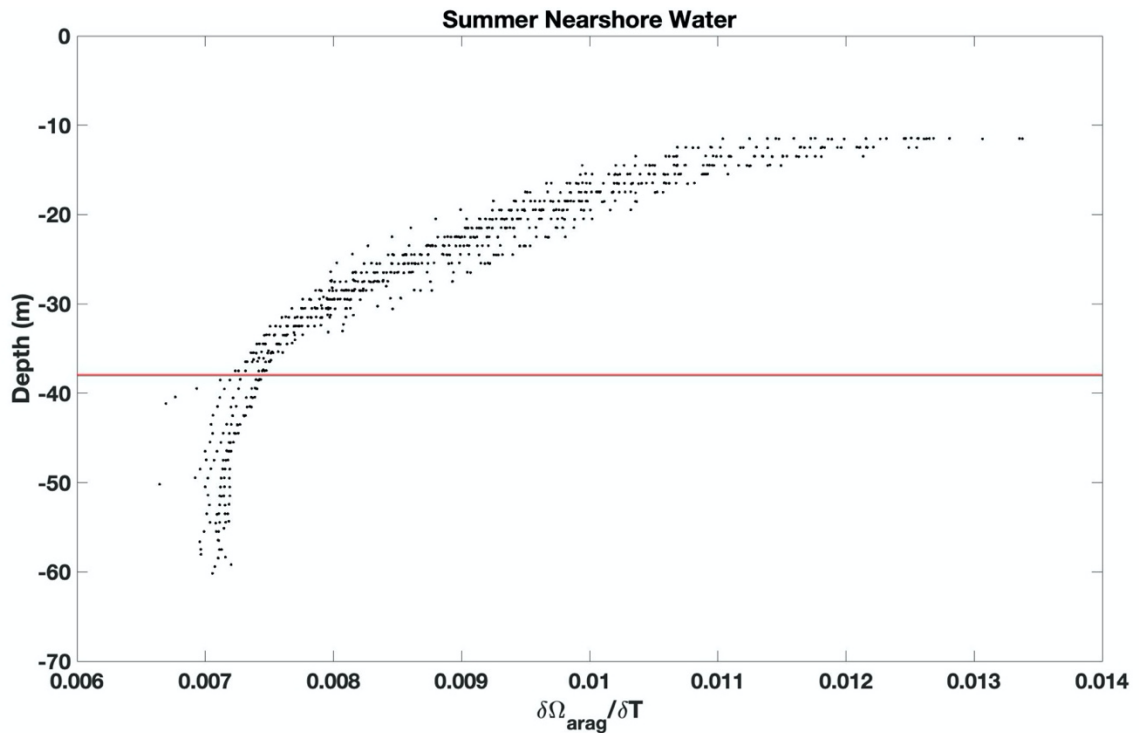


Figure S3.1. Ω_{arag} sensitivity to changes in temperature ($\frac{\partial\Omega_{arag}}{\partial T}$) vs. depth, the relationship which was used to identify deep water masses; in this example, the relationship is shown for summer nearshore water. There is a break in the slope of the relationship around 38 m, indicating the transition from subsurface water to deep water. Similar breaks were seen in each driver variable's sensitivity. Deep water was identified in spring, summer, and fall.

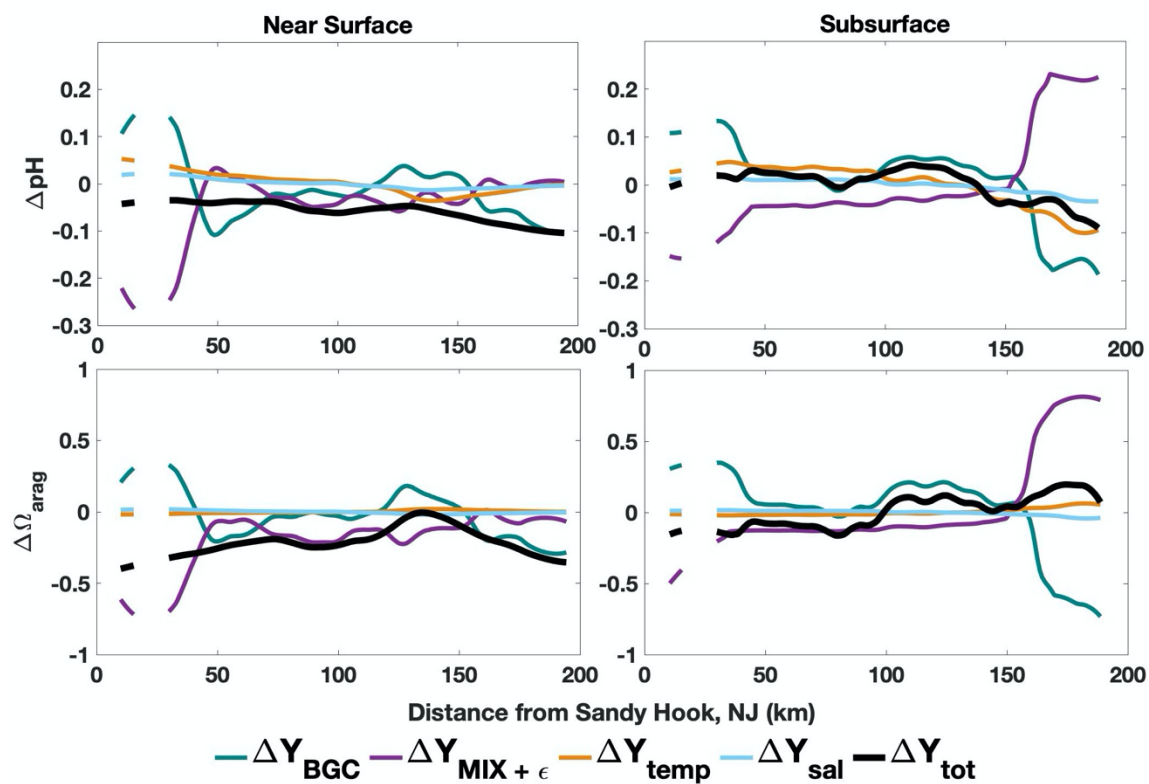


Figure S3.2. Drivers of change in Ω_{arag} and pH in Winter 2019. ΔY_{tot} indicates the change in a variable from the seasonal mean in that depth layer (Analysis 1). A robust loess smoothing filter, spanning 10% of the data points, was applied for visualization purposes.

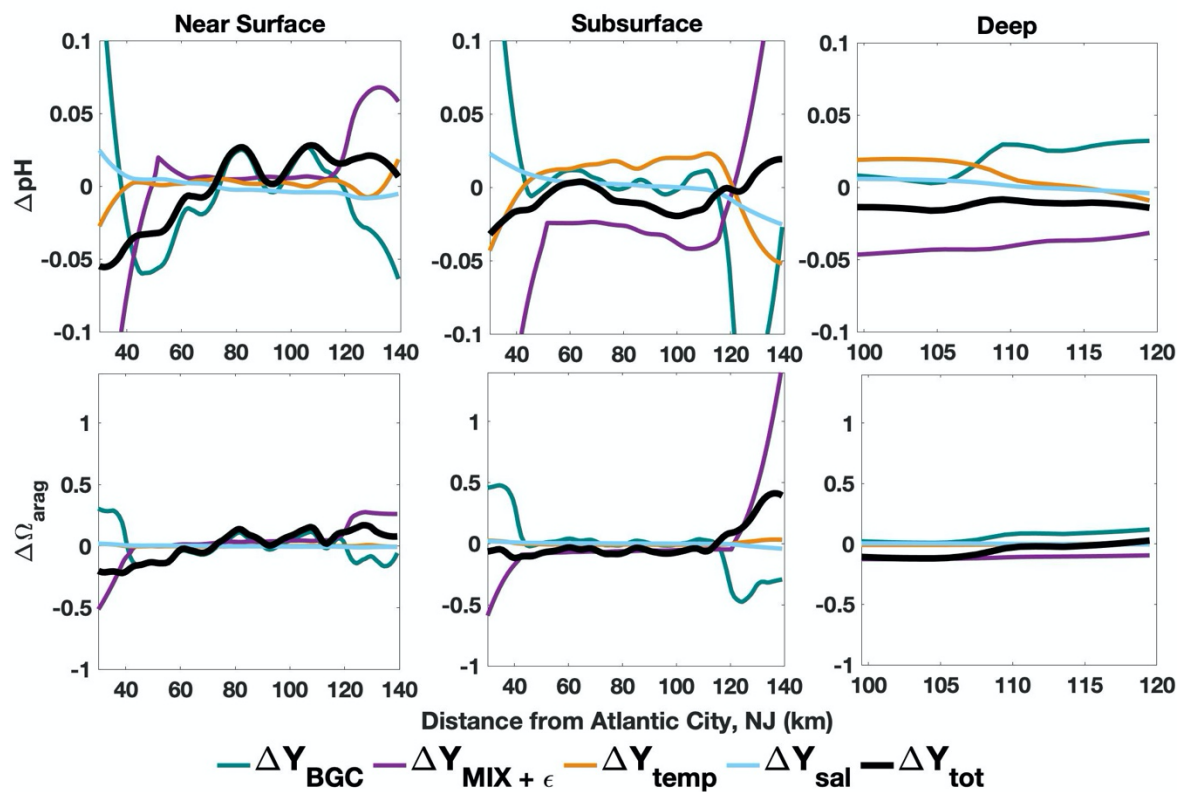


Figure S3.3. Drivers of change in Ω_{arag} and pH in Spring 2018. ΔY_{tot} indicates the change in a variable from the seasonal mean in that depth layer (Analysis 1). A robust loess smoothing filter, spanning 10% of the data points, was applied for visualization purposes.

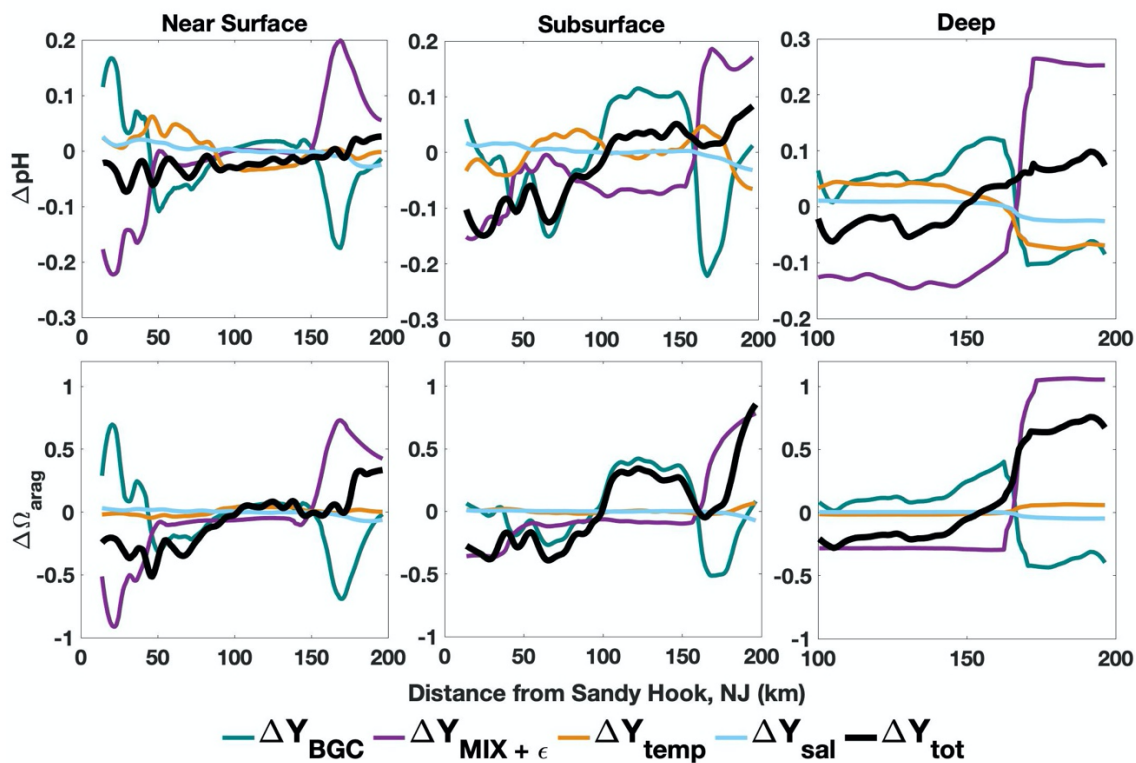


Figure S3.4. Drivers of change in Ω_{arag} and pH in Summer 2019. ΔY_{tot} indicates the change in a variable from the seasonal mean in that depth layer (Analysis 1). A robust loess smoothing filter, spanning 10% of the data points, was applied for visualization purposes.

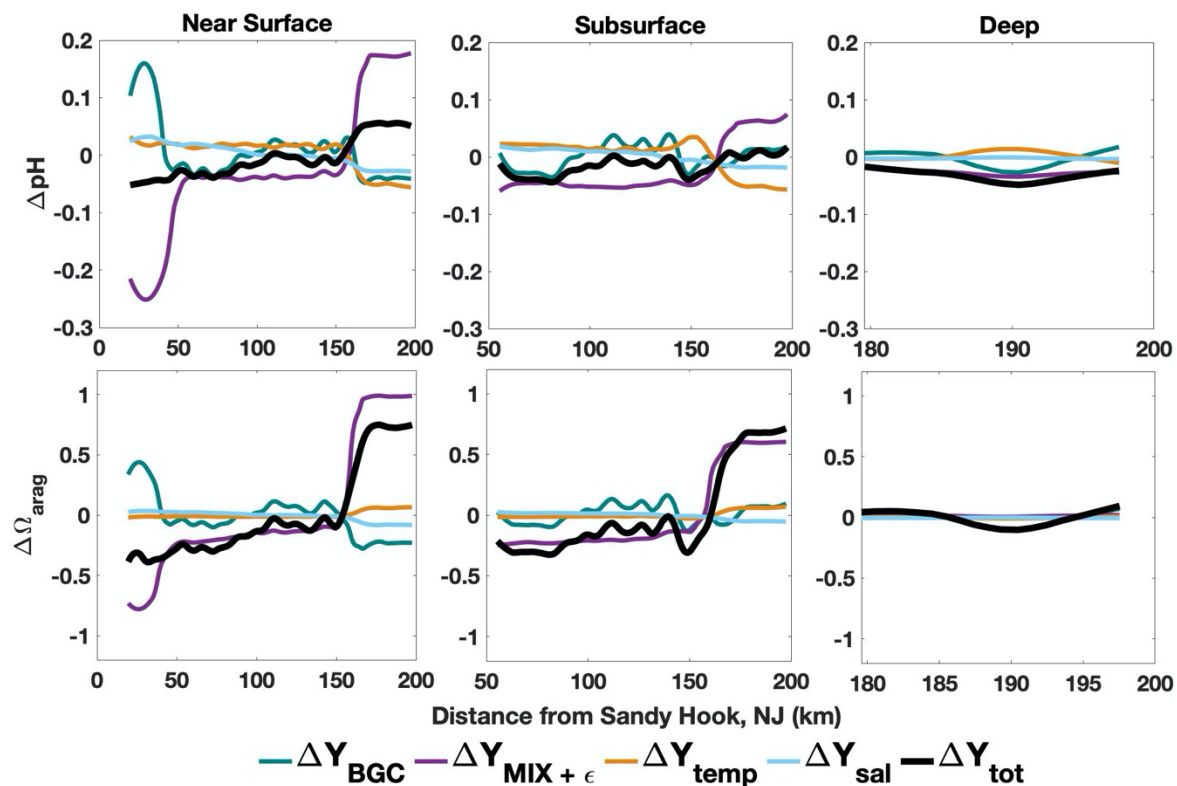


Figure S3.5. Drivers of change in Ω_{arag} and pH in Fall 2019. ΔY_{tot} indicates the change in a variable from the seasonal mean in that depth layer (Analysis 1). A robust loess smoothing filter, spanning 10% of the data points, was applied for visualization purposes.

3.12 Supplemental Tables

Table S3.1. Sensitivities of H^+ and Ω_{arag} to changes in temperature, salinity, TA, DIC, and salinity-normalized DIC (nDIC). Equations are split by season and region as defined in Table 1. Sensitivities for TA, DIC, and nDIC were used to compute changes in pH and Ω_{arag} due to biogeochemistry and water mass mixing as described in section 2.3.

	$\frac{\partial H^+}{\partial T}$	$\frac{\partial H^+}{\partial S}$	$\frac{\partial H^+}{\partial TA}$	$\frac{\partial H^+}{\partial DIC}$	$\frac{\partial H^+}{\partial nDIC}$	$\frac{\partial \Omega_{arag}}{\partial T}$	$\frac{\partial \Omega_{arag}}{\partial S}$	$\frac{\partial \Omega_{arag}}{\partial TA}$	$\frac{\partial \Omega_{arag}}{\partial DIC}$	$\frac{\partial \Omega_{arag}}{\partial nDIC}$
Winter										
<i>Nearshore Near-Surface</i>	0.2828	0.2307	-0.0446	0.0467	0.0485	0.0074	-0.0125	0.0093	-0.0089	-0.0088
<i>Nearshore Subsurface</i>	0.3081	0.2451	-0.0473	0.0495	0.0513	0.0082	-0.0136	0.0093	-0.0089	-0.0088
<i>Midshelf Near-Surface</i>	0.2515	0.2027	-0.0344	0.0364	0.0404	0.0090	-0.0215	0.0097	-0.0092	-0.0092
<i>Midshelf Subsurface</i>	0.3108	0.2453	-0.0454	0.0477	0.0495	0.0091	-0.0156	0.0094	-0.0089	-0.0089
<i>Shelf Break Near-Surface</i>	0.2712	0.2158	-0.0384	0.0405	0.0418	0.0089	-0.0209	0.0096	-0.0091	-0.0091
<i>Shelf Break Subsurface</i>	0.3551	0.2741	-0.0489	0.0516	0.0522	0.0115	-0.0194	0.0094	-0.0090	-0.0090
Spring										
<i>Nearshore Near-Surface</i>	0.3709	0.3145	-0.0618	0.0646	0.0656	0.0103	-0.0136	0.0095	-0.0090	-0.0090
<i>Nearshore Subsurface</i>	0.3633	0.2986	-0.0600	0.0626	0.0634	0.0095	-0.0129	0.0093	-0.0089	-0.0089

Table S3.1 Continued

<i>Midshelf Near-Surface</i>	0.3293	0.2722	-0.0490	0.0516	0.0525	0.0105	-0.0166	0.0096	-0.0092	-0.0092
<i>Midshelf Subsurface</i>	0.3428	0.2702	-0.0541	0.0565	0.0569	0.0087	-0.0133	0.0092	-0.0088	-0.0088
<i>Midshelf Deep Water</i>	0.3729	0.2868	-0.0616	0.0639	0.0646	0.0083	-0.0117	0.0089	-0.0085	-0.0085
<i>Shelf Break Near-Surface</i>	0.3142	0.2576	-0.0442	0.0468	0.0470	0.0109	-0.0184	0.0097	-0.0093	-0.0093
<i>Shelf Break Subsurface</i>	0.3355	0.2610	-0.0470	0.0495	0.0515	0.0105	-0.0182	0.0095	-0.0090	-0.0090
<i>Shelf Break Deep Water</i>	0.3572	0.2735	-0.0484	0.0511	0.0511	0.0118	-0.0200	0.0094	-0.0089	-0.0089
Summer										
<i>Nearshore Near-Surface</i>	0.3611	0.3372	-0.0534	0.0569	0.0574	0.0164	-0.0230	0.0105	-0.0100	-0.0100
<i>Nearshore Subsurface</i>	0.4979	0.4031	-0.0989	0.1017	0.1016	0.0093	-0.0087	0.0086	-0.0082	-0.0082
<i>Nearshore Deep Water</i>	0.5902	0.4304	-0.1329	0.1346	0.1350	0.0072	-0.0040	0.0073	-0.0070	-0.0070
<i>Midshelf Near-Surface</i>	0.3266	0.3021	-0.0441	0.0475	0.0632	0.0180	-0.0324	0.0107	-0.0101	-0.0099
<i>Midshelf Subsurface</i>	0.4001	0.3229	-0.0696	0.0722	0.0748	0.0097	-0.0126	0.0091	-0.0087	-0.0086
<i>Midshelf Deep Water</i>	0.4624	0.3474	-0.0908	0.0930	0.0937	0.0074	-0.0072	0.0082	-0.0078	-0.0078
<i>Shelf Break Near-Surface</i>	0.2802	0.2507	-0.0328	0.0358	0.0439	0.0192	-0.0434	0.0109	-0.0102	-0.0101

Table S3.1 Continued

<i>Shelf Break Subsurface</i>	0.3639	0.2880	-0.0547	0.0574	0.0665	0.0108	-0.0170	0.0094	-0.0090	-0.0087
<i>Shelf Break Deep Water</i>	0.3702	0.2842	-0.0505	0.0533	0.0534	0.0121	-0.0202	0.0094	-0.0090	-0.0090
Fall										
<i>Nearshore Near-Surface</i>	0.3548	0.3050	-0.0515	0.0546	0.0547	0.0132	-0.0195	0.0100	-0.0095	-0.0095
<i>Nearshore Subsurface</i>	0.3899	0.3199	-0.0574	0.0605	0.0605	0.0127	-0.0187	0.0097	-0.0092	-0.0092
<i>Midshelf Near-Surface</i>	0.3418	0.2857	-0.0459	0.0489	0.0515	0.0138	-0.0226	0.0100	-0.0096	-0.0095
<i>Midshelf Subsurface</i>	0.3554	0.2904	-0.0480	0.0510	0.0520	0.0136	-0.0221	0.0099	-0.0094	-0.0094
<i>Shelf Break Near-Surface</i>	0.2983	0.2420	-0.0315	0.0345	0.0347	0.0179	-0.0365	0.0105	-0.0099	-0.0099
<i>Shelf Break Subsurface</i>	0.3100	0.2506	-0.0338	0.0367	0.0371	0.0175	-0.0344	0.0103	-0.0098	-0.0098
<i>Shelf Break Deep Water</i>	0.3649	0.2847	-0.0474	0.0504	0.0506	0.0136	-0.0233	0.0097	-0.0092	-0.0092

Table S3.2. Anomalies of pH and Ω_{arag} caused by temperature, salinity, mixing and air-sea gas exchange, and biogeochemical activity during four seasonal glider deployments in the MAB. Values reported here are seasonal mean anomalies as calculated in Analysis 1, in which values were compared to a seasonal mean to evaluate spatial variability.

	ΔpH_{tot}	ΔpH_T	ΔpH_S	ΔpH_{MIX}	ΔpH_{BGC}	$\Delta \Omega_{tot}$	$\Delta \Omega_T$	$\Delta \Omega_S$	$\Delta \Omega_{MIX}$	$\Delta \Omega_{BGC}$
Winter										
<i>Nearshore Surface</i>	-0.04	0.04	0.02	-0.24	0.13	-0.37	-0.02	0.02	-0.67	0.30
<i>Nearshore Subsurface</i>	0.01	0.04	0.01	-0.17	0.13	-0.14	-0.02	0.01	-0.47	0.33
<i>Midshelf Surface</i>	-0.05	0.00	0.00	-0.03	-0.02	-0.17	0.00	-0.01	-0.19	0.02
<i>Midshelf Subsurface</i>	0.01	0.01	0.00	-0.03	0.03	-0.01	-0.01	0.00	-0.10	0.09
<i>Shelf Break Surface</i>	-0.09	-0.01	-0.01	0.00	-0.08	-0.28	0.01	-0.01	-0.07	-0.21
<i>Shelf Break Subsurface</i>	-0.05	-0.08	-0.03	0.22	-0.17	0.19	0.05	-0.03	0.78	-0.61
Spring										
<i>Nearshore Surface</i>	-0.05	-0.02	0.02	-0.19	0.13	-0.21	0.01	0.02	-0.53	0.29
<i>Nearshore Subsurface</i>	-0.03	-0.03	0.02	-0.23	0.21	-0.07	0.02	0.02	-0.56	0.45
<i>Midshelf Surface</i>	0.00	0.00	0.00	0.01	-0.01	-0.01	0.00	0.00	0.01	-0.02
<i>Midshelf Subsurface</i>	-0.01	0.02	0.00	-0.03	0.01	-0.05	-0.01	0.00	-0.06	0.02
<i>Midshelf Deep Water</i>	-0.01	0.01	0.00	-0.04	0.02	-0.06	-0.01	0.00	-0.12	0.06
<i>Shelf Break Surface</i>	0.02	0.00	-0.01	0.06	-0.03	0.13	0.00	-0.01	0.26	-0.13

Table S3.2 Continued

<i>Shelf Break Subsurface</i>	0.01	-0.04	-0.02	0.17	-0.11	0.27	0.02	-0.03	0.66	-0.39
<i>Shelf Break Deep Water</i>	0.00	-0.07	-0.02	0.17	-0.09	0.39	0.05	-0.03	0.73	-0.35
Summer										
<i>Nearshore Surface</i>	-0.04	0.02	0.02	-0.20	0.12	-0.30	-0.02	0.02	-0.71	0.41
<i>Nearshore Subsurface</i>	-0.12	-0.03	0.01	-0.14	0.03	-0.28	0.01	0.01	-0.36	0.06
<i>Nearshore Deep Water</i>	-0.14	0.01	0.02	-0.17	-0.01	-0.41	0.00	0.00	-0.40	-0.01
<i>Midshelf Surface</i>	-0.03	0.00	0.00	-0.01	-0.03	-0.11	0.01	0.00	-0.08	-0.08
<i>Midshelf Subsurface</i>	-0.02	0.01	0.00	-0.05	0.01	0.01	0.00	0.00	-0.09	0.10
<i>Midshelf Deep Water</i>	-0.02	0.03	0.01	-0.13	0.05	-0.18	-0.01	0.00	-0.29	0.12
<i>Shelf Break Surface</i>	0.01	0.00	-0.02	0.12	-0.08	0.21	0.01	-0.06	0.64	-0.33
<i>Shelf Break Subsurface</i>	0.04	0.00	-0.02	0.17	-0.12	0.30	0.01	-0.03	0.63	-0.32
<i>Shelf Break Deep Water</i>	0.08	-0.07	-0.02	0.26	-0.08	0.69	0.06	-0.04	1.06	-0.38
Fall										
<i>Nearshore Surface</i>	-0.04	0.02	0.03	-0.23	0.15	-0.35	-0.01	0.03	-0.76	0.39
<i>Nearshore Subsurface</i>	-0.07	0.02	0.02	-0.11	0.00	-0.43	-0.01	0.02	-0.44	0.01
<i>Midshelf Surface</i>	-0.02	0.01	0.01	-0.04	0.00	-0.15	-0.01	0.01	-0.16	0.01
<i>Midshelf Subsurface</i>	-0.02	0.02	0.01	-0.05	0.00	-0.19	-0.01	0.01	-0.20	0.01
<i>Shelf Break Surface</i>	0.05	-0.05	-0.03	0.17	-0.05	0.69	0.05	-0.07	0.97	-0.26

Table S3.2 Continued

<i>Shelf Break Subsurface</i>	0.00	-0.04	-0.02	0.07	-0.01	0.57	0.05	-0.04	0.58	-0.02
<i>Shelf Break Deep Water</i>	-0.03	0.00	0.00	-0.03	0.00	0.00	0.00	0.00	0.00	0.00

Table S3.3. Anomalies of pH and Ω_{arag} caused by temperature, salinity, mixing and air-sea gas exchange, and biogeochemical activity during four seasonal glider deployments in the MAB. Values reported here are annual mean anomalies as calculated in Analysis 2, in which values were compared to an annual mean to evaluate seasonal variability.

	ΔpH_{tot}	ΔpH_T	ΔpH_S	ΔpH_{MIX}	ΔpH_{BGC}	$\Delta \Omega_{tot}$	$\Delta \Omega_T$	$\Delta \Omega_S$	$\Delta \Omega_{MIX}$	$\Delta \Omega_{BGC}$
Winter										
<i>Nearshore Surface</i>	0.08	0.20	0.00	-0.05	-0.07	-0.32	-0.08	0.00	0.02	-0.27
<i>Nearshore Subsurface</i>	0.10	0.06	0.00	0.04	0.00	0.16	-0.03	0.00	0.17	0.02
<i>Midshelf Surface</i>	0.09	0.13	0.00	-0.02	-0.02	-0.15	-0.08	-0.01	-0.08	0.02
<i>Midshelf Subsurface</i>	0.05	0.06	0.00	0.01	-0.01	0.00	-0.03	0.00	0.06	-0.02
<i>Shelf Break Surface</i>	-0.01	0.20	0.01	-0.19	-0.03	-0.73	-0.09	0.01	-0.58	-0.07
<i>Shelf Break Subsurface</i>	-0.03	0.04	0.00	0.03	-0.10	-0.22	-0.02	-0.01	0.14	-0.34
Spring										
<i>Nearshore Surface</i>	-0.05	0.05	0.00	0.04	-0.13	-0.26	-0.02	0.00	0.14	-0.38
<i>Nearshore Subsurface</i>	0.02	-0.01	0.00	-0.02	0.05	0.11	0.01	0.00	-0.05	0.15
<i>Midshelf Surface</i>	0.03	0.06	0.00	0.00	-0.03	-0.09	-0.04	0.00	0.06	-0.11
<i>Midshelf Subsurface</i>	0.00	0.06	0.00	-0.03	-0.03	-0.16	-0.03	0.00	-0.05	-0.08
<i>Midshelf Deep Water</i>	-0.02	0.00	0.00	-0.01	0.00	-0.63	0.00	0.00	-0.64	0.00
<i>Shelf Break Surface</i>	-0.01	0.10	0.01	-0.10	-0.03	-0.42	-0.05	0.01	-0.29	-0.09

Table S3.3 Continued

<i>Shelf Break Subsurface</i>	-0.01	0.08	0.01	-0.05	-0.04	-0.27	-0.04	0.01	-0.13	-0.11
<i>Shelf Break Deep Water</i>	0.00	0.04	0.00	-0.02	-0.02	-0.18	-0.02	0.00	-0.09	-0.07
Summer										
<i>Nearshore Surface</i>	-0.07	-0.13	0.02	-0.32	0.36	0.15	0.13	0.02	-0.83	0.83
<i>Nearshore Subsurface</i>	-0.14	-0.07	0.01	-0.05	-0.04	-0.23	0.03	0.00	-0.20	-0.06
<i>Nearshore Deep Water</i>	-0.23	0.00	0.00	-0.24	0.00	-1.21	0.00	0.00	-1.21	0.00
<i>Midshelf Surface</i>	-0.04	-0.13	0.02	-0.44	0.51	0.31	0.16	0.04	-0.88	0.96
<i>Midshelf Subsurface</i>	-0.09	-0.01	0.01	-0.14	0.05	-0.21	0.00	0.01	-0.40	0.18
<i>Midshelf Deep Water</i>	-0.11	0.00	0.00	-0.12	-0.01	-0.97	0.00	0.00	-0.97	0.00
<i>Shelf Break Surface</i>	-0.06	-0.11	0.02	-0.21	0.27	0.16	0.15	0.05	-0.85	0.89
<i>Shelf Break Subsurface</i>	-0.05	0.06	0.02	-0.13	0.01	-0.36	-0.02	0.01	-0.48	0.13
<i>Shelf Break Deep Water</i>	-0.01	0.02	0.00	0.00	-0.03	-0.10	-0.01	0.00	0.02	-0.11
Fall										
<i>Nearshore Surface</i>	-0.02	-0.04	-0.02	0.16	-0.13	0.13	0.03	-0.02	0.61	-0.48
<i>Nearshore Subsurface</i>	-0.01	-0.11	-0.02	0.21	-0.09	0.46	0.09	-0.03	0.71	-0.31
<i>Midshelf Surface</i>	0.02	-0.03	-0.01	0.14	-0.07	0.31	0.03	-0.02	0.56	-0.25
<i>Midshelf Subsurface</i>	-0.01	-0.09	-0.01	0.13	-0.03	0.41	0.08	-0.02	0.45	-0.10
<i>Shelf Break Surface</i>	0.03	-0.07	-0.03	0.20	-0.08	0.69	0.08	-0.08	1.08	-0.39

Table S3.3 Continued

<i>Shelf Break Subsurface</i>	0.00	-0.09	-0.01	0.04	0.06	0.74	0.11	-0.03	0.38	0.28
<i>Shelf Break Deep Water</i>	-0.03	-0.02	0.00	-0.03	0.02	0.09	0.02	0.00	-0.01	0.09

CHAPTER 4: Meta-Analysis of Larval Bivalve Growth in Response to Ocean Carbonate Chemistry and its Application to Sea Scallop Larval Dispersal in the Mid-Atlantic Bight*

* This chapter is in preparation for submission to the Journal of Shellfish Research as “Wright-Fairbanks, E.K., Munroe, D., Hunter, E., Wilkin, J., and Saba, G.K. Meta-Analysis of Larval Bivalve Growth in Response to Ocean Acidification and its Application to Sea Scallop Larval Dispersal in the Mid-Atlantic Bight.”

4.1 Abstract

Ocean acidification due to increasing atmospheric CO₂ and coastal physical, biological, and chemical processes is an ongoing threat to carbonate-utilizing organisms living in productive coastal shelves. Bivalves exposed to acidification have shown reduced growth, reproduction, and metabolic processes, with larval stages exhibiting the greatest susceptibility. Here, we compile results from published studies on larval bivalve growth responses to acidification to estimate a relationship between larval growth and aragonite saturation state. We then apply this relationship to a larval dispersal individual-based model for Atlantic sea scallops (*Placopecten magellanicus*), an economically vital species in the Mid-Atlantic Bight that is historically under-studied in acidification research. To date, there have been no published studies on sea scallop larval response to ocean acidification. Model simulations allow the identification of potential impacts of acidification on scallop success in the region. Results show that the degree of susceptibility to acidification sea scallop exhibit will influence their ability to successfully settle in major fisheries habitats in the MAB on a seasonal and annual basis. Additionally, an interaction between drivers of larval success is identified, in which temperature and the state of ocean acidification determine success based on organism sensitivity to acidification. This balance between drivers influences larval settlement success across spatial and interannual scales in the MAB.

4.2. Introduction

Ocean acidification (OA) due to increasing atmospheric CO₂ has caused global surface water pH to decline by 0.017-0.027 pH units per decade since the late 1980s

(Gledhill et al., 2015; IPCC, 2019; Sutton et al., 2016; Zeebe, 2012). This pH decline is associated with a simultaneous decline in calcium carbonate saturation state (Ω), indicating potential negative effects to organisms that utilize calcium carbonate to make shells. Ocean acidification can be compounded in coastal zones by various physical, biological, and chemical processes (“coastal acidification”). Freshwater inputs, nutrient loading, productivity-respiration cycles, coastal currents, and water mass intrusions can alter local seawater chemistry, resulting in episodic extremes of carbonate chemistry on daily to interannual time scales (Cai et al., 2011; Gledhill et al., 2015; Siedlecki et al., 2017; Wright-Fairbanks et al., 2020; Wright-Fairbanks & Saba, in review).

Organisms that build structures with calcium carbonate are especially susceptible to ocean acidification because decreased Ω can result in reduced calcification rates or depression of metabolic processes (Cooley et al., 2015; Doney et al., 2009; Gazeau et al., 2013; Kroeker et al., 2013). While calcifying organisms can upregulate calcification internally, this upregulation is an energetic cost that comes at the expense of other functions including metabolism, respiration, growth, body condition, excretion, and reproduction (Clements & Chopin, 2017). Adult shellfish exposed to elevated levels of $p\text{CO}_2$ can exhibit thin or malformed shells with impaired hinge development, making them more vulnerable to predators or environmental stressors (Doney et al., 2009; Gazeau et al., 2013). Larval bivalves exposed to acidified waters have been shown to exhibit decreased survival, metamorphosis, growth, shell thickness and integrity, lipid accumulation, calcium uptake, calcification, feeding initiation, and juvenile settlement (Gobler & Talmage, 2013; Green et al., 2012; Kurihara et al., 2008; Ries et al., 2009; Talmage & Gobler, 2010; Waldbusser et al., 2014). Trochophore larvae are the most

sensitive life-history stage in marine bivalves (Kapsenberg et al., 2018). This transitional stage includes the first deposition of amorphous calcium carbonate which lacks crystalline structure and therefore is susceptible to dissolution (Parker et al., 2013). While larval bivalves can elevate Ω somewhat at the shell-tissue interface under moderate acidification levels, this acid-base regulation is an energetic drain and leads to declines in calcification rate (Ramesh et al., 2017).

The Atlantic sea scallop (*Placopecten magellanicus*), hereafter ‘scallops’, is one of the most economically important shellfish in the United States, with a fishery valued at \$486 million in 2020 (NOAA, 2021b). Scallops are found along the Atlantic coast from Cape Hatteras, North Carolina to Newfoundland, Canada, living at depths from 25-200 meters with an active fishery operating between 25-100 meters year-round in the U.S. (NEFSC, 2014). In this coastal region, scallops are exposed to daily, seasonal, and interannual environmental fluctuations, including episodic and ongoing gradual ocean acidification (Wright-Fairbanks et al., 2020; Xu et al., 2017; Xu et al., 2020). In the Mid-Atlantic, scallop spawning and transport occur during periods of transition in the water column, either in the spring as seasonal warming increases stratification or in the fall during seasonal overturn and mixing (Neima & Kenchington, 1997). During development, larval scallops can be transported hundreds of kilometers alongshore over a period of ~35 days (Culliney, 1974; Munroe et al., 2018), encountering variable environmental conditions including pockets of low pH and/or Ω that may affect processes such as growth. Despite their economic importance and susceptibility to acidification, the effects of OA on larval scallop growth and development have not been determined in a laboratory setting.

In this study, we compiled results from published literature to estimate a comprehensive larval bivalve growth rate vs. aragonite saturation state relationship. This relationship was then applied to a model simulation of larval sea scallop growth and dispersal in the Mid-Atlantic Bight. This allowed observation of the effects of short-term fluctuations in OA on the growth, settlement success, and population connectivity of an economically crucial, yet under-studied species. Lastly, this study highlights the need for standardized laboratory methods in shellfish OA research, and the importance of species-specific investigations.

4.3 Methods

4.3.1 Larval bivalve growth parameter

4.3.1.1 Study selection

A literature review was conducted on studies that investigated the effects of ocean acidification on larval bivalve growth. Through a comprehensive search for keywords “ocean acidification”, “bivalve”, “growth”, “larvae”, and combinations of these phrases on Google Scholar and ISI Web of Science, we identified studies published at any time that reported bivalve larval growth responses to ocean acidification. Further, we went through the references of all studies to identify any additional relevant works. Overall, 27 studies were analyzed (Supplemental Table 1). Variables recorded in the review included study species, life stages of study species, treatment groups, and when available, pH, the partial pressure of carbon dioxide ($p\text{CO}_2$), dissolved inorganic carbon (DIC), total alkalinity (TA), concentration of carbonate ions ($[\text{CO}_3^{2-}]$), calcite saturation state (Ω_{cal}), aragonite saturation state (Ω_{arag}), salinity, temperature, and dissolved oxygen for each

treatment group. Additionally, applicable response variables (larval growth rate or shell size over time), values of response variables in each treatment group, and notes on other variables studied were collected. When response variable values were not explicitly stated in the text, corresponding authors were contacted and asked to provide values for analysis.

All studies were filtered through the following criteria to determine those that generated an applicable relationship between larval bivalve growth and ocean acidification relevant to species inhabiting waters along the U.S. East Coast. Studies included in the final analysis provided exact values of larval shell growth rates (length/time) or larval shell size, measured at the longest length parallel to the hinge, and age at length so growth rate could be calculated as $\frac{\text{change in length}}{\text{time}}$. Additionally, selected studies included explicit values for all carbonate chemistry parameters (pH, $p\text{CO}_2$, TA, and DIC), or at least 2 out of the 4 so that the remaining parameters could be derived. Lastly, the studies were narrowed down to only those that investigated species commonly found along the U.S. East Coast, including those in Atlantic coastal or bay waters. Focusing on organisms from this region removed variability in larval responses due to drivers of carbonate chemistry in different coastal zones. Some studies only included response variables or treatment values for certain treatment groups. Treatment groups without specific response or treatment values were excluded from the meta-analysis, unless information was provided by the corresponding authors. In the end, results from 9 studies encompassing 5 bivalve species were used to determine a relationship between larval bivalve growth rate and Ω_{arag} . The five bivalve species were *Argopecten irradians* (bay scallop), *Crassostrea virginica* (Eastern oyster), and *Mercenaria mercenaria*

(quahog/hard clam) *Mytilus edulis* (blue mussel), and *Spisula solidissima* (Atlantic surfclam).

4.3.1.2 Growth parameter development

Studies that only provided a final length and time of growth were held under the assumption that initial length was 50 μm , an estimate of average bivalve egg size in the study region (Allen, 1953; Barber & Blake, 1983; Gallager & Mann, 1986; Langton et al., 1987; Schweinitz & Lutz, 1976). This assumption removed the bias of growth rates being calculated from a starting size of 0 μm , which discounts egg size and skews growth rate higher. After the adjusted growth rates were calculated, outliers in each species were defined as >1.5 inter-quartile range away from the median growth rate and were subsequently removed. Then, regression analyses were run on the relationship between carbonate saturation state with respect to aragonite (Ω_{arag}) and growth rates. Ω_{arag} was selected as the variable of choice for this parameter due to its importance in the early development of larval bivalve shells and susceptibility to negative impacts of ocean acidification (Waldbusser et al., 2014).

Larval growth rate and carbonate chemistry relationships were investigated in three ways. First, absolute Ω_{arag} and absolute growth rates ($\mu\text{m}/\text{day}$) were compared using a logarithmic regression.

$$growth\ rate = a + b * \log(\Omega_{arag}) \quad (1)$$

The logarithmic regression was calculated using the MATLAB (v. 2019b) Curve Fitting Toolbox, which provides coefficients of the logarithmic relationship a and b as well as goodness of fit indicators (e.g., R-square and root mean square error (RMSE)). Next, changes in Ω_{arag} and changes in growth rate (overall change and percent change) were

compared using the following first degree polynomial regressions that were also calculated using the MATLAB (v. 2019b) Curve Fitting Toolbox.

$$\Delta growth\ rate = a * \Delta \Omega_{arag} + b \quad (2)$$

$$\% \Delta growth\ rate = a * \% \Delta \Omega_{arag} + b \quad (3)$$

4.3.2 Atlantic sea scallop (*Placopecten magellanicus*) larval dispersal model

A coupled physical-individual behavior model (IBM) was developed to test the applicability of the derived larval bivalve growth rate-OA parameters, wherein modeled scallop larval swimming behavior is impacted by larval size and environment. This model simulated sea scallop larval dispersal along the MAB shelf during two spawning seasons in each of seven years. This approach builds on prior work modeling bivalve larval transport in the MAB (Hart et al., 2020; Munroe et al., 2018; Narváez et al., 2012; Zhang et al., 2015; Zhang et al., 2016), and uses an offline larval tracking model with behavior applied to archived environmental model output rather than using an IBM integrated synchronously within the circulation model. The circulation, OA, and IBM models are described in detail below.

4.3.2.1 Regional Ocean Modeling System (ROMS)

An implementation of the Regional Ocean Modeling System (ROMS; www.myroms.org; Haidvogel et al., 2008; Shchepetkin & McWilliams, 2005) provides the ocean physical and OA environmental properties that force the larval dispersal model. The model is described in detail by López et al. (2020). The domain extends from Cape Hatteras, North Carolina to Halifax, Nova Scotia, and from the coast to beyond the Gulf Stream. It thus encompasses Gulf Stream ring and meander activity, the Gulf of Maine, and the Scotian Shelf, all of which are remote drivers of MAB processes. Model

horizontal resolution is 7 km, with 40 terrain-following coordinate vertical levels. Model open boundary conditions are from the Mercator-Océan global daily analysis (Lellouche et al., 2018), adjusted to remove seasonal biases (Levin et al., 2018), and augmented with harmonic tides (Egbert & Erofeeva, 2002). Surface meteorological forcing is 3-hourly data from the North American Regional Reanalysis (NARR) (Mesinger et al., 2006). River inflows at 27 locations use USGS daily data adjusted to account for ungauged portions of the watershed (López, 2020).

The ROMS simulations used in this study incorporated a biogeochemical (BGC) model that simulates 16 ecosystem constituents (Druon et al., 2010; Fennel & Wilkin, 2009; Hofmann et al., 2011), among them dissolved inorganic and organic nitrogen, semi-labile and refractory organic carbon, dissolved oxygen, alkalinity, and total dissolved inorganic carbon, from which pH and Ω_{arag} can be calculated. The BGC model parameter choices are close to those of Feng et al. (2015), and López (2020) presents further details of the initial and open boundary conditions and features of the BGC model solution. The circulation and BGC models are integrated synchronously (i.e., at every model time-step) to capture the full interaction of BGC processes with tidal mixing, mixed layer variability, and the diurnal cycle of light. This coordinated model-based estimate of circulation, temperature, salinity, pH, and Ω_{arag} allows an investigation of the impacts of full water column carbonate chemistry on larval bivalve dispersal in the MAB.

4.3.2.2 *ROMSPath*

ROMSPath (Hunter, 2021), is based on the LTRANS model (North et al., 2006; Schlag & North, 2012) but works in the native curvilinear and terrain-following

coordinate system of the ROMS model for greater accuracy. To date, applications include studies of algal blooms in the Gulf of Maine (Clark et al., 2016) and mussel larvae in Delaware Bay (Garwood et al., 2021).

4.3.2.2.1 Growth and behavior

Larval scallop behavior was integrated into ROMSPath using algorithms developed for the bivalve larval growth and swimming behavior in the individual-based model (IBM) developed by Munroe et al. (2018). The scallop IBM is described in detail in (Munroe et al., 2018) and the major components used in this study are summarized below.

In Munroe et al. (2018), larval scallop growth was derived using published growth rates taking into account the dependence of growth on water temperature. Larvae were assumed to be spherical for growth purposes, though sinking and swimming rates were based on reported values of non-spherical larvae (Munroe et al., 2018). Details of the temperature-growth relationship can be found in section 2.2 of Munroe et al. (2018). Here, we sought to improve the temperature-based growth relationship by incorporating the relationship between growth and ocean carbonate chemistry, specifically Ω_{arag} .

To integrate Ω_{arag} into the growth parameter, we used the $\Delta growth rate - \Delta\Omega_{arag}$ relationship (Equation 10) to determine the change in growth caused by a change in a reference Ω_{arag} of 1.92. The reference value was determined as the average full-water column Ω_{arag} in the MAB during the modeled seasons (spring, summer, and fall) based on high-resolution autonomous seasonal measurements (Wright-Fairbanks et al., 2020). We added the change in growth due to Ω_{arag} to temperature-derived growth, resulting in overall daily growth.

$$\text{daily_growth} = \text{temperature_growth} + \Omega_{arag_delta_growth} \quad (4)$$

Because dissolution is not thermodynamically favorable when $\Omega_{arag} > 1.0$, if the model predicted a negative growth value but $\Omega_{arag} > 1.0$, growth was set to 0 for that time period.

Larval vertical swimming behavior was determined based on temperature and larval size. Size was derived using the growth equations described above. Vertical movement was a product of passive sinking rates, upward swimming speed, and downward swimming speed, all of which varied with larval length. Vertical movement of larvae over time ($\frac{dz}{dt}$) is determined using Equation 5, reproduced here from Munroe et al. (2018).

$$\frac{dz}{dt} = -Sk(L)(1 - Fu(T)) + (Us_s(L) \times Fu(T)) - Ds_s(L)(1 - Fu(T)) \quad (5)$$

Where passive sinking (Sk), upward swimming speed (Us_s), and downward swimming speed (Ds_s) vary with length (L) as:

$$Sk(L) = Sk_0 L^{Sk_1} \quad (6)$$

$$Us_s(L) = Us_0 + Us_1 L + Us_2 L^2 \quad (7)$$

$$Ds_s(L) = Ds_0 + Ds_1 L + Ds_2 L^2 \quad (8)$$

And the fraction of time spent swimming upward (Fu) varies with temperature (T), where larvae move upwards to warmer water when temperature is below a 16 °C threshold and downwards to cooler water when temperature is above that threshold until they reach settlement size (Munroe et al., 2018).

$$Fu(T) = Fu_{s0} \left(1 - \tanh \left(\frac{T - T_{Us1}}{T_{Us2}} \right) \right) \quad (9)$$

Coefficients of the upward swimming function U_{s0} , U_{s1} , and U_{s2} are -0.381 mm s^{-1} , $9.262 \times 10^{-3} \text{ mm s}^{-1} \mu\text{m}^{-1}$, and $-2.692 \times 10^{-5} \text{ mm s}^{-1} \mu\text{m}^{-2}$, respectively. Coefficients of the downward swimming function D_{s0} , D_{s1} , and D_{s2} are -0.561 mm s^{-1} , $1.749 \times 10^{-2} \text{ mm s}^{-1} \mu\text{m}^{-1}$, and $-6.538 \times 10^{-5} \text{ mm s}^{-1} \mu\text{m}^{-2}$. The initial upward swimming time fraction $F_{u_{s0}}$ is 0.5, and the temperature coefficients that determine the fraction of time spent swimming T_{Us1} and T_{Us2} are $16.5 \text{ }^\circ\text{C}$ and $0.9 \text{ }^\circ\text{C}$.

4.3.2.3 Model runs

ROMSPath particle tracking simulations were run for the years 2007-2013 using 1-day mean velocity, temperature, and ecosystem fields from the coupled ROMS model solution. Using daily average fields as input to ROMSPath, rather than the fully time synchronous particle tracking in Munroe et al. (2018), incurs errors associated with unresolved net effects of high frequency velocity variability. However, over the 45-day time scale of the scallop larval cycle, this effect is not expected to be important.

Modeled larval release quantities were scaled to the scallop spawning biomass observed in each region (Table 4.1; Munroe et al., 2018; NEFSC, 2018). Larvae were released across four broad geographical regions which reflect federal management zones for Atlantic sea scallops (from south to north: Virginia Beach (VB), Delmarva (DMV), New York Bight (NYB), and Long Island (LI); Table 4.1; Figure 4.1). A fifth region, Block Island (BI), was included as a settlement zone but no larvae were released from there due to a lack of spawning population (Munroe et al., 2018). These regions additionally have been the focus of ongoing carbonate system monitoring (Goldsmith et al., 2019; Hunt et al., 2021; Saba et al., 2019; Wright-Fairbanks et al., 2020; Xu et al., 2017; Xu et al., 2020). Larval passage between and successful settlement in the different

management zones indicated population connectivity, which was monitored due to its importance in sustaining populations along the entire coast. Larval release was simulated in each month from May-October, capturing the recognized spring and fall scallop spawning seasons, as well as the influence of summer stratification on larval dispersal (Dupaul et al., 1989). Larvae were released at intervals of 0.1° latitude and 0.25° longitude throughout each release zone, for a total of 57 release points in LI, 61 release points in NYB, 20 release points in DMV, and 13 release points in VB. Release occurred on days 1, 6, 11, 16, 21, and 26 of each month. Larvae were released at bottom water depth at each release point and entered the water column at a $75 \mu\text{m}$, capable of growth and movement via swimming and sinking.

Larvae that reached lengths $>250 \mu\text{m}$ within 45 days (an upper limit of scallop larval viability), in water of depth $<100 \text{ m}$, inside the designated habitat bounds, and without interacting with the model boundary were deemed to have settled successfully. Other causes of natural mortality, such as predation and food availability, were not included in this model.

Four distinct simulations were run. First, a simulation for passive particles with no behavior was run to determine how passive interaction with the environment influenced success (Group 1). Next, a simulation for particles exhibiting growth and behavior derived from temperature was run to understand larval scallop success and population connectivity when OA was not a factor (Group 2). Last, simulations were run to examine potential responses of sea scallop larvae to changes in ocean carbonate chemistry. One OA simulation was run for passive particles with OA-sensitive growth (Group 3), and another was run for particles with OA-sensitive growth and swimming behavior (Group

4). Due to a lack of data indicating the response of larval sea scallops to carbonate chemistry, simulation groups 2 and 4 were used to understand differences between scallop larvae that are OA sensitive and non-OA sensitive (Equations 5 and 6).

Population connectivity and larval success were compared across experiments to understand how sensitivity to OA may impact sea scallop larval dispersal seasonally and interannually. In the analysis of seasonal distinctions that follow, spring comprises May/June release, summer indicates July/August release, and fall is defined as September/October release.

4.4. Results

4.4.1 Larval bivalve growth parameter

Figure 4.2 depicts the results of the larval growth rate vs. Ω_{arag} parameter creation. The derived growth rate- Ω_{arag} and Δ growth rate- $\Delta\Omega_{arag}$ relationships (Figure 4.2) were analyzed to determine which relationship yielded the highest R-square value and fit best into the existing sea scallop larval dispersal model framework (section 4.3.2). The Δ growth rate- $\Delta\Omega_{arag}$ had an R^2 value of 0.35 and the growth rate- Ω_{arag} relationship had an R^2 of 0.25, so the Δ relationship was selected for integration into the model. The Δ relationship was used to alter the existing relationship between larval scallop growth rate and temperature previously determined by Munroe et al. (2018). Including both temperature and Ω_{arag} effects on growth rate provided a more complete picture of how the environment may influence larval bivalve growth rates.

Through parameter selection, two separate response types of larval bivalve growth to changes in carbonate chemistry were identified. One response group

(*Argopecten irradians*, *Crassostrea virginica*, and *Mercenaria mercenaria*) showed sensitivity to changes in carbonate chemistry (i.e., Δ growth rate and $\Delta\Omega_{arag}$ are positively correlated). *Mytilus edulis* showed no sensitivity to these changes (i.e., no linear correlation between Δ growth rate and $\Delta\Omega_{arag}$ with an R-square value of approximately zero) (Figure 4.3). Because there were only two Δ growth rate- $\Delta\Omega_{arag}$ data points for *Spisula solidissima*, a linear relationship could not be determined. However, in the growth rate vs. Ω_{arag} logarithmic analysis, *S. solidissima* showed no correlation between growth rate and Ω_{arag} with an R^2 value of ~ 0 , so it was grouped with *M. edulis* (Figure 4.2). Accordingly, two separate relationships were derived for these two sensitivity groups (Equation 10: OA sensitive; Equation 11: non-OA sensitive).

$$\Delta growth\ rate = 3.71 * \Delta\Omega_{arag} - 3.78; R^2 = 0.3538 \quad (10)$$

$$\Delta growth\ rate = -0.0024 * \Delta\Omega_{arag} + 0.19; R^2 = 0.0000 \quad (11)$$

Because these results indicate that the relationship between changes in Ω_{arag} and larval growth for *M. edulis* and *S. solidissima* is not statistically significant, these non-OA sensitive trials were run without integrating any carbonate system effect into the growth parameter.

4.4.2 Modeled larval scallop sensitivity to OA

Modeled scallop larval dispersal had variable outcomes based on season, year, region, behavior, and the assumption of species sensitivity to OA (Table 4.3). The greatest success for non-OA sensitive larvae occurred in spring 2007 in LI (77.6%), and the greatest average success for OA sensitive scallops occurred in spring 2012 in LI (59.8%). The greatest non-OA sensitive population connectivity occurred in 2007 in LI (34.7%) (Table 4.4), and the greatest OA-sensitive population connectivity occurred in

2011 in DMV (18.3%) (Table 4.5). Scallops exhibiting swimming behavior were 12% and 0.3% more successful than their non-swimming counterparts in the non-OA sensitive and OA sensitive. Regional, seasonal, and annual differences in settlement success and population connectivity are described in detail below.

4.4.2.1 Settlement success

Settlement success rates varied greatly over location, season, and year. But overall, scallops grown under the assumption of OA sensitivity had a success rate 17% lower than scallops growing without OA impacts (Table 4.3). Every year exhibited higher annual average success rates across all locations in the non-OA sensitive trial compared to the OA sensitive trial. However, there were eight instances where the OA sensitive trial had higher success (VB and DMV in fall 2010; VB in summer 2011; NYB, DMV, and NYB in fall 2011; DMV and VB in spring 2012). In those instances, the high success of OA-sensitive larvae occurred when Ω_{arag} was at least 0.4 higher than the 7-year average Ω_{arag} in that location and season. In fall 2011, Ω_{arag} was as much as 1.17 greater than the interannual fall average (VB). Additionally, in 6/8 instances, average temperature was more than 0.9°C higher than average, and up to 6.59°C higher (spring 2012, VB) (Table 4.6).

The greatest differences in success between OA sensitive vs. non-OA sensitive trials occurred in the Long Island region in 6 out of the 7 modeled years, and in New York Bight in the other year (Table 4.3). Long Island also experienced the lowest Ω_{arag} values in the majority of seasons during each year (Table 4.6). Seasonally, the greatest differences in success between OA sensitivity trials occurred in spring or summer in each year and location, with OA-sensitive larvae experiencing lower success than non-

sensitive larvae. The exception to that rule occurred in 2011 in VB and DMV. There, Ω_{arag} was highest in fall which corresponded to success rates 45% (VB) and 50% (DMV) higher in the OA sensitive group than the non-OA sensitive group.

4.4.2.2 Population connectivity

Larval transport allowed for population connectivity between regions in the model domain (Tables 4 and 5). In both the OA sensitive and non-OA sensitive groups, most successful larvae were released in LI and NYB and settled in those same two northern release regions. Larvae released in LI and NYB also settled successfully in DMV, VB, and BI. Larvae released in DMV settled mostly in NYB, with some settling in DMV, LI, and BI. The least successful larvae in both sensitivity groups were released in VB. Of those released there, the highest percentage settled in DMV, with some reaching NYB, LI, and BI. A low percentage of non-OA sensitive larvae and zero OA sensitive larvae successfully settled in VB. Though OA sensitive larvae were more successful in the southern regions and non-OA sensitive larvae were more successful in the north, patterns in regional connectivity did not differ between sensitivity groups. In both OA sensitivity groups, NYB fed the most regions (non-OA sensitive: average 3.9 regions/year; OA sensitive: average 1.9 regions/year) and received larvae from the most regions (non-OA sensitive: average 3.4 regions/year; OA sensitive: average 2 regions/year), making it the most connected region modeled, followed closely by LI.

4.4.2.3 Seasonality

Seasonal patterns of settlement success differed between OA sensitivity groups (Table 4.3). Non-OA sensitive larvae in every region were the most successful in spring and least successful in fall. Conversely, OA sensitive larvae were the most successful in

fall in every region except LI, where high success in spring 2012 skewed the average success to spring. Non-OA sensitive success was highest in spring, when temperature was lowest in each region averaged over all years (Table 4.6). Larvae experienced the warmest temperatures in fall, which was higher than the model cutoff temperature for larval growth (19 °C) in DMV and VB in most years. OA sensitive success was generally highest in fall, when larvae experienced the highest average Ω_{arag} value in every region. In spring 2012, unusually high OA sensitive larval success in the LI region corresponded to the highest seasonal average Ω_{arag} in LI that year.

4.5 Discussion

The review of OA-larval bivalve studies resulted in the successful development of a larval growth rate- Ω_{arag} relationship. The relationship was applied to sea scallops, a species that has not been studied in the laboratory, allowing for conclusions to be drawn about the potential impacts of OA on this understudied group. Sea scallop larval success and population connectivity were dependent on region, season, year, and sensitivity to OA. Larval scallops that are sensitive to OA exhibited overall lower success and population connectivity than non-sensitive larvae. However, OA sensitivity also presented a compensatory mechanism by which high Ω_{arag} made up for declines in growth due to high temperature at the southern extent of the species range. Projected future increases in Ω_{arag} in scallop habitat at the MAB shelf break may increase species success in northern management regions.

4.5.1 Meta-analysis of larval bivalve growth under OA

4.5.1.1 Species-specific responses

The meta-analysis of OA-larval bivalve studies revealed two separate OA response groups, with *Mytilus edulis* and *Spisula solidissima* showing no definitive response to OA and *Argopecten irradians*, *Crassostrea virginica*, and *Mercenaria mercenaria* responding negatively to OA. While all five species are found in the Mid-Atlantic region, they inhabit different environments that may affect their ability to endure acidification.

The three OA sensitive species, *A. irradians*, *C. virginica*, and *M. mercenaria*, are commonly found in shallow estuarine mud or sand flats along the U.S. east coast (Bricelj, 1993; Mackenzie Jr., 2008; NOAA, 2021a). All three species tolerate large swings in salinity and temperature ranging from 5-46 ppt and -2-33 °C (Table 4.2). They have a wide geographic distribution, stretching north of the MAB into the Gulf of St. Lawrence and south of the MAB to the Gulf of Mexico or further (*C. virginica*). *C. virginica* often form dense reefs by attaching to and growing upon each other (Shumway, 1996). *M. mercenaria* live on sandy or muddy sea beds, burying themselves in the sediment, and can also be found among oyster reefs (Roegner & Mann, 1990). *A. irradians* live in aggregations on the sea floor, but are able to swim freely to avoid predators using water propulsion (Mackenzie Jr., 2008).

One non-OA sensitive species, *M. edulis*, inhabits intertidal as well as subtidal habitats, tolerates large swings in salinity (10-35 ppt), but prefers cooler temperatures (5-20 °C) (FAO, 2021). The other non-OA sensitive species, *S. solidissima*, lives in the coastal ocean and can tolerate salinities of 14-52 ppt and temperatures of 15-26 °C, but cannot withstand hypoxic conditions often found in estuaries (Acquafredda et al., 2019; Cargnelli et al., 1999). Both non-OA sensitive species have MAB-centric distributions,

with the southern extent of their ranges ending around Cape Hatteras (FAO, 2021; NEFSC, 2017). *M. edulis* form beds by using byssal threads to attach to various surfaces along the coastline, from rock to vegetation (FAO, 2021). *S. solidissima* adults often burrow in sandy sediments where they are protected from predators (Cargnelli et al., 1999).

Given the habitat preferences of the meta-analysis species, it is difficult to discern differences that would cause certain species to show OA sensitivity and others not to. One difference between the two groups is that the OA sensitive species (*A. irradians*, *C. virginica*, and *M. mercenaria*) tend to have larger geographical ranges, with all three found, at a minimum, along the entire U.S. east coast from Cape Cod to the Gulf of Mexico. The non-OA sensitive species (*M. edulis* and *S. solidissima*) have a smaller range, generally found only in the north Atlantic and no farther south than Cape Hatteras. This could indicate that the bivalve species with smaller geographic ranges are more suited for survival in the Mid-Atlantic due to specialization to the region as opposed to more widespread environmental tolerance. However, it is beyond the scope of this paper to identify the evolutionary differences between bivalve species inhabiting the MAB. Further studies identifying the specific ranges of OA tolerance for individual species are necessary to clarify patterns of and reasons for OA susceptibility.

4.5.1.2 Other environmental considerations

The bivalves investigated here are subject to additional environmental stressors that may affect their long-term survival. Bivalves are generally able to withstand a wide range of temperatures within their dynamic environments, but have an upper temperature threshold at which metabolic processes deteriorate. The upper temperature threshold

varies between species in the meta-analysis, with *M. edulis* being the lowest (20°C), and the remaining species reaching their upper threshold in the mid 20s to mid 30s (Table 4.2). The model used in this study reported average annual temperatures as high as 23.6°C in its southern coastal range (Table 4.6), which would likely be higher in the shallow bays and estuaries. While the meta-analysis species are likely not yet living at their upper temperature thresholds, ocean temperatures are projected to increase by 3°C in the MAB under a doubling of atmospheric CO₂ (Saba et al., 2016). Continued warming in shallow coastal zones will negatively impact bivalve populations, especially those which are unable to seek refuge by moving throughout the water column. Negative impacts will likely be felt more in the southern Mid-Atlantic, which experiences warmer temperatures year-round than its more northern counterpart (Table 4.6).

The meta-analysis species all live near the coast or in bays and estuaries, and are therefore exposed to freshwater river outputs to the sea. Freshwater has lower buffering capacity for CO₂ than seawater, and is therefore more prone to acidification (Cai et al., 2020; Kwiatkowski & Orr, 2018). Because of this, nearshore regions have been shown to have lower pH and Ω_{arag} than offshore regions (Wright-Fairbanks et al., 2020; Xu et al., 2017). Though bivalves in coastal zones are able to withstand present environmental conditions, precipitation events and coastal storms are projected to increase in strength and number, delivering larger quantities of freshwater into these habitats (Voynova & Sharp, 2012; Wetz & Yoskowitz, 2013). It is currently unknown how close these species are living to their tolerance thresholds for acidification, and if they are close to those limits, increased freshwater intrusion may cause declines in the health of their populations.

4.5.1.3 OA experiment needs

The literature review conducted here identified several studies investigating the effect of ocean acidification on larval bivalve growth and development. While many studies measured similar metrics, there was not a consensus on experimental design for reporting of treatment values and response variables. This likely stems from the novelty of the OA research field and multitude of viable methods for conducting OA laboratory experiments.

There are few published studies on larval bivalve responses to OA. The number of studies focused on each bivalve species is even fewer, and in the case of Atlantic sea scallops, zero. Here, we apply a generalized larval bivalve growth curve to sea scallops, but in order to strengthen this relationship and/or determine the sensitivity of sea scallops to OA, it is necessary to utilize species-specific experimental data. It is imperative that responses of key species, like *P. magellanicus*, to projected environmental change are experimentally tested and repeated with confidence in order to project future changes in their contribution to economic, social, and environmental wellbeing. This understanding will not be achieved without experimental data. Further, it would be extremely beneficial to pair chemical and biological measurements in the field to understand organismal responses to realistic environmental conditions.

4.5.2 Sea scallop larval dispersal model

4.5.2.1 Comparison to a previous temperature-based model

The larval model developed here is founded on the temperature-based growth and behavior model for larval sea scallops of Munroe et al. (2018). The non-OA sensitive trials run here mimic those results. Our settlement success results showed some

similarities to those of Munroe et al. (2018), but a few key differences arose. Both models showed the greatest settlement success in the Long Island region (less one year in which New York Bight was more successful in our results), and settlement success decreased from north to south over the range of the model. However, the models diverged in seasonal success. Our model showed higher success in spring than in fall across all regions and years, while theirs showed little spring success and the majority of successful settlement in fall in all regions. The success rates in our non-OA sensitive scenario were low in fall due to high temperatures at particle locations, averaging greater than 19°C, at which mass mortalities of larval scallops have been recorded (Hart & Chute, 2004). These high fall temperatures suppressed success in VB in 5/7 simulated calendar years, in DMV 4/7 years, and in LI 3/7 years.

The OA sensitive group had lower success rates than those reported in Munroe et al. (2018) across the board, which is likely a result of the negative impacts of OA on larval growth. However, the OA sensitive group had similar seasonal patterns to Munroe et al. (2018), with higher success in fall than in spring due to high Ω_{arag} . It is unlikely that multiple years would experience 0% settlement success as our OA-sensitive model suggests. This result likely arose due to a small number of larvae being released (only a fraction of the numbers expected each year), and strict settlement success criteria. In years with 0% success, there were many otherwise successful larvae that happened to settle outside of the bounds of the fisheries management areas. Those larvae were not considered successful here, but may well grow successfully in the ocean.

Population connectivity patterns were similar to those reported in Munroe et al. (2018), with LI and NYB the most well-connected regions. They supplied and received

the majority of larvae to and from the other regions. Because VB was at the edge of the range and received very few successful larvae, its population is potentially in jeopardy compared to those of the northern regions. Our model displayed northward connection in all regions, while Munroe et al. (2018) exhibited a majority southward down-coast dispersal. Like differences in larval success, this may be the result of release depths, release locations, and integration of advection in each model. Though the major current pattern in the MAB is southward alongshore, the continued success of northern populations indicates that larvae must be dispersing northward. Our model iterations supported this theory. Northward movement of larval organisms in the MAB should be investigated further to clarify the intersection of physical dynamics and ecological patterns.

Differences in release depth, exact release location, individual-based model particle tracking, and ROMS iteration may account for differences in environmental conditions that would cause our model to deviate from Munroe et al. (2018) in terms of settlement and seasonality of success. Whether synchronous online particle tracking versus ROMSPath calculations based on daily average model output could account for those differences would require detailed further analysis.

4.5.2.2 Seasonality

Particles experienced environmental differences based on location, with temperature increasing from north (LI) to south (VB) in each year (Table 6). Additionally, particles experienced different temperature based on season, increasing from spring through fall in LI and NYB all years, in DMV in 6/7 years, and in VB 4/7 years (Table 6). Average temperatures are higher in fall than summer likely due to

particles dispersing through cold, subsurface water trapped on the shelf in summer (the Mid-Atlantic Cold Pool) (Castelao et al., 2008; Chen et al., 2018; Houghton et al., 1982).

Additionally, particles experienced a spatial gradient in Ω_{arag} , which increased from north (LI) to south (VB) each year (Table 6). Ω_{arag} also showed seasonal patterns, with particles experiencing an increase from spring to fall, though in some years (2007, 2012) particles experienced the lowest Ω_{arag} in summer in all areas. The north to south gradient of Ω_{arag} in the MAB has been recorded previously (Wanninkhof et al., 2015), and is a result of Gulf Stream influence in the south, the Labrador Current in the north, and spatial temperature gradients (Cai et al., 2020). Seasonal differences in average Ω_{arag} might occur due to nearshore freshwater mixing in the spring, biological respiration and stratification in the summer decreasing Ω_{arag} in the Cold Pool water mass, and mixing of the high- Ω_{arag} Gulf Stream onto the continental shelf in fall (Wright-Fairbanks et al., 2020). In years when particles experienced higher-than-average seasonal Ω_{arag} , it is possible that a Gulf Stream ring carried a large volume of high- Ω_{arag} water onto the shelf (Andres, 2016).

The differences in seasonal settlement success between OA sensitivity groups indicates a compensatory mechanism by which high Ω_{arag} can make up for low success due to high temperatures for OA sensitive scallops (Figure 4.4). Non-OA sensitive scallop larvae exhibited low success due to average temperatures above their temperature range of optimal growth (10-15 °C), and above their growth cutoff temperature (19°C), which occurred most often in southern regions in the fall. However, high Ω_{arag} in those regions caused OA sensitive scallop larvae to have their highest seasonal success averaged over the entire model time period. This occurred expressly in NYB, DMV, and

VB in fall 2011 and DMV and VB spring 2012, which had both high temperatures and well-above-seasonal average Ω_{arag} . Other instances, like summer and fall 2012 in DMV and VB, experienced high temperatures, but Ω_{arag} values were lower than the interannual seasonal averages, and therefore did not compensate for the negative effect of temperature. If sea scallops are non-OA sensitive, success will likely be driven by temperature. If sea scallops are sensitive to OA, larval success rates will be influenced by Ω_{arag} , especially in high-temperature scenarios. Laboratory determination of scallop sensitivity to OA is necessary to establish which scenario is more likely for this species.

4.5.2.3 Implications of OA on stock management

As demonstrated in this study, sea scallop development and success can be linked to ocean temperature and the state of acidification. The U.S. northeast and MAB region have experienced substantial long-term ocean warming in surface and bottom waters in the past four decades (Chen et al., 2020; Kavanaugh et al., 2017). This warming has already caused a shift in suitable habitat to deeper and more northern areas for some commercial species (Bell et al., 2015; Kleisner et al., 2017; Pinsky et al., 2013), and will likely cause scallop southern range to shift northward. While there is some possible relief from high Ω_{arag} in southern regions that are heavily influenced by the high- Ω_{arag} Gulf Stream, at some point the compensatory action will not be enough for scallops to overcome high temperatures. Southern regions (VB, DMV) acted as source stocks in this simulation, with little settlement and population connectivity. Together with warming temperatures, this could mean that southern stocks are in danger of failing as time progresses.

Model results showed the highest settlement success in the northern regions (LI and NYB), meaning these regions could be critical to the ongoing success of scallop populations in the MAB. In these northern regions where temperatures are more suited to scallop development, an increase in Gulf Stream intrusions has been observed and is projected to continue over the coming decades (Gangopadhyay et al., 2019; Gawarkiewicz et al., 2018). These intrusions will deliver high- Ω_{arag} water to the well-connected source stocks in NYB and LI, which will aid in compensating for increased temperatures there. This could allow stocks in NYB, LI, and the northern regions they feed (namely BI) to remain intact even under the threat of warming. However, it is difficult to predict when Gulf Stream intrusions will occur and which areas of the shelf they will influence, and this will become even more difficult under projections of increasing Gulf Stream instability (Gangopadhyay et al., 2019). Further investigation of source vs. stock populations is imperative to stock management. Additionally, the response of scallop larvae to high Ω_{arag} needs to be determined to draw conclusions about the influence of temperature and Ω_{arag} on larval success and population dynamics.

4.6 Conclusions

This study presents the development of a larval bivalve growth rate-ocean acidification relationship that was successfully applied to a larval dispersal model for Atlantic sea scallops in the Mid-Atlantic Bight. Development of the growth rate-OA parameter revealed species-specific responses which are important to consider in predicting the response of bivalve larvae to acidification. While it is helpful to derive relationships for general use, future studies of species-specific responses would benefit

from standardized, high-quality ocean acidification laboratory research. When larval scallop sensitivity to OA was assumed, model simulations showed negative effects of OA on scallop growth, settlement success, and population connectivity in MAB fisheries habitats. However, OA sensitivity mitigated the negative effects of high temperature on larval scallop growth and settlement success in areas of high Ω_{arag} . As such, the interplay between temperature and OA can potentially determine the success of larval scallops in the MAB. Further investigation of source vs. stock populations and species-specific responses to OA will benefit management of Atlantic sea scallop stock in the Mid-Atlantic Bight.

4.7 References

- Acquafredda, M. P., Munroe, D. M., Ragnoe Calvo, L. M., & De Luca, M. (2019). The effect of rearing temperature on the survival and growth of early juvenile Atlantic surfclams (*Spisula solidissima*). *Aquaculture Reports*, 13:100176.
- Allen, R. D. (1953). Fertilization and artificial activation in the egg of the surf-clam, *Spisula solidissima*. *The Biological Bulletin Published by the Marine Biological Laboratory*, 105(2).
- Andres, M. (2016). On the recent destabilization of the Gulf Stream path downstream of Cape Hatteras. *Geophysical Research Letters*, 43, 9836-9842. doi:10.1002/
- Barber, B. J., & Blake, N. J. (1983). Growth and reproduction of the bay scallop, *Argopecten irradians* (Lamarck) at its southern distributional limit. *Journal of Experimental Marine Biology and Ecology*, 66, 247-256.
- Bell, R. J., Richardson, D. E., Hare, J. A., Lynch, P. D., & Fratantoni, P. S. (2015). Disentangling the effects of climate, abundance, and size on the distribution of marine fish: an example based on four stocks from the Northeast US shelf. *ICES Journal of Marine Science*, 72(5), 1311-1322. doi:10.1093/icesjms/fsu217
- Bricelj, V. M. (1993). Aspects of the Biology of the Northern Quahog, *Mercenaria mercenaria*, with Emphasis on Growth and Survival during Early Life History. *Proceedings of the Second Rhode Island shellfish industry conference*.
- Cai, W.-J., Hu, X., Huang, W.-J., Murrell, M. C., Lehrter, J. C., Lohrenz, S. E., Chou, W.-C., Zhai, W., Hollibaugh, J. T., Wang, Y., Zhao, P., Guo, X., Gundersen, K., Dai, M., & Gong, G.-C. (2011). Acidification of subsurface coastal waters

- enhanced by eutrophication. *Nature Geoscience*, 4(11), 766-770.
doi:10.1038/ngeo1297
- Cai, W.-J., Xu, Y. Y., Feely, R. A., Wanninkhof, R., Jonsson, B., Alin, S. R., Barbero, L., Cross, J. N., Azetsu-Scott, K., Fassbender, A. J., Carter, B. R., Jiang, L. Q., Pepin, P., Chen, B., Hussain, N., Reimer, J. J., Xue, L., Salisbury, J. E., Hernandez-Ayon, J. M., Langdon, C., Li, Q., Sutton, A. J., Chen, C. A., & Gledhill, D. K. (2020). Controls on surface water carbonate chemistry along North American ocean margins. *Nat Commun*, 11(1), 2691. doi:10.1038/s41467-020-16530-z
- Cargnelli, L. M., Griesbach, S. J., Packer, D. B., & Weissberger, E. (1999). Essential Fish Habitat Source Document: Atlantic Surfclam, *Spisula solidissima*, Life History and Habitat Characteristics. *NOAA Technical Memorandum NMFS-NE Series*(142).
- Castelao, R., Glenn, S., Schofield, O., Chant, R., Wilkin, J., & Kohut, J. (2008). Seasonal evolution of hydrographic fields in the central Middle Atlantic Bight from glider observations. *Geophysical Research Letters*, 35(3). doi:10.1029/2007gl032335
- Chen, Z., Curchitser, E., Chant, R., & Kang, D. (2018). Seasonal Variability of the Cold Pool Over the Mid-Atlantic Bight Continental Shelf. *Journal of Geophysical Research: Oceans*, 123(11), 8203-8226. doi:10.1029/2018jc014148
- Chen, Z., Kwon, Y. O., Chen, K., Fratantoni, P., Gawarkiewicz, G., & Joyce, T. M. (2020). Long-Term SST Variability on the Northwest Atlantic Continental Shelf and Slope. *Geophysical Research Letters*, 47(1). doi:10.1029/2019gl085455
- Clark, S., Hubbard, K. A., McGillicuddy, D. J. J., Ralston, D. K., & Shankar, S. (2016). Investigating Pseudo-nitzschia australis introduction to the Gulf of Maine with observations and models. *Continental Shelf Research*, 228:104493.
- Clements, J. C., & Chopin, T. (2017). Ocean acidification and marine aquaculture in North America: potential impacts and mitigation strategies. *Reviews in Aquaculture*, 9, 326-341. doi:10.1111/raq.12140
- Cooley, S. R., Rheuban, J. E., Hart, D. R., Luu, V., Glover, D. M., Hare, J. A., & Doney, S. C. (2015). An Integrated Assessment Model for Helping the United States Sea Scallop (*Placopecten magellanicus*) Fishery Plan Ahead for Ocean Acidification and Warming. *PLoS One*, 10(5), e0124145. doi:10.1371/journal.pone.0124145
- Culliney, J. L. (1974). Larval development of the giant scallop *Placopecten magellanicus* (gmelin). *Biol. Bull*, 147, 321-332.
- Doney, S. C., Fabry, V. J., Feely, R. A., & Kleypas, J. A. (2009). Ocean acidification: the other CO2 problem. *Ann Rev Mar Sci*, 1, 169-192.
doi:10.1146/annurev.marine.010908.163834
- Druon, J. N., Mannino, A., Signorini, S., McClain, C., Friedrichs, M., Wilkin, J., & Fennel, K. (2010). Modeling the dynamics and export of dissolved organic matter in the Northeastern U.S. continental shelf. *Estuarine, Coastal and Shelf Science*, 88, 488-507. doi:10.1016/j.ecss.2010.05.010

- Dupaul, W. D., Kirkley, J. E., & Schmitzer, A. C. (1989). Evidence of a semiannual reproductive cycle for the sea scallop, *Placopecten magellanicus* (Gmelin, 1791), in the Mid-Atlantic Region. *Journal of Shellfish Research*, 8(1), 173-178.
- Egbert, G. D., & Erofeeva, S. Y. (2002). Efficient inverse modeling of barotropic ocean tides. *Journal of Atmospheric and Oceanic Technology*, 19, 183-204.
- FAO. (2021). *Mytilus edulis* (Lineaeus, 1758). *Species Fact Sheets*. Retrieved from fao.org/fishery/species/2688/en
- Feng, Y., Friedrichs, M., Wilkin, J., Tian, H., Yang, Q., Hofmann, E., Wiggert, J., & Hood, R. (2015). Chesapeake Bay nitrogen fluxes derived from a land-estuarine-ocean biogeochemical modeling system: Model description, evaluation, and nitrogen budgets. *Journal of Geophysical Research: Biogeosciences*, 120, 1666-1695. doi:doi:10.1002/2015JG002931.
- Fennel, K., & Wilkin, J. (2009). Quantifying biological carbon export for the northwest North Atlantic continental shelves. *Geophysical Research Letters*, 36, L18605. doi:10.1029/2009GL039818.
- Gallager, S. M., & Mann, R. (1986). Growth and Survival of Larvae of *Mercenaria mercenaria* (L.) and *Crassostrea virginica* (Gmelin) Relative to Broodstock Conditioning and Lipid Content of Eggs. *Aquaculture*, 56, 106-121.
- Gangopadhyay, A., Gawarkiewicz, G., Silva, E. N. S., Monim, M., & Clark, J. (2019). An Observed Regime Shift in the Formation of Warm Core Rings from the Gulf Stream. *Sci Rep*, 9(1), 12319. doi:10.1038/s41598-019-48661-9
- Garwood, J. C., Fuchs, H. L., Gerbi, G. P., Hunter, E., Chant, R. J., & Wilkin, J. (2021). Estuarine larval retention enhanced by observed larval responses to turbulence but not by responses to waves. *Limnology and Oceanography*.
- Gawarkiewicz, G., Todd, R., Zhang, W., Partida, J., Gangopadhyay, A., Monim, M.-U.-H., Fratantoni, P., Malek Mercer, A., & Dent, M. (2018). The Changing Nature of Shelf-Break Exchange Revealed by the OOI Pioneer Array. *Oceanography*, 31(1), 60-70. doi:10.5670/oceanog.2018.110
- Gazeau, F., Parker, L. M., Comeau, S., Gattuso, J.-P., O'Connor, W. A., Martin, S., Pörtner, H.-O., & Ross, P. M. (2013). Impacts of ocean acidification on marine shelled molluscs. *Marine Biology*, 160(8), 2207-2245. doi:10.1007/s00227-013-2219-3
- Gledhill, D., White, M., Salisbury, J., Thomas, H., Misna, I., Liebman, M., Mook, B., Grear, J., Candelmo, A., Chambers, R. C., Gobler, C., Hunt, C., King, A., Price, N., Signorini, S., Stancioff, E., Stymiest, C., Wahle, R., Waller, J., Rebuck, N., Wang, Z., Capson, T., Morrison, J. R., Cooley, S., & Doney, S. (2015). Ocean and Coastal Acidification off New England and Nova Scotia. *Oceanography*, 25(2), 182-197. doi:10.5670/oceanog.2015.41
- Gobler, C. J., & Talmage, S. C. (2013). Short- and long-term consequences of larval stage exposure to constantly and ephemerally elevated carbon dioxide for marine bivalve populations. *Biogeosciences*, 10(4), 2241-2253. doi:10.5194/bg-10-2241-2013

- Goldsmith, K. A., Lau, S., Poach, M. E., Sakowicz, G. P., Trice, T. M., Ono, C. R., Nye, J., Shadwick, E. H., StLaurent, K. A., & Saba, G. K. (2019). Scientific considerations for acidification monitoring in the U.S. Mid-Atlantic Region. *Estuarine, Coastal and Shelf Science*, 225. doi:10.1016/j.ecss.2019.04.023
- Green, M. A., Waldbusser, G. G., Hubazc, L., Cathcart, E., & Hall, J. (2012). Carbonate Mineral Saturation State as the Recruitment Cue for Settling Bivalves in Marine Muds. *Estuaries and Coasts*, 36(1), 18-27. doi:10.1007/s12237-012-9549-0
- Haidvogel, D. B., Arango, H. G., Budgell, W. P., Cornuelle, B., Churchitser, E., Di Lorenzo, E., Fennel, K., Geyer, W. R., Hermann, A. J., Lanerolle, L., Levin, J., McWilliams, J. C., Miller, A., Moore, A., Powell, T., Shchepetkin, A. F., Sherwood, C., Signell, R., Warner, J. C., & Wilkin, J. (2008). Ocean forecasting in terrain-following coordinates: Formulation and skill assessment of the Regional Ocean Modeling System. *Journal of Computational Physics*, 227, 3595-3624.
- Hart, D. R., & Chute, A. S. (2004). Sea Scallop, *Placopecten magellanicus*, Life History and Habitat Characteristics. *NOAA Technical Memorandum NMFS-NE Series*, 189.
- Hart, D. R., Munroe, D. M., Caracappa, J. C., Haidvogel, D., Shank, B. V., Rudders, D. B., Klinck, J. M., Hofmann, E. E., Powell, E. N., & Kaplan, D. M. (2020). Spillover of sea scallops from rotational closures in the Mid-Atlantic Bight (United States). *ICES Journal of Marine Science*, 77(5), 1992-2002. doi:10.1093/icesjms/fsaa099
- Hofmann, G. E., Smith, J. E., Johnson, K. S., Send, U., Levin, L. A., Micheli, F., Paytan, A., Price, N. N., Peterson, B., Takeshita, Y., Matson, P. G., Crook, E. D., Kroeker, K. J., Gambi, M. C., Rivest, E. B., Frieder, C. A., Yu, P. C., & Martz, T. R. (2011). High-frequency dynamics of ocean pH: a multi-ecosystem comparison. *PLoS One*, 6(12), e28983. doi:10.1371/journal.pone.0028983
- Houghton, R. W., Shlitz, R., Beardsley, R. C., Butman, B., & Chamberlin, J. L. (1982). The Middle Atlantic Bight Cold Pool: Evolution of the Temperature Structure During Summer 1979. *American Meteorological Society*, 12, 1019-1029.
- Hunt, C. W., Salisbury, J. E., Vandemark, D., Abmann, S., Fietzek, P., Melrose, C., Wanninkhof, R., & Azetsu-Scott, K. (2021). Variability of USA East Coast surface total alkalinity distributions revealed by automated instrument measurements. *Marine Chemistry*, 232. doi:10.1016/j.marchem.2021.103960
- Hunter, E. (2021). imcslatte/ROMSPath: ROMSPath Second Release (v1.0.1). Zenodo.
- IPCC. (2019). Summary for Policymakers. *IPCC Special Report on the Ocean and Cryosphere in a Changing Climate*.
- Kapsenberg, L., Miglioli, A., Bitter, M. C., Tambutté, E., Dumollard, R., & Gattuso, J. P. (2018). Ocean pH fluctuations affect mussel larvae at key developmental transitions. *Proceedings of the Royal Society B: Biological Sciences*, 285(1893). doi:10.1098/rspb.2018.2381
- Kavanaugh, M. T., Rheuban, J. E., Luis, K. M. A., & Doney, S. C. (2017). Thirty-Three Years of Ocean Benthic Warming Along the U.S. Northeast Continental Shelf and

- Slope: Patterns, Drivers, and Ecological Consequences. *J Geophys Res Oceans*, 122(12), 9399-9414. doi:10.1002/2017JC012953
- Kleisner, K. M., Fogarty, M. J., McGee, S., Hare, J. A., Moret, S., Perretti, C. T., & Saba, V. S. (2017). Marine species distribution shifts on the U.S. Northeast Continental Shelf under continued ocean warming. *Progress in Oceanography*, 153, 24-36. doi:10.1016/j.pocean.2017.04.001
- Kroeker, K. J., Kordas, R. L., Crim, R., Hendriks, I. E., Ramajo, L., Singh, G. S., Duarte, C. M., & Gattuso, J. P. (2013). Impacts of ocean acidification on marine organisms: quantifying sensitivities and interaction with warming. *Glob Chang Biol*, 19(6), 1884-1896. doi:10.1111/gcb.12179
- Kurihara, H., Asai, T., Kato, S., & Ishimatsu, A. (2008). Effects of elevated pCO₂ on early development in the mussel *Mytilus galloprovincialis*. *Aquatic Biology*, 4, 225-233. doi:10.3354/ab00109
- Kwiatkowski, L., & Orr, J. C. (2018). Diverging seasonal extremes for ocean acidification during the twenty-first century. *Nature Climate Change*, 8(2), 141-145. doi:10.1038/s41558-017-0054-0
- Langton, R. W., Robinson, W. E., & Schick, D. (1987). Fecundity and reproductive effort of sea scallops *Placopecten magellanicus* from the Gulf of Maine. *Marine Ecology Progress Series*, 37, 19-25.
- Lellouche, J.-M., Greiner, E., Le Galloudec, O., Garric, G., Regnier, C., Drevillon, M., Benkiran, M., Testut, C.-E., Bourdalle-Badie, R., Gasparin, F., Hernandez, O., Levier, B., Drillet, Y., Remy, E., & Le Traon, P.-Y. (2018). Recent updates to the Copernicus Marine Service global ocean monitoring and forecasting real-time 1/12° high-resolution system. *Ocean Science*, 14(5), 1093-1126. doi:<https://doi.org/10.5194/os-14-1093-2018>
- Levin, J., Wilkin, J., Fleming, N., & Zavala-Garay, J. (2018). Mean circulation of the Mid-Atlantic Bight from a climatological data assimilative model. *Ocean Modelling*, 128, 1-14. doi:10.1016/j.ocemod.2018.05.003
- López, A. G. (2020). Modeling the circulation and timescales of the Mid-Atlantic Bight and Gulf of Maine. *PhD thesis, Rutgers, The State University of New Jersey, New Brunswick, NJ*, 127 pp. doi:<https://doi.org/doi:10.7282/t3-d1e6-jz61>
- López, A. G., Wilkin, J., & Levin, J. C. (2020). Doppio - a ROMS (v3.6)-based circulation model for the Mid-Atlantic Bight and Gulf of Maine: configuration and comparison to integrated coastal observing network observations. *Geoscientific Model Development*, 13, 3709-3729. doi:10.5194/gmd-13-3709-2020
- Mackenzie Jr., C. L. (2008). The Bay Scallop, *Argopecten irradians*, Massachusetts Through North Carolina: Its Biology and the History of Its Habitats and Fisheries. *Marine Fisheries Review*, 70(3-4).
- Mesinger, F., DiMego, G., Kalnay, E., Mitchell, K., Shafran, P. C., Ebisuzaki, W., Jovi'c, D., Woollen, J., Rogers, E., Berbery, E. H., Ek, M. B., Fan, Y., Grumbine, R., Higgins, W., Li, H., Lin, Y., Manikin, G., Parrish, D., & Shi, W. (2006). North

- American Regional Reanalysis. *Bulletin of the American Meteorological Society*, 87, 343-360.
- Munroe, D. M. H., D., Caracappa, J. C., Klinck, J. M., Powell, E. N., Hofmann, E. E., Shank, B. V., & Hart, D. R. (2018). Modeling larval dispersal and connectivity for Atlantic sea scallop (*Placopecten magellanicus*) in the Middle Atlantic Bight. *Fisheries Research*, 208, 7-15. doi:10.1016/j.fishres.2018.06.020
- Narváez, D. A., Klinck, J. M., Powell, E. N., Hofmann, E. E., Wilkin, J., & Haidvogel, D. B. (2012). Modeling the dispersal of eastern oyster (*Crassostrea virginica*) larvae in Delaware Bay. *Journal of Marine Research*, 70, 381-409.
- NEFSC. (2014). 59th Northeast Regional Stock Assessment Workshop (59th SAW) Assessment Report. *U.S. Department of Commerce Northeast Fisheries Science Center Reference Document*, 14-09.
- NEFSC. (2017). 61st Northeast Regional Stock Assessment Workshop (61st SAW) Assessment Report. *U.S. Department of Commerce Northeast Fisheries Science Center Reference Document*, 17-05. doi:10.7289/V5/RD-NEFSC-17-05
- NEFSC. (2018). 65th Northeast Regional Stock Assessment Workshop (65th SAW) assessment report. doi:<https://doi.org/10.25923/zapm-ga75>
- Neima, P. G., & Kenchington, E. (1997). Report of Commercial Scallop Hatchery Design. *Canadian Technical Report of Fisheries and Aquatic Sciences*.
- NOAA. (2021a). *Eastern Oyster*. Retrieved from <https://www.fisheries.noaa.gov/species/eastern-oyster>
- NOAA. (2021b). *Landings data*. Retrieved from <https://fisheries.noaa.gov/foss/>
- North, E. W., Hood, R., Chao, S.-Y., & Sanford, L. P. (2006). Using a random displacement model to simulate turbulent particle motion in a baroclinic frontal zone: a new implementation scheme and model performance tests. *Journal of Marine Systems*, 60, 365-380. doi:10.1016/j.jmarsys.2005.08.003
- Parker, L. M., Ross, P. M., O'Connor, W. A., Portner, H. O., Scanes, E., & Wright, J. M. (2013). Predicting the response of molluscs to the impact of ocean acidification. *Biology (Basel)*, 2(2), 651-692. doi:10.3390/biology2020651
- Pinsky, M. L., Worm, B., Fogarty, M. J., Sarmiento, J. L., & Levin, S. A. (2013). Marine Taxa Track Local Climate Velocities. *Science*, 341(6151), 1239-1242.
- Ramesh, K., Hu, M. Y., Thomsen, J., Bleich, M., & Melzner, F. (2017). Mussel larvae modify calcifying fluid carbonate chemistry to promote calcification. *Nat Commun*, 8(1), 1709. doi:10.1038/s41467-017-01806-8
- Ries, J. B., Cohen, A. L., & McCorkle, D. C. (2009). Marine calcifiers exhibit mixed responses to CO₂-induced ocean acidification. *Geology*, 37(12), 1131-1134. doi:10.1130/G30210A.1;1figure;1table;DataRepositoryitem2009279
- Roegner, G. C., & Mann, R. (1990). Habitat Requirements for the Hard Clam, *Mercenaria mercenaria*, in Chesapeake Bay. *College of William and Mary Special Scientific Report*, 126.

- Saba, G. K., Wright-Fairbanks, E., Chen, B., Cai, W.-J., Barnard, A. H., Jones, C. P., Branham, C. W., Wang, K., & Miles, T. (2019). The Development and Validation of a Profiling Glider Deep ISFET-Based pH Sensor for High Resolution Observations of Coastal and Ocean Acidification. *Frontiers in Marine Science*, 6. doi:10.3389/fmars.2019.00664
- Saba, V. S., Griffies, S. M., Anderson, W. G., Winton, M., Alexander, M. A., Delworth, T. L., Hare, J. A., Harrison, M. J., Rosati, A., Vecchi, G. A., & Zhang, R. (2016). Enhanced warming of the Northwest Atlantic Ocean under climate change. *Journal of Geophysical Research: Oceans*, 121(1), 118-132. doi:10.1002/2015jc011346
- Schlag, Z. R., & North, E. W. (2012). *Lagrangian TRANSport model (LTRANS v2) User's Guide*. Retrieved from Cambridge, MD, USA:
- Schweinitz, E. H., & Lutz, R. A. (1976). Larval development of the northern horse mussel, *Modiolus modiolus* (L.) including a comparison with the larvae of *Mytilus edulis* L. as an aid in planktonic identification. *Biological Bulletin*, 150, 348-360.
- Shchepetkin, A. F., & McWilliams, J. C. (2005). The regional oceanic modeling system (ROMS): a split-explicit, free-surface, topography-following-coordinate oceanic model. *Ocean Modelling*, 9(4), 347-404. doi:10.1016/j.ocemod.2004.08.002
- Shumway, S. E. (1996). *The Eastern Oyster, Crassostrea virginica* (V. S. Kennedy, R. I. E. Newell, & A. F. Eble Eds.): Maryland Sea Grant.
- Siedlecki, S. A., Pilcher, D. J., Hermann, A. J., Coyle, K., & Mathis, J. (2017). The Important of Freshwater to Spatial Variability of Aragonite Saturation State in the Gulf of Alaska. *Journal of Geophysical Research: Oceans*, 122, 8482-8502. doi:10.1002/
- Sutton, A. J., Sabine, C. L., Feely, R. A., Cai, W.-J., Cronin, M. F., McPhaden, M. J., Morell, J. M., Newton, J. A., Noh, J.-H., Ólafsdóttir, S. R., Salisbury, J. E., Send, U., Vandemark, D. C., & Weller, R. A. (2016). Using present-day observations to detect when anthropogenic change forces surface ocean carbonate chemistry outside preindustrial bounds. *Biogeosciences*, 13(17), 5065-5083. doi:10.5194/bg-13-5065-2016
- Talmage, S. C., & Gobler, C. J. (2010). Effects of past, present, and future ocean carbon dioxide concentrations on the growth and survival of larval shellfish. *Proc Natl Acad Sci U S A*, 107(40), 17246-17251. doi:10.1073/pnas.0913804107
- Voynova, Y. G., & Sharp, J. H. (2012). Anomalous biogeochemical response to a flooding event in the Delaware Estuary: a possible typology shift due to climate change. *Estuaries and Coasts*, 35, 943-958.
- Waldbusser, G. G., Hales, B., Langdon, C. J., Haley, B. A., Schrader, P., Brunner, E. L., Gray, M. W., Miller, C. A., & Gimenez, I. (2014). Saturation-state sensitivity of marine bivalve larvae to ocean acidification. *Nature Climate Change*, 5(3), 273-280. doi:10.1038/nclimate2479

- Wanninkhof, R., Barbero, L., Byrne, R., Cai, W.-J., Huang, W.-J., Zhang, J.-Z., Baringer, M., & Langdon, C. (2015). Ocean acidification along the Gulf Coast and East Coast of the USA. *Continental Shelf Research*, 98, 54-71. doi:10.1016/j.csr.2015.02.008
- Wetz, M. S., & Yoskowitz, D. W. (2013). An 'extreme' future for estuaries? Effects of extreme climate events on estuarine water quality and ecology. *Marine Pollution Bulletin*, 69, 7-18.
- Wright-Fairbanks, E. K., Miles, T. N., Cai, W. J., Chen, B., & Saba, G. K. (2020). Autonomous Observation of Seasonal Carbonate Chemistry Dynamics in the Mid-Atlantic Bight. *Journal of Geophysical Research: Oceans*. doi:10.1029/2020jc016505
- Xu, Y. Y., Cai, W.-J., Gao, Y., Wanninkhof, R., Salisbury, J., Chen, B., Reimer, J. J., Gonski, S., & Hussain, N. (2017). Short-term variability of aragonite saturation state in the central Mid-Atlantic Bight. *Journal of Geophysical Research: Oceans*, 122. doi:10.1002/
- Xu, Y. Y., Cai, W.-J., Wanninkhof, R., Salisbury, J., Reimer, J., & Chen, B. (2020). Long-Term Changes of Carbonate Chemistry Variables Along the North American East Coast. *Journal of Geophysical Research: Oceans*, 125(7). doi:10.1029/2019jc015982
- Zeebe, R. E. (2012). History of Seawater Carbonate Chemistry, Atmospheric CO₂, and Ocean Acidification. *Annual Review of Earth and Planetary Sciences*, 40(1), 141-165. doi:10.1146/annurev-earth-042711-105521
- Zhang, X., Haidvogel, D., Munroe, D., Powell, E. N., Klinck, J., Mann, R., & Castruccio, F. S. (2015). Modeling larval connectivity of the Atlantic surfclams within the Middle Atlantic Bight: Model development, larval dispersal and metapopulation connectivity. *Estuarine, Coastal and Shelf Science*, 153, 38-53. doi:10.1016/j.ecss.2014.11.033
- Zhang, X., Munroe, D., Haidvogel, D., & Powell, E. N. (2016). Atlantic surfclam connectivity within the Middle Atlantic Bight: Mechanisms underlying variation in larval transport and settlement. *Estuarine, Coastal and Shelf Science*, 173, 65-78. doi:10.1016/j.ecss.2016.02.019

4.8 Figures

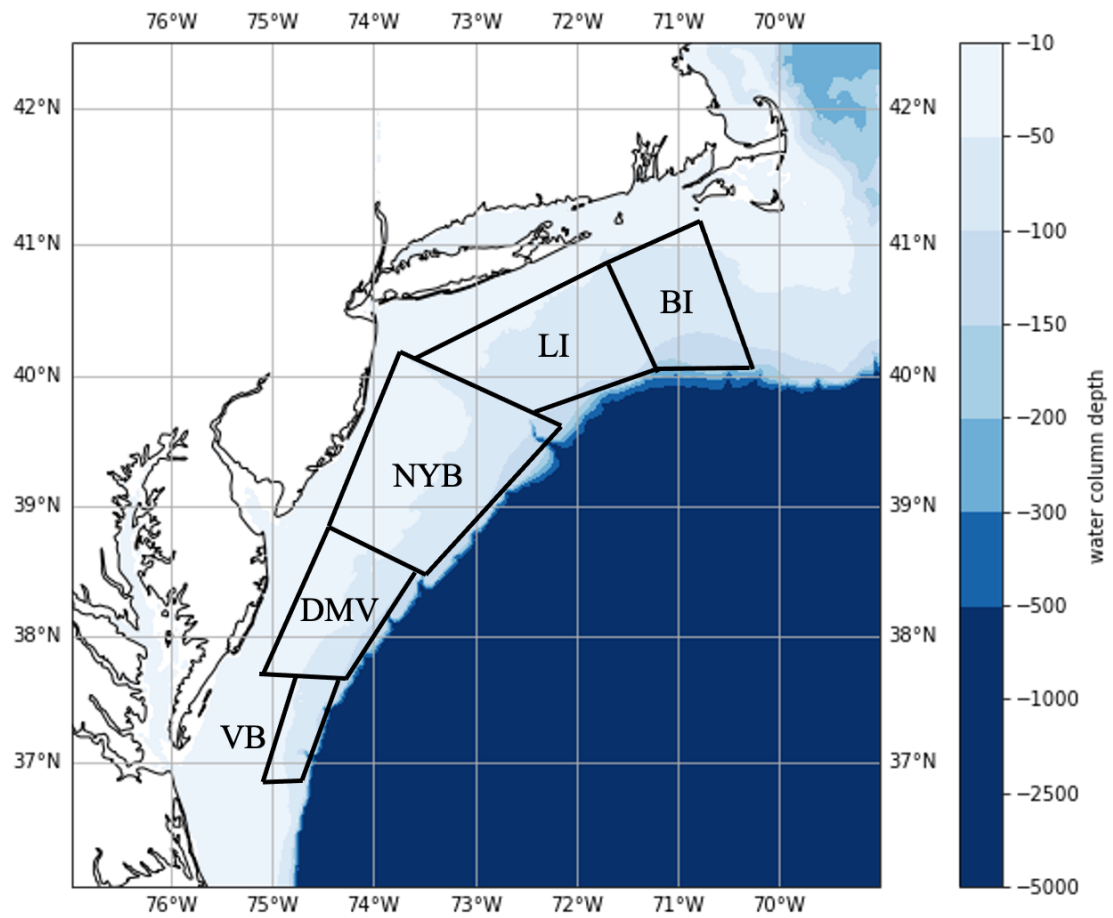


Figure 4.1: Map of regions defined for larval release and determination of larval success and population connectivity. Regions are based on federal management zones for Atlantic sea scallops. Regions are defined as follows: Block Island (BI), Long Island (LI), New York Bight (NYB), Delmarva (DMV), Virginia Beach (VB).

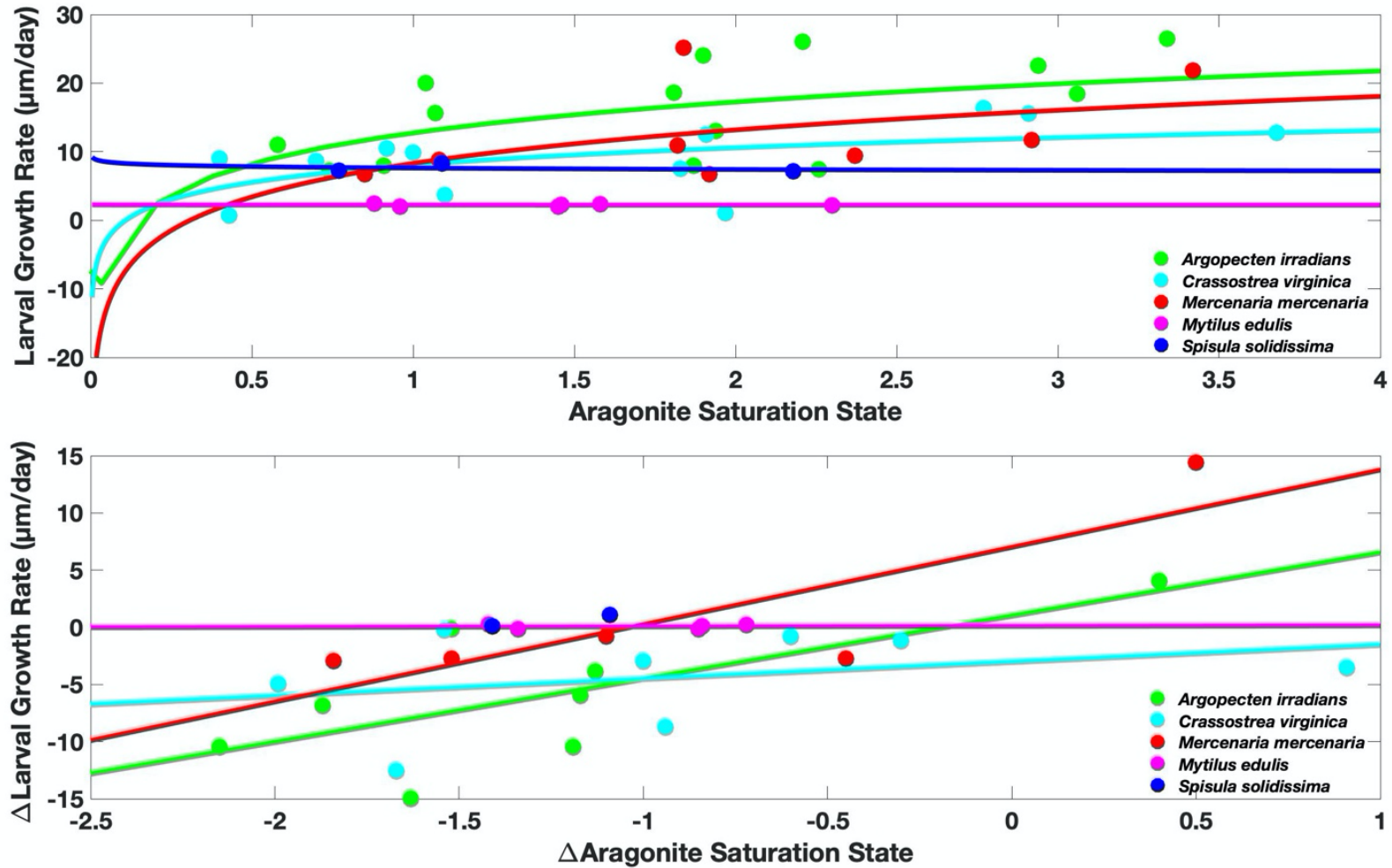


Figure 4.2: Larval bivalve growth vs. OA relationship development by species. The top panel shows absolute growth as a function of aragonite saturation state. The bottom panel shows changes in growth rate as a function of changes in aragonite saturation state.

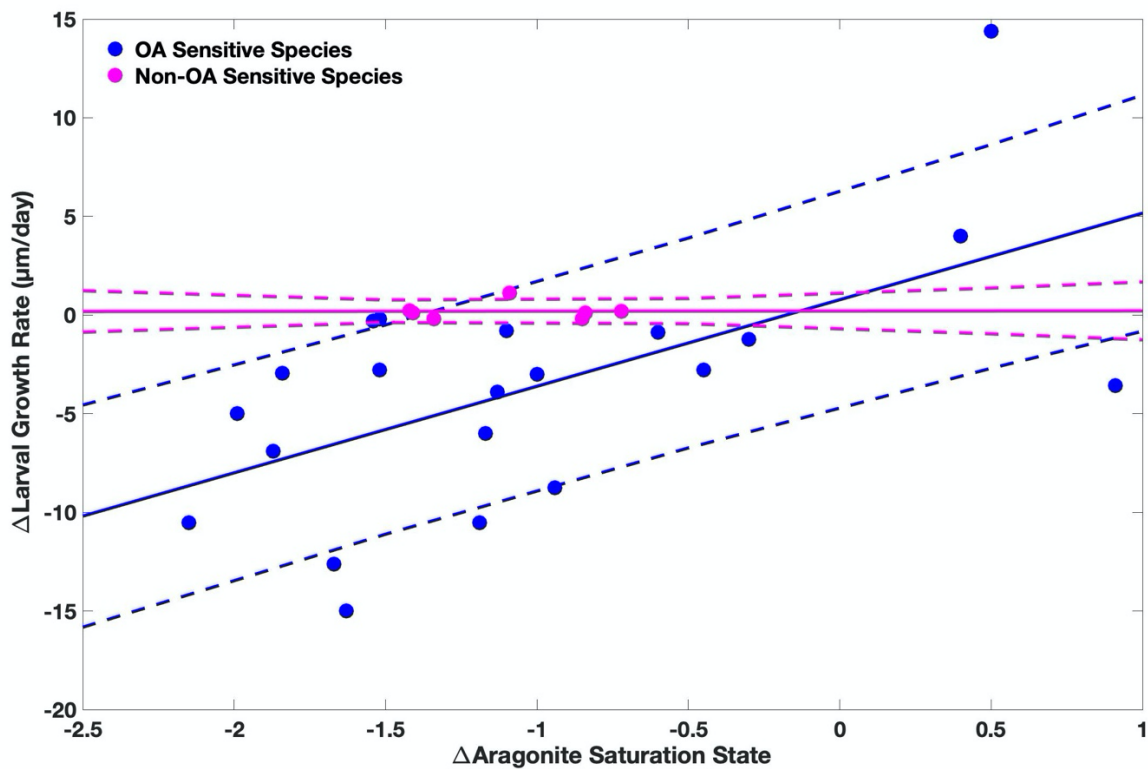


Figure 4.3: Changes in larval bivalve growth rate due to changes in aragonite saturation state (Ω_{arag}). Species are grouped by sensitivity to OA, with non-OA sensitive species in pink and OA sensitive species in blue. Solid lines are the best fit and dashed lines indicate 1 standard error.

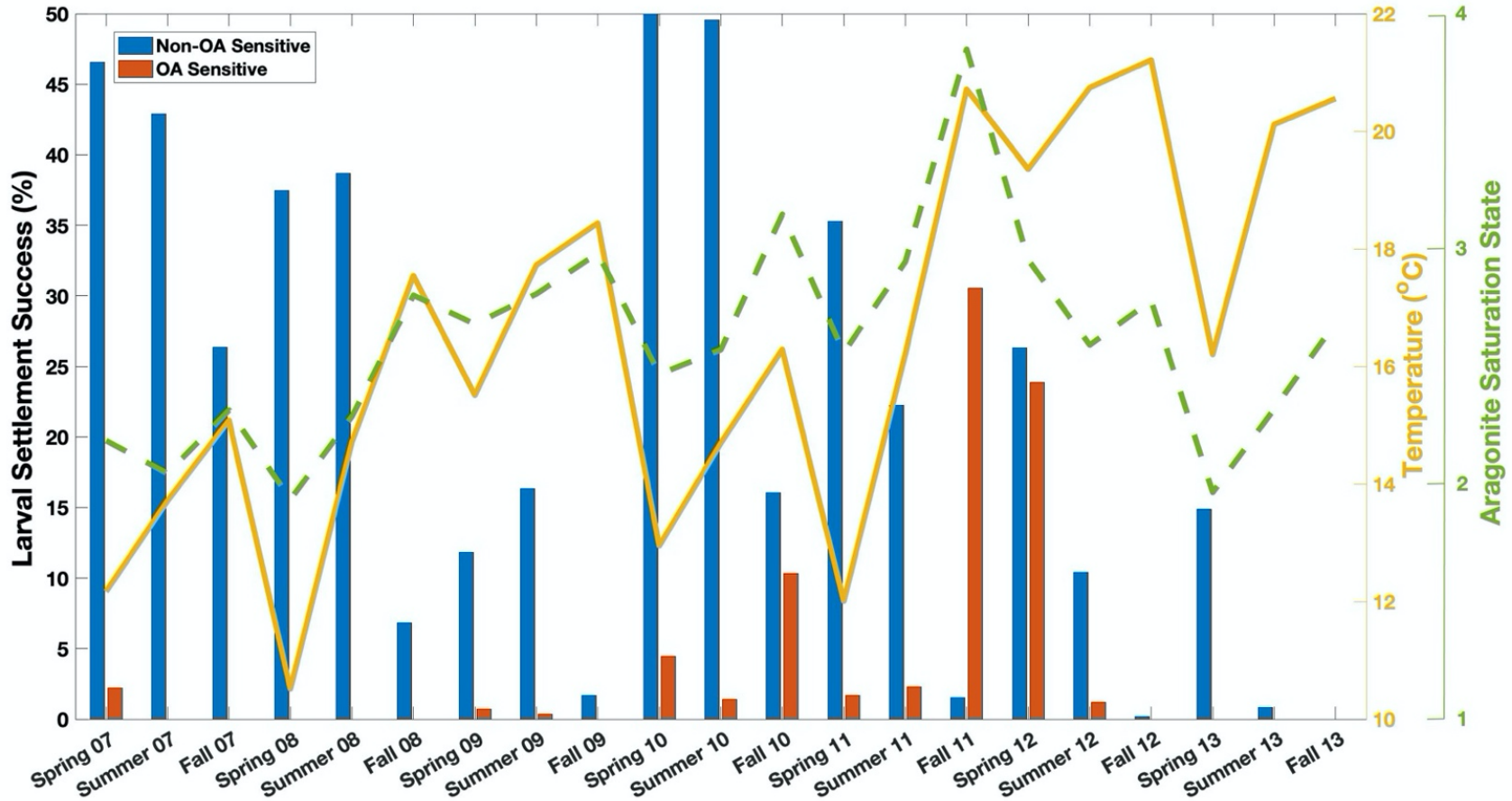


Figure 4.4: Seasonal settlement success for sea scallop larvae over the course of 7 years, with 3 seasons modeled per year. Success values are the average of settlement success over 4 dispersal regions (LI, NYB, DMV, VB). Average temperature and aragonite saturation state at particle locations in each season/year are overlaid as line graphs.

4.9 Tables

Table 4.1: Sea scallop larval dispersal model region bounds and number of particles released in each region every year.

Region	Release point latitude range	Release point longitude range	Particles released per year
Long Island	[39.8,40.8]	[-73.25, -71.25]	2052
New York Bight	[38.5, 40.2]	[-74, -72.25]	1980
Delmarva	[37.7, 38.5]	[-74.75, -73.75]	900
Virginia Beach	[36.9, 37.6]	[-75, -74.5]	252

Table 4.2: Habitat preferences and ranges for the five bivalve species included in the development of the larval growth vs. Ω_{arag} parameter.

Species	Salinity (PSU)	Temperature (°C)	Habitat	Geographic range
<i>Argopecten irradians</i>	>14	15-35	Estuarine/shallow flats	Cape Cod to Gulf of Mexico
<i>Crassostrea virginica</i>	5-42, prefer >12.5	-2-36	Shallow estuarine or intertidal	Gulf of St. Lawrence to Panama
<i>Mercenaria mercenaria</i>	12.5-46, prefer 20-35	0-33, prefer >16	Intertidal, mud flats/sand flats	Gulf of St. Lawrence to Gulf of Mexico
<i>Mytilus edulis</i>	10-35, prefer >20	5-20	Subtidal and intertidal beds	North Atlantic
<i>Spisula solidissima</i>	14-52	15-26	Coastal <36 m	Nova Scotia to Cape Hatteras

Table 4.3: Seasonal settlement success for larval sea scallops spawned in four release regions over a 7-year period, with success shown for 3 seasons per year. Larvae were released from each region and deemed successful if they settled within 45 days at size 250 μm , in <100 meters of water, and in a designated habitat region (Long Island (LI), New York Bight (NYB), Delmarva (DMV), Virginia Beach (VB), or Block Island (BI)). Numbers in each box indicate the percent of larvae released from each area that settled successfully in any other designated area. No larvae were released from the BI region because of a lack of spawning population; therefore, it is not included in this table.

Year	Season	Non-OA Sensitive				OA Sensitive			
		LI	NYB	DMV	VB	LI	NYB	DMV	VB
2007	Spring	77.6	63.0	39.7	5.9	0.0	1.2	6.3	1.2
	Summer	72.8	74.1	24.7	0.0	0.0	0.0	0.0	0.0
	Fall	47.8	52.3	5.3	0.0	0.0	0.0	0.0	0.0
2008	Spring	33.8	32.0	37.7	46.4	0.0	0.0	0.0	0.0
	Summer	23.1	62.0	43.3	26.2	0.0	0.0	0.0	0.0
	Fall	13.7	13.6	0.0	0.0	0.0	0.0	0.0	0.0
2009	Spring	23.8	18.8	4.7	0.0	0.2	0.6	2.0	0.0
	Summer	51.8	13.5	0.0	0.0	1.3	0.0	0.0	0.0
	Fall	6.4	0.3	0.0	0.0	0.0	0.0	0.0	0.0
2010	Spring	55.4	57.1	38.7	48.8	0.0	0.2	5.7	11.9
	Summer	57.8	67.1	55.3	17.9	0.0	0.0	4.3	1.2
	Fall	39.3	24.8	0.0	0.0	4.7	0.0	20.0	16.7
2011	Spring	56.5	41.1	29.3	14.3	0.2	0.3	2.7	3.6
	Summer	41.2	34.7	13.0	0.0	0.5	2.1	5.3	1.2
	Fall	5.6	0.5	0.0	0.0	0.9	26.1	50.0	45.2
2012	Spring	72.7	32.3	0.3	0.0	59.8	19.4	6.7	9.5
	Summer	34.4	7.3	0.0	0.0	4.4	0.3	0.0	0.0
	Fall	0.7	0.0	0.0	0.0	0.0	0.0	0.0	0.0
2013	Spring	28.2	27.3	4.0	0.0	0.0	0.0	0.0	0.0
	Summer	1.3	2.0	0.0	0.0	0.0	0.0	0.0	0.0
	Fall	0.0	0.0	0.0	0.0	0.0	0.0	0.0	0.0

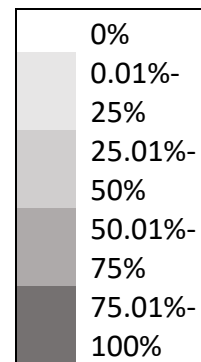


Table 4.4: Non-OA sensitive scallop population connectivity. Numbers indicate the percent of larvae spawned in each release region that successfully settled in each other release region. Regions that experienced no settlement success are indicated with a dash.

Year	Release Region	Settled in LI	Settled in NYB	Settled in DMV	Settled in VB	Settled in BI
2007	LI	34.7	18	0.3	0	13
	NYB	24.2	30.1	1.7	0	7.2
	DMV	3.4	12.2	4	0	3.6
	VB	0.4	0	1.6	0	0
2008	LI	9.5	2.6	0	0	11.5
	NYB	19.6	10.5	0.1	0	5.7
	DMV	8.4	10	1	0.3	7.2
	VB	9.9	6.7	0.8	0	6.7
2009	LI	11.6	7.7	0	0	8
	NYB	3.6	6	0	0	1.2
	DMV	0.6	0.6	0	0	0.4
	VB	-	-	-	-	-
2010	LI	26.8	8.8	0	0	15.3
	NYB	24.1	19.1	0.2	0	6.3
	DMV	5.3	22.6	3.2	0.1	0.1
	VB	0.8	8.3	13.1	0	0
2011	LI	9.1	19.8	2.8	0	2.7
	NYB	5.1	12.5	5.5	0.3	2.1
	DMV	2.9	7.3	2.7	0.7	0.6
	VB	0	4.4	0.4	0	0
2012	LI	14.8	13.5	0.3	0.1	7.3
	NYB	3.7	8.2	0.4	0	0.9
	DMV	0	0.1	0	0	0
	VB	-	-	-	-	-
2013	LI	2.6	1.8	0	0	5.4
	NYB	5.4	1.3	0	0	3.1
	DMV	0.2	0.9	0	0	0.2
	VB	-	-	-	-	-

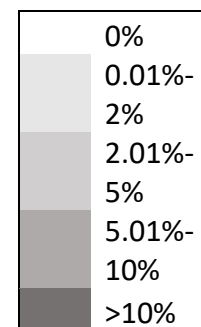


Table 4.5: OA sensitive scallop population connectivity. Numbers indicate the percent of larvae spawned in each release region that successfully settled in each other release region. Regions that experienced no settlement success are indicated with a dash.

Year	Release Region	Settled in LI	Settled in NYB	Settled in DMV	Settled in VB	Settled in BI
2007	LI	-	-	-	-	-
	NYB	0	0.4	0.1	0	0
	DMV	0	2.0	0.1	0	0
	VB	0	0	0.4	0	0
2008	LI	-	-	-	-	-
	NYB	-	-	-	-	-
	DMV	-	-	-	-	-
	VB	-	-	-	-	-
2009	LI	0.1	0	0	0	0.3
	NYB	0.1	0	0	0	0.2
	DMV	0.4	0.2	0	0	0
	VB	-	-	-	-	-
2010	LI	0.1	0	0	0	1.5
	NYB	0.1	2.6	0	0	0.1
	DMV	0.1	8.3	1.6	0	0
	VB	0	2.4	7.5	0	0
2011	LI	0.1	0.1	0	0	0.3
	NYB	0.4	8.9	0	0	0.2
	DMV	0.6	18.3	0	0	0.4
	VB	0.4	16.3	0	0	0
2012	LI	10.2	6.6	0	0	4.6
	NYB	2.5	3.7	0	0	0.3
	DMV	0	1.9	0.3	0	0
	VB	0	0.8	2.4	0	0
2013	LI	-	-	-	-	-
	NYB	-	-	-	-	-
	DMV	-	-	-	-	-
	VB	-	-	-	-	-

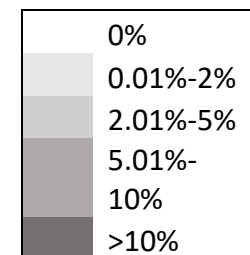


Table 4.6: Average temperature and Ω_{arag} at particle locations in each region over a 7-year period, with both metrics shown for 3 seasons per year. Averages include environmental conditions experienced by all particles released from each region.

Year	Season	Temperature ($^{\circ}\text{C}$)				Ω_{arag}			
		LI	NYB	DMV	VB	LI	NYB	DMV	VB
2007	Spring	8.14	9.51	13.66	17.36	1.83	2.07	2.33	2.50
	Summer	9.09	11.00	15.94	18.82	1.71	1.90	2.26	2.31
	Fall	11.41	13.46	16.96	18.50	1.76	2.26	2.50	2.74
2008	Spring	9.06	9.17	10.44	13.39	1.65	1.76	2.03	2.29
	Summer	11.47	12.96	16.00	18.41	1.83	2.06	2.50	2.76
	Fall	15.15	16.64	18.33	20.05	2.33	2.66	3.04	3.19
2009	Spring	11.56	13.59	17.64	19.25	2.14	2.47	2.97	3.15
	Summer	14.56	16.81	18.95	20.57	2.34	2.64	3.00	3.25
	Fall	16.46	17.50	19.10	20.69	2.59	2.82	3.14	3.38
2010	Spring	10.75	11.10	13.65	16.30	2.11	2.29	2.63	2.85
	Summer	11.83	13.25	15.38	18.31	2.08	2.27	2.70	3.23
	Fall	14.22	15.85	17.05	18.04	2.36	2.84	3.55	3.84
2011	Spring	9.03	10.29	12.86	15.85	2.01	2.26	2.74	3.23
	Summer	10.42	13.43	19.15	21.81	2.00	2.45	3.46	3.88
	Fall	17.27	20.04	21.95	23.60	3.03	3.67	4.19	4.50
2012	Spring	14.82	15.95	21.92	24.71	2.84	2.78	2.92	3.27
	Summer	16.06	18.85	22.70	25.36	2.46	2.33	2.61	2.97
	Fall	18.74	20.06	22.48	23.58	2.50	2.74	2.94	2.94
2013	Spring	12.39	14.20	18.25	19.96	1.87	1.85	1.96	2.18
	Summer	17.83	19.05	20.58	23.00	2.06	2.25	2.36	2.60
	Fall	18.80	19.60	21.18	22.64	2.60	2.72	2.68	2.75

CHAPTER 5: Conclusions

Understanding ocean acidification in the coastal zone is critical due to its influence on living marine resources. The ocean carbonate system is complex, with multiple physical, chemical, and biological forcings making it difficult to discern and predict along the continental shelf. The aim of this dissertation was to explain this complex system in the Mid-Atlantic Bight by investigating the cycles, drivers, and impacts of seasonal carbonate chemistry dynamics. The previous chapters outline a framework by which marine technology and modeling techniques can be used to disentangle the drivers and impacts of coastal carbonate chemistry on a seasonal, shelf-wide scale.

In Chapter 2, I described the implementation of recently developed marine technology, specifically a deep-sea pH sensor integrated into an autonomous glider. This observing platform is cost-effective and able to provide high-resolution measurements year-round in challenging ocean conditions. Here, it allowed a high-resolution description of seasonal changes in the Mid-Atlantic carbonate system for the first time. In Chapter 3, I further decomposed the seasonal cycles of carbonate chemistry into their component parts, identifying water mass mixing and biological productivity and respiration as the major drivers of carbonate chemistry in the region. In Chapter 4, I applied seasonal carbonate system changes to a biological framework using modeling techniques. By incorporating carbonate chemistry effects into larval sea scallop growth and dispersal simulations, I determined that acidification may decrease scallop larval success in the Mid-Atlantic. Additionally, I found that the level of scallop sensitivity to acidification will determine the driver of larval success, with temperature having a greater influence on

non-OA sensitive scallops and aragonite saturation state influencing OA sensitive scallops.

This work underscores and supports the need for continued development of acidification observing networks, laboratory-based OA experimentation, and paired chemical and biological observations. As technology progresses, acidification observing networks will be able to grow regionally, nationally, and globally. It is important to track local drivers and effects of acidification, but also understand how local systems interact within a national economic framework and within the broader global ocean. pH gliders represent one important component of such carbonate system observing networks. The data collected by observing networks is extremely valuable for determining responses of organisms to realistic environmental conditions and change. As shown in Chapter 4, it is also necessary to establish species-specific responses to environmental disturbances to understand how those organisms will respond to episodic and long-term change. Continued monitoring of acidification and its effects on commercially vital organisms is imperative to ensuring the sustained health and well-being of coastal ocean ecosystems.